Evaluation of Optical Images Sub-Pixel Correlation for Estimating Ground Deformation

Muhammad Yaseen

March, 2009

Evaluation of Optical Images Sub-Pixel Correlation for Estimating Ground Deformation

by

Muhammad Yaseen

Thesis submitted to the International Institute for Geo-information Science and Earth Observation in partial fulfilment of the requirements for the degree of Master of Science in Geo-information Science and Earth Observation, Specialisation: (fill in the name of the specialisation)

Thesis Assessment Board

Prof. Dr. Freek van der Meer	(Chairman)
Dr. P.M. (Paul) van Dijk	(External examiner)
Dr. M. (Mark) van der Meijde	(First supervisor)
Dr. H.M.A. (Harald) van der Werff	(Second supervisor)
Drs. T.M. (Tom) Loran	(Course director AES)

INTERNATIONAL INSTITUTE FOR GEO-INFORMATION SCIENCE AND EARTH OBSERVATION
ENSCHEDE, THE NETHERLANDS

Disclaimer

This document describes work undertaken as part of a programme of study at the International Institute for Geo-information Science and Earth Observation. All views and opinions expressed therein remain the sole responsibility of the author, and do not necessarily represent those of the institute.

…….to my father

in the loving memory of my father (Abbou)

Abstract

Sub-pixel correlation of optical images can give valuable information for terrain change monitoring and estimating ground deformation. The evaluation of a newly developed sub-pixel correlation technique (COSI-Corr) can give a better understanding of the process characterizing the change. The present study aims at evaluating its performance in terms of sensitivity, repeatability, robustness and applicability. The sub-pixel correlation of optical images bracketing an earthquake (2005 Kashmir earthquake) event, through their precise orthorectification and coregistration, was carried out with different datasets, DEM options and methodological parameters. The correlated images, their derived maps and graphs were compared and interpreted in order to evaluate the technique with respect to the above mention functionalities. After analyzing the correlated images, their derived maps and graphs, it was found that the technique may be applied for terrain change monitoring. It can assist in giving preliminary damages assessments as soon as pre- and post-event images are available. However, in estimating ground deformation such as displacement along a fault, the results after applying different datasets, DEM options and methodological parameters are varying and inconsistent. The Sinc 25 resampling method and Frequential correlator give comparatively accurate results while the Bilinear resampling method and Statistical correlator results were found to be relatively stable but less accurate. The third resampling method, Bicubic, did not provide accurate results and in most cases the results were unrealistic too. There is still need to go into deeper theoretical details of the methodology in order to understand the behaviour of change of different parameters and its effects on the results. For checking the repeatability and accuracy of displacement estimation, a flat area should be selected in order to minimize DEM inherent errors.

.

Acknowledgements

Alhamadulillah: all praises and pride for almighty ALLAH who give me capabilities and expertise to complete my studies. I would like to thanks to HEC (Higher Education Commission) the Govt. of Pakistan who sponsors my studies abroad.

I am thankful to my supervisors for their kind guidance, encouragements, and critical remarks for correcting and improvements of my research work. Their scientific ideas and suggestions were always a source of guidance to me during my research work.

I would like to appreciate my Father's ambitions despite of very tough circumstances, he helped and encouraged me in getting the education, so I reached at this highest level of education. His struggles for my education are incredible.

I would like to extend my heartiest gratitude to my wife who is also studying with me, despite of busy schedule, she always tried to look after the house and taking care for cooking and clothing, etc. etc. During the writing of my thesis she really helped me a lot for the correct formulating of the thesis. Particularly I am obliged to her for giving two beautiful kids while studying here at ITC and she does not compromising any thing for their looking after. I also would like to acknowledge my children (Asma and Muhammad Taha Yaseen) who really want my attention and company in their child hood. During my studies particularly they suffer a lot during my thesis work due to not giving any time to them.

Finally I acknowledge my family who is bearing difficulties in my absence at home, being the eldest in the home and due to responsibilities my presence is required at home. I am thankful to my younger siblings who suffered and are suffering my absence. At the end and most importantly I would like to acknowledge my mother for her love, affections and prayers are always a source of inspiration for me.

May ALLAH give me courage and knowledge that I can apply for bringing peace and welfare to the humanity.

Muhammad Yaseen
March 09, 2009
Enschede, The Netherlands.

Table of contents

1. **Introduction** **1**
   1.1. Background 1
   1.2. Problem Definition 1
   1.3. Main Objective 2
      1.3.1. Sub Objectives 2
   1.4. Research Questions 3
   1.5. Hypothesis 3
2. Literature Review **5**
   2.1. Location of Study Area 5
   2.2. Geology and Tectonics Settings 5
   2.3. Overview of Remote Sensing Methods 8
      2.3.1. SAR/InSAR 8
      2.3.2. Optical Image Correlation 9
      2.3.3. Aerial Photography 11
      2.3.4. Digital Elevation Model (DEM) 11
3. Methods and Materials **13**
   3.1. Introduction 13
   3.2. Overview of Methodology 13
      3.2.1. Preprocessing 14
      3.2.2. Co-registration 14
      3.2.3. Correlation 17
      3.2.4. Measuring Displacements 17
      3.2.5. Vector Field 18
   3.3. Analysis & Interpretation 18
   3.4. Quantification of Results 19
   3.5. Sensitivity Analysis 19
   3.6. Repeatability 19
   3.7. Robustness 19
   3.8. Applicability 20
   3.9. Materials 20
      3.9.1. Satellite Data 20
      3.9.2. Software 21
4. Results **23**
   4.1. Introduction 23
   4.2. DEM based Analysis 27
   4.3. Sensitivity Analysis 29
      4.3.1. Resampling Methods 29
         4.3.1.1. Kernel size of Sinc resampling method 31
      4.3.2. Correlation Methods 32
         4.3.2.1. Window Size 33
         4.3.2.2. Step Size 35
         4.3.2.3. Threshold 36

4.4. Measuring Displacements along the Fault 37
4.4.1. DEMs Selection Effects 38
4.4.2. Resampling Methods 38
4.4.2.1. Kernel Size 38
4.4.3. Correlation Method 38
4.4.3.1. Window Size 39
4.4.3.2. Step Size 40
4.4.3.3. Threshold 40
4.5. Repeatability 40
4.6. Robustness 41
4.7. Mapping and Analysis of Fault Rupture 42
4.8. Applicability 44
5. Discussion and Conclusions 45
5.1. Discussion 45
5.2. Conclusion 47
5.3. Recommendations 48
References 49
Appendix A 51
Appendix B 83

List of figures

Figure 2-1. A) The study area of the 2005 Kashmir earthquake in northern Pakistan. B) Regional tectonic map of the westernmost part of the frontal Himalaya. Solid black lines are major tectonic lines. Red lines show active faults. The 2005 surface rupture along BBF is denoted by aligned red circles. 6

Figure 2-2. Geology in and around the epicentral area of the 2005 Kashmir earthquake. Trace of the 2005 surface rupture is also shown by red lines with teeth on the up thrown side (Kaneda et al., 2008). 7

Figure 3-1 Flowchart of Methodology showing basic steps for estimating co-seismic ground deformation 14

Figure 3-2 Methodological parameters of COSI-Corr technique used to get the different correlated images (results) 16

Figure 4-1 Sub-pixel correlation of optical images result showing horizontal displacement values in North-South direction 23

Figure 4-2 Vector field map, from a correlation image, showing displacement directions and magnitudes in the form of vectors....24

Figure 4-3 Displacement measured along the fault at a specified location 25

Figure 4-4 A displacement image after making the sub-pixel correlation of pre- and post-earthquake ASTER images 25

Figure 4-5 Average resultant displacement of defined intervals for different Options of selecting DEM....27

Figure 4-6 Vector Field comparisons of displacement for different-date-DEMs used to orthorectify the images....28

Figure 4-7. Average resultant displacement of different intervals for resampling methods....30

Figure 4-8. Rose diagrams showing displacement directions for three kernel sizes (25, 31, 37) of Sinc resampling method....31

Figure 4-9. Mean and standard deviation of North-South and East-West components of displacement for correlation methods....32

Figure 4-10. Rose diagrams showing the displacement direction distribution for window sizes of Frequential correlation method....34

Figure 4-11. Average angle (direction of displacement) of different intervals for window sizes of Frequential correlation method....34

Figure 4-12. Mean and standard deviation, both N-S and E-W displacement components, for different step sizes of Frequential correlation method....35

Figure 4-13. Histograms of displacement in North-South direction for different Threshold values of Frequential correlation method....36

Figure 4-14. Histograms of displacement in East-West direction for different Threshold values of Frequential correlation method 37

Figure 4-15. Displacement measurements along the fault at selected locations using different options of selecting DEMs 38

Figure 4-16. Displacement measurement along the fault at selected locations using different window sizes for Sinc 25 resampling method 39

Figure 4-17. Displacement measurements along the fault at selected locations for two pairs of images bracketing the earthquake 41

Figure 4-18. A) Correlation Image (N-S displacements) B) Shaded Relief Image 43

List of figures in Appendix A

Figure A- 1. Histograms of displacement in North-South direction for different date DEMs used to orthorectify the images....51

Figure A- 2. Histograms of displacement in East-West direction for different date DEMs used to orthorectify the images....51

Figure A- 3. Mean and standard deviation both for North-South and East-West components of displacement for different date DEMs used to orthorectify the images....52

Figure A- 4. Average angle (direction of displacement) of different intervals for different date DEMs used to orthorectify the images....52

Figure A- 5. Rose diagrams showing displacement directions for different DEM options using Sinc25 resampling method and Frequential correlator....53

Figure A- 6. Histograms of displacement in North-South direction for different resampling methods....53

Figure A- 7. Histograms of displacement in East-West direction for different resampling methods....54

Figure A- 8. Mean and standard deviation both for North-South and East-West components of displacement for resampling methods....54

Figure A- 9. Scatter plot for comparison of resultant displacement for Sinc 25 & Bilinear resampling methods....55

Figure A- 10. Average angle (direction of displacement) of different intervals for resampling methods....55

Figure A- 11. Vector Field comparisons of displacement for resampling methods....56

Figure A- 12. Rose diagrams showing displacement directions for three resampling methods....57

Figure A- 13. Average angle (direction of displacement) at defined different intervals for resampling methods....57

Figure A- 14. Histograms of displacement in North-South direction for kernel sizes of Sinc resampling method....58

Figure A- 15. Histograms of displacement in East-West direction for kernel sizes of Sinc resampling method....58

Figure A- 16. Average resultant displacement of different kernel sizes of Sinc resampling method 59

Figure A- 17. Mean and standard deviation both for North-South and East-West components of displacement for kernel sizes of Sinc resampling method....59

Figure A- 18. Vector Field comparisons of displacement for Kernel Size of Sinc resampling method....60

Figure A- 19. Histograms of displacement in North-South direction for different correlation methods....61

Figure A- 20. Histograms of displacement in East-West direction for different correlation methods 61
Figure A- 21. Average resultant displacement of different intervals for correlation methods using Bilinear resampling method 62
Figure A- 22. Average resultant displacement of different intervals for correlation methods using Sinc25 resampling method 62
Figure A- 23. Vector Field comparisons of displacement for correlation methods 63
Figure A- 24. Average angle (direction of displacement) of different intervals for correlation methods using Bilinear resampling method 64
Figure A- 25. Average angle (direction of displacement) of different intervals for correlation methods using Sinc25 resampling method 64
Figure A- 26. Histograms of displacement in North-South direction for different window sizes of Frequential correlation method 65
Figure A- 27. Histograms of displacement in East-West direction for different window sizes of Frequential correlation method 65
Figure A- 28. Average resultant displacement of different intervals for window sizes of Frequential correlation method 66
Figure A- 29. Mean and standard deviation both for North-South and East-West components of displacement for window sizes of Frequential correlation method 66
Figure A- 30. Vector Field comparisons of displacement for window sizes of Frequential correlation method 67
Figure A- 31. Histograms of displacement in North-South direction for different step sizes of Frequential correlation method 68
Figure A- 32. Histograms of displacement in East-West direction for different step sizes of Frequential correlation method 68
Figure A- 33. Average resultant displacement of different intervals for step sizes of Frequential correlation method 69
Figure A- 34. Vector Field comparisons of displacement for step sizes of Frequential correlation method 70
Figure A- 35. Average angle (direction of displacement) of different intervals for Step sizes of Frequential correlation method 71
Figure A- 36. Rose diagrams showing displacement directions for different step sizes of Sinc resampling method 71
Figure A- 37. Average resultant displacement of different intervals for Threshold of Frequential correlation method 72
Figure A- 38. Mean and standard deviation both for North-South and East-West components of displacement for Threshold of Frequential correlation method 72

Figure A- 39. Vector Field comparisons of displacement for Threshold of Frequential correlation engine using Bilinear resampling method....73

Figure A- 40. Vector Field comparisons of displacement for Threshold of Frequential correlation engine using Sinc25 resampling method....74

Figure A- 41. Average angle (direction of displacement) of different intervals for Threshold of Frequential correlation method....75

Figure A- 42. Rose diagrams showing displacement directions for different threshold values using Sinc25 and Bilinear resampling methods....75

Figure A- 43. Displacement measurement along the fault at selected locations using different resampling methods....76

Figure A- 44. Displacement measurement along the fault at selected locations using different kernel sizes of Sinc resampling method....76

Figure A- 45. Displacement measurement along the fault at selected locations using different Correlators....77

Figure A- 46. Displacement measurement along the fault at selected locations using different window sizes for Bilinear and Bicubic resampling methods....77

Figure A- 47. Displacement measurement along the fault at selected locations using different step sizes....78

Figure A- 48. Displacement measurement along the fault at selected locations using different threshold values....78

Figure A- 49. Correlation image of 2nd pair of image bracketing the earthquake....79

Figure A- 50. Histograms of displacement in North-South direction for two pairs of images bracketing the earthquake....79

Figure A- 51. Histograms of displacement in East-West direction for two pairs of images bracketing the earthquake....80

Figure A- 52. Average resultant displacement of different intervals for two pairs of images bracketing the earthquake....80

Figure A- 53. Mean and standard deviation both for North-South and East-West components of displacement for two pairs of images bracketing the earthquake....81

Figure A- 54. Average angle (direction of displacement) of different intervals and their respective rose diagrams for two pairs of images bracketing the earthquake....81

Figure A- 55. Vector Field comparison of displacement for two pairs of images....82

List of tables

Table 3-1. Provided ASTER imagery description 20
Table 4-1 The quantification of results based on visual comparison and interpretation of results 26

1. Introduction

1.1. Background

Tectonic activity plays a major role in developing the landforms of an area. Different geological/surface processes or phenomena are the direct manifestation of the subsurface forces of dynamic earth. Geological structures have promising importance for the understanding of variety of problems related to physical processes. Many applications, like earth resource exploration, hazards due to earthquakes, volcanoes, landslides, flooding and engineering infrastructures, involve both the qualitative and quantitative assessment/evaluation/analysis of geological structures.

Among all the geological structures identification of active faults bears significant importance for researchers in recognizing the seismic potential and assessing their associated seismic hazards. It is necessary to know the accurate locations and geometry of active faults for proper seismic hazard estimation. The available Remote Sensing techniques, after adequate processing, have a great potential for detecting the location of active faults with reasonable accuracy.

On October 8th, 2005 a powerful earthquake of M_w 7.6 magnitude hit the Northern areas and Azad Kashmir region of Pakistan causing loss of about 80,000 lives and severe damage to the infrastructure of the area. The area is marked with high seismic activity since it lies in the region where two major tectonic plates, namely Indian tectonic plate and Eurasian tectonic plate, collide past each other. The earthquake produced the thrust surface rupture which is rarely produced by the earthquakes in past. This surface rupture extended for seventy-five (75) kilometres. and is the result of an abrupt movement along a shallow fault (Avouac et al., 2006). Most of the surface rupture follows the pre-existing traces of several active faults or fault segments, collectively called the Balakot–Bagh fault (BBF). The NW trending ground fractures occurred largely in the hanging wall zone of the south-eastern extension of the earthquake causative BBF fault (Kaneda et al., 2008).Thus the Kashmir earthquake provides a unique opportunity for the researchers to study earthquake mechanism in a complex geological settings.

1.2. Problem Definition

Surface ruptures as a result of major destructive earthquakes produce a large number of geomorphic features. Thrust type surface ruptures, as produced by the Kashmir earthquake, are much less common than the strike-slip or normal ones. Detailed and accurate mapping of co-seismic surface rupture provides key information to understand the earthquake mechanism and to study the tectonic geomorphic features. (Rubin, 1996).

Remote sensing techniques are now widely used in various earth observation studies due to its effective results and time saving methodologies. Satellite InSAR imaging is capable of measuring earthquake-induced ground deformation with sub-centimeter accuracy (Pavez et al., 2006). However, its applicability for problem solving like ground deformation estimation may require deep knowledge regarding image acquisition, processing and interpretation. A big disadvantage of InSAR technique, in

measuring ground deformation associated with active faults is the loss of accuracy near the fault due to loss of coherence of radar signals. At this point a newly developed technique of sub-pixel correlation of optical images (from push broom sensors) before and after the seismic event can greatly help for the measurement of ground deformation near faults (or fault zone). This technique may be very helpful for the early assessment of damages caused by an earthquake. The sub-pixel correlation of optical images technique measures horizontal displacement component in E-W and N-S direction, and its results are more accurate at shorter wavelength (Avouac et al., 2006). Where as the InSAR provide results in measuring the vertical component of the displacement. Both techniques can complement the information in order to have a complete characterization of faults.

The mapping of 2005 Kashmir earthquake surface rupture along the fault is not straightforward due to the mountainous terrain and massive landslides close to the fault trace. Balakot–Bagh Fault (BBF); which is termed as the causative fault of the 2005 Kashmir earthquake, is subdivided into several faults or fault segments with different geological, geomorphological, and geometrical characteristics.

Present study "Evaluation of Optical Images Sub-Pixel Correlation for Estimating Ground Deformation" uses the newly developed COSI-Corr (Co-Registration of Optically Sensed Images and Correlation) software technique for estimating ground deformation. There is need to evaluate this newly developed methodology for its wider use in solution to Earth Science related problems like change (caused due to different dynamic processes of the Earth) detection. Specifically the study is aimed at assessing the technique's performance and functionality in terms of its applicability, sensitivity, repeatability and robustness for terrain change detection particularly for mapping surface rupture and displacement along the fault. After completing the study it will give an assessment of the usefulness of the technique for solving the problems associated with conventional ways and other techniques for measuring ground deformation along the fault. If the assessment goes in favour of the technique, it will give a confidence for its quick applicability to earthquake-induced deformation along fault(s) which would assist in estimating the early damages as soon as the imagery is available. Also the extracted information would be used in characterizing different geological faults to understand their mechanics in relation to the geological frame work of the area.

1.3. Main Objective

To assess the sensitivity, repeatability, robustness and applicability of the newly developed sub-pixel correlation technique "Co-Registration of Optically Sensed Images and Correlation (COSI-Corr)" for measuring coseismic ground deformation.

1.3.1. Sub Objectives

1. Sensitivity analysis by comparison of results with the change of different methodological parameters to check the robustness of the COSI-Corr technique.
2. Testing the technique for repeatability using different-date data set of the same area.
3. Evaluate applicability of the technique for detecting and mapping surface deformation for the study area.
4. Characterizing the fault rupture detected by sub-pixel correlation of multi-date ASTER images bracketing the earthquake using best parameters of the technique.

1.4. Research Questions

1. How are the different parameters of the adopted methodology sensitive in measuring displacement along an active fault?
2. Are the results affected when the sub-pixel correlation process is repeated using different pre-earthquake remote sensing dataset?
3. Does the technique prove to be robust after sensitivity and repeatability analysis?
4. Is the technique suitably applicable for the purpose of estimating the ground deformation caused by an earthquake?
5. How does the selection of Digital Elevation Models (DEMs) from different dates affect the sub-pixel correlation?
6. How do different features along a fault rupture affect the correlation of images and measurement of displacement?

1.5. Hypothesis

As the study area lies in high seismic hazard zone, there is a continuous accumulation of stress in the subsurface due to two continental plate convergences. This built-up stress is released or is prone to release along active faults in the form of seismic events (earthquakes). Due to deformation caused by release of energy along active faults, surface deformation can act as an identifier for active faults. Since active faults have implications on the development of landscape, geomorphic features, manifesting themselves on the earth surface, bear indications for identifying and characterizing the active faults.

2. Literature Review

2.1. Location of Study Area

The study area is located in the state of Azad Jammu and Kashmir in the Lesser Himalaya of northern Pakistan (Fig. 2.1 A). Most of the terrain is mountainous with the highest peaks exceeding 15,000 feet above sea level, particularly the epicentral area of 2005 Kashmir earthquake is a very rugged mountainous area with deep narrow valleys and relief of 5,000 feet or more and slopes of 45-50 degrees. The region is drained by the Jhelum River and its two tributaries Neelum and Kunhar. Due to Rapid discharge flow of rivers, erosion rate is high, which produces steep lower valley slopes. Muzaffarabad, about 10 Km south west of the epicenter, is the largest city in the region, with a population of about 200,000 and was severely damaged during the 2005 Kashmir earthquake (EERI_Report., 2005), (Jayangondaperumal and Thakur, 2008).

2.2. Geology and Tectonics Settings

The Indian plate is colliding with the Eurasian plate at geologic and geodetic convergence rates of 30–50 mm/year. Himalayan mountain ranges have been developed by the tectonic movement of the two colliding plates (Figure 2.1B) and still continue to uplift the mountain ranges. (Durrani et al., 2005). In Pakistan Himalayan arc abruptly changes its strike from west- northwest to east-west, to form the Hazara arc (Fig. 2.1 B). The Salt Range thrust (SRT), a local name to the Main Frontal Thrust (MFT), forms the southern margin of the Hazara arc.

As shown in Figure 2.2 the region encloses the Hazara–Kashmir Syntaxis (HKS), which is formed due the bend of Tertiary strata along the Main Boundary Thrust (MBT). (Kazmi and Qasim Jan, 1997). Main Boundary Thrust (MBT) separates the Sub-Himalayan (Miocene and underlying Precambrian) rocks from Lesser-Himalayan (Precambrian) rocks. The epicenter of the 2005 Kashmir earthquake lies within the core of the syntaxial (HKS) bend which is a part of Indus Kohistan Seismic Zone (IKSZ) (Kaneda et al., 2008). The Indus Kohistan Seismic Zone (IKSZ) is characterized by a step in topography between the Lesser and the High Himalayas, Known as a ramp in the Main Himalayan Thrust (MHT) decollement. This abrupt rise in topography is recognized across the IKSZ also (Jayangondaperumal and Thakur, 2008).

After analyzing ASTER images, (Avouac et al., 2006) estimated a 75 km length of the rupture zone that apparently reactivated the Muzaffarabad–Tanda faults and is now collectively called the Balakot–Bagh Fault (BBF) (Kaneda et al., 2008). The presumed fault trace is shown in Figure 2.1 B. The length of the rupture is reported by Harvard Seismology to be about 90 km (different as given by (Avouac et al., 2006)). The fault plane dips about 37 degrees and the mechanism is mostly thrust. The average slip is between 2-4 meters, confirmed from several sources (COMET, Harvard, (Bilham and Ambraseys, 2004)).

The Sub-Himalaya in the north of MFT (or SRT) is bounded by Main Boundary Thrust (MBT), which is mainly composed of folded and faulted sedimentary rocks of Mesozoic and Tertiary age. (Kaneda et al., 2008). In river valleys, the basement rocks are sedimentary and metamorphic and overlain by coarse fluvio-glacial gravels (up to boulder size) with very few fines (sand, silt and clay) of Quaternary age.(Dellow et al., 2006).

Figure 2.2 shows Hazara Kashmir Syntaxis contains mostly Murree Formation, including red beds (north of Muzaffarabad) of slaty cleavage (Bossart et al., 1988). Northwest of Muzaffarabad, the sinuous Muzaffarabad fault (part of BBF) bifurcates from the MBT to separate the Muzaffarabad formation to the northeast from the Murree formation to the southwest (Kaneda et al., 2008). Murree Formation is overlain by the Kamlial Formation in South of Muzaffarabad, and in further south by younger formations of the Siwalik Group. While from Muzaffarabad to Balakot, the Murree Formation is underlain by marine Palaeocene strata and Precambrian Muzaffarabad Limestone (Calkins et al., 2004).

Near Muzaffarabad the Balakot–Bagh Fault (BBF) dips northeast and separates Precambrian limestone & shale from Miocene Murree Formation, towards southeast BBF is entirely within the Murree Formation or forms contact between Murree and Kamlial formations (Figure 2.2). Concentration of large landslides and damages were on its hanging-wall side close to the fault.

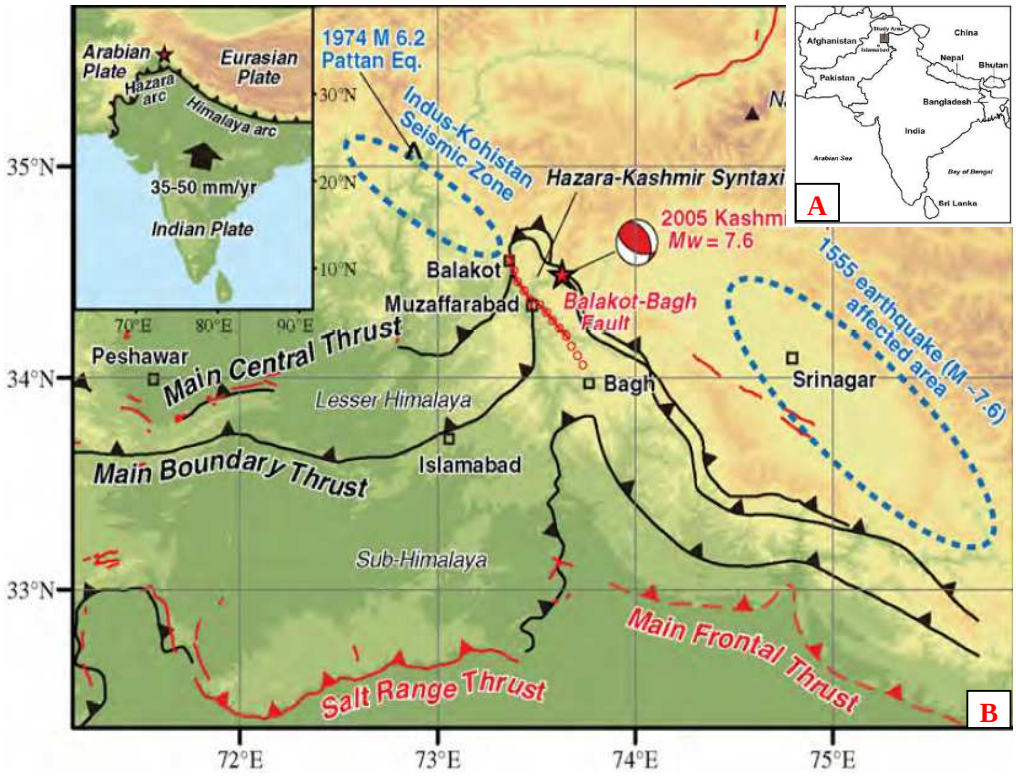

Figure 2-1. A) The study area of the 2005 Kashmir earthquake in northern Pakistan. B) Regional tectonic map of the westernmost part of the frontal Himalaya. Solid black lines are major tectonic lines. Red lines show active faults. The 2005 surface rupture along BBF is denoted by aligned red circles.

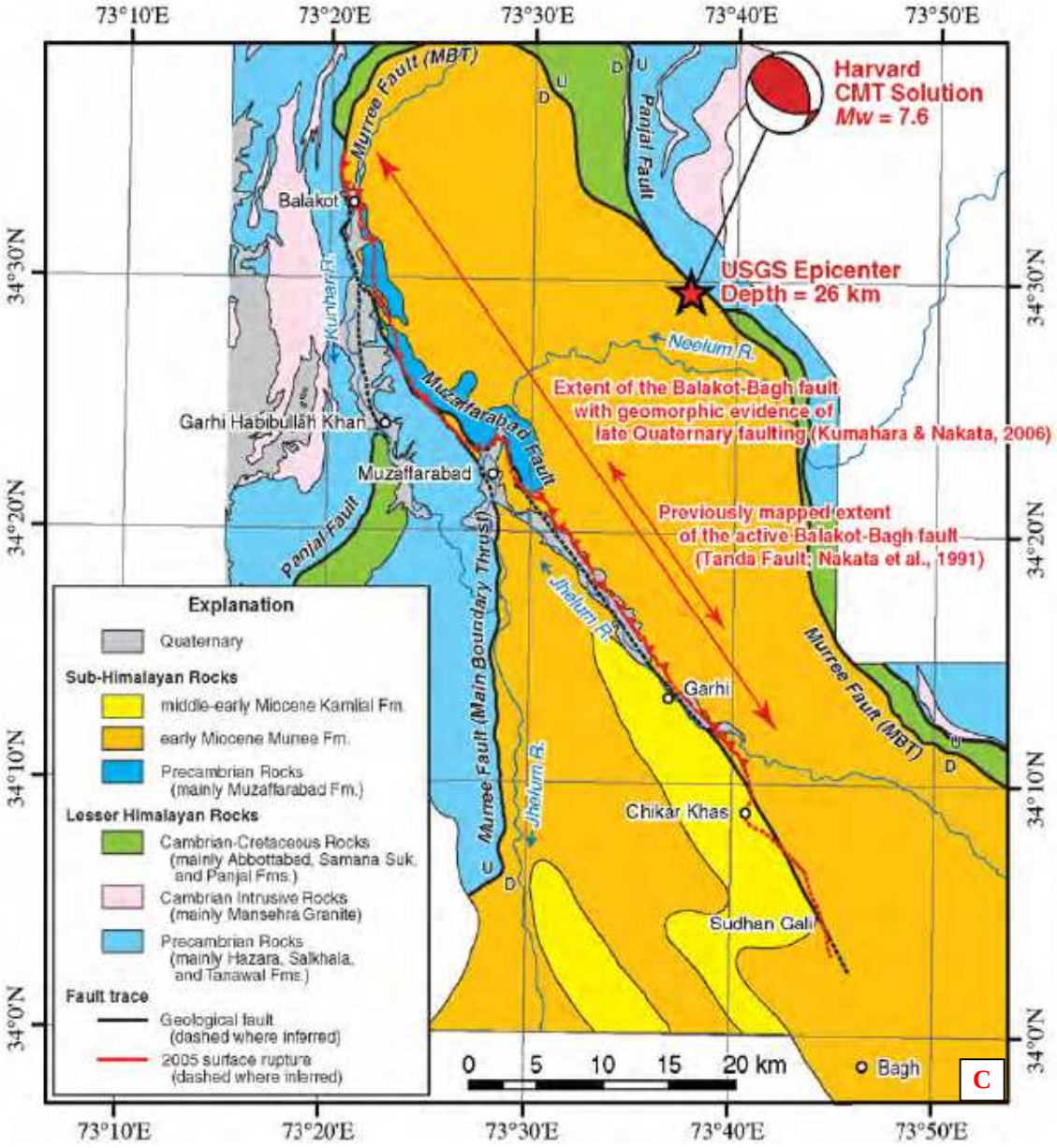

Figure 2-2. Geology in and around the epicentral area of the 2005 Kashmir earthquake. Trace of the 2005 surface rupture is also shown by red lines with teeth on the up thrown side (Kaneda et al., 2008).

2.3. Overview of Remote Sensing Methods

Satellite remote sensing provides a systematic, synoptic framework for advancing scientific knowledge of the Earth as a complex system of geophysical phenomena. During the last two decades use of remote sensing has been increasing for various applications in earth sciences. This geospatial information can be integrated to the scientific knowledge for understanding the physical processes on earth surface.

Remote sensing information acts as a good complement to traditional field and airborne observations for solving problems in seismology, volcanology, geomorphology and hydrology. Today applied research is rapidly transforming due to the use of different types of remote sensing data like for high resolution topography (InSAR, Lidar, digital photgrammetry etc.), hyper-spectral (such as ASTER, MODIS and Hyperion) and active microwave imaging to understand the physical processes of solid earth (Tralli et al., 2005).

Understanding the different environmental processes including natural hazards, specifically measurement of sub-resolution horizontal terrain displacements which are associated with earthquakes, sand dunes migration, coastal processes, glacial motion and pre-eruptive volcanic processes is increasing rapidly (Crippen, 1992). Remote sensing studies have a potential to provide a valuable first step in the identification and analysis of active faulting in deforming regions (Walker, 2006).

Following are some basic remote sensing techniques which can provide crucial information for characterizing faults (tectonic and structures), measuring ground deformation, fault ruptures and fault slip distribution due to earthquakes (particularly).

2.3.1. SAR/InSAR

Synthetic aperture radar (SAR) is a form of radar, active remote sensing technique, in which sophisticated processing of radar data is used to produce a very narrow effective beam. The antenna transmits radiation which is then reflected from the target, as opposed to passive remote sensing where the reflections detected come from ambient illumination. Therefore radar remote sensing does not require natural illumination and images can be taken at night. Radar uses electromagnetic radiation with microwave frequencies; the atmospheric effects do not disturb the radar signals, allowing to acquire remote sensing data in any weather.
Wikipedia (http://en.wikipedia.org/wiki/InSAR)

InSAR method uses two (or more) SAR images, from two SAR antennas with different viewing geometries, for measuring phase differences of two SAR signals. As a result, the terrain displacements associated with faults, fractures and subsidence can be measured to centimetre/millimetre accuracy (Tronin, 2006). Synthetic aperture radar interferometry (InSAR) from Earth-orbiting spacecraft provides a new tool to map global topography and deformation of the Earth's surface (Burgmann et al., 2000). In seismotectonics accurate measurement of ground displacement is very crucial and requires pre and post event satellite images. The availability of satellite imagery has made it easier to get accurate measurement of ground displacement especially in remote/inaccessible areas.

Satellite radar interferometry (InSAR) has become a popular method for the study of earthquakes. There are however some severe limitations to this technique related to the geometry and to the concept of coherence. InSAR is very sensitive to parameters like time interval, the surface type, the climate, the relief type and the sensor wavelength (Kervyn, 2001), also to phase decorrelation, the determination of displacements requires phase unwrapping which is often difficult. Another limitation is that interferograms are saturated when the gradient of the displacement exceeds half a fringe per pixel and therefore do not give accurate measurements near faults or any other complex geological settings (Michel et al., 1999).

Beside these there some technical limitations, such as relative variations in the radar's trajectory or variations in its frequency standard (Massonnet and Feigl, 1998). Availability of SAR images may also be the big issue compare to optical remote sensing data. InSAR results are also degraded due to dense vegetation like in tropical and subtropical areas in measuring the surface deformation. Despite all, the technique (InSAR) is still a useful high-resolution tool for monitoring the different types of crustal deformation (Chung-Pai Chang et al., year missing).

2.3.2. Optical Image Correlation

Optical remote sensing can also be helpful in monitoring the terrain changes using image processing algorithms that measure apparent offsets in the geographic locations of corresponding pixels from two (or more) different dates images of the same portion of the Earth's surface. Pixel offsets of two images are represented in the form of vectors whose orientations indicate the direction of terrain displacement and whose lengths denote the magnitude of that displacement. Theoretically, this can be accomplished using different mathematical approaches:

i. Imageodesy using cross-correlation (Crippen and Blom, 1991)
ii. Wavelet analysis (Strang et al., 1997).
iii. Fourier analysis (Van Puymbroeck et al., 2000)
iv. Co-Registration of Optically Sensed Images and Correlation (COSI-Corr) (Leprince et al., 2007)

Imageodecy

The concept of "imageodesy" was first developed by (Crippen and Blom, 1991). This determines the pixel offsets statistically between two time- separated images. The basic assumption is that pixel offset measurement errors are normally distributed throughout the image, mean and standard deviation of the probability density function can be defined by this large number of measurements. In this way pixel offset vectors are determined through the comparison of pixels in pre-to-post-event image.
The imageodesy technique is based on normalised-cross correlation and phase correlation for measuring horizontal terrain shift at sub-pixel accuracy, thus it is a powerful tool for monitoring surface changes (e.g. due to earthquake). Although imageodesy is capable of detecting changes at sub-pixel accuracy and is robust to environment conditions, it demands intensive data processing computing, which might be the major limitation for its wider use (Liu and Ma).

Wavelet analysis

The use of wavelet analysis to do change detection can use boxcar functions to approximate pixel boundaries, which can result in better approximation of pixel shifts than the sine and cosine expansions used in Fourier analysis (Strang et al., 1997). However use of this technique is limited to well define fault scarps and its results are not good in complex geological settings (Cara, 2004).

Fourier analysis

(Van Puymbroeck et al., 2000) applied Fourier analysis to measure pixel offsets. By taking the Fourier transform of an image, it can be separated into a set of spatial frequency components. The analysis in the frequency domain examines the phase difference between the varying frequency components of the two images. In the spatial domain, this difference represents the sum of apparent and true pixel offsets

Co-Registration of Optically Sensed Images and Correlation (COSI Corr)

In the present study a newly developed technique, implemented in a software package Co-Registration of Optically Sensed Images and Correlation (COSI-Corr), is used. It measures the horizontal ground deformation, surface ruptures and co-seismic offsets from optical images in the Fourier domain.

InSAR (interferometric synthetic aperture radar), geodetic and field surveys are common techniques to measure coseismic deformation. However near the faults or fault zones having complex surface ruptures and cracks these techniques do not provide detailed and accurate results. The distribution of slip across a fault zone and its along-strike variability is very critical for understanding the earthquake dynamics and the damaging near-field seismic waves, and might be best estimated from correlating optical images instead of InSAR or field techniques (Avouac et al., 2006).

Optical images correlation can give valuable information that can complement InSAR measurements and field observations for better estimation of displacements at Earth's surface. Also this technique provides the two components (east-west and north-south) of the horizontal displacement field and it is more robust against de-correlation (Leprince et al., 2007).

Surface ruptures are generally produced by large earthquakes, which may provide important source of information for understanding the earthquake mechanics in complement to geodetic and seismological measurements. Conventional field measurements suffer from a numerous limitations which may includes: fault ruptures have a complex geometry; fault slip can generally be measured only on a limited number of locations where clear offset points are observable such as roads or terrace risers. The fault-perpendicular component is generally not measurable in the field. Here optical satellite imagery comes to solve these limitations. Basic principle of the approach is that surface deformation can be measured by comparing pre and post earthquake images (Van Puymbroeck et al., 2000).

Optical images correlation has some considerations regarding the resolution of satellite images (e.g., 2.5–10m for SPOT, 15m for ASTER), sometimes insufficient to measure subtle ground deformations, especially where fault displacement is less than 1m (Leprince et al., 2007), which is typically the case for earthquakes with magnitude less than Mw 7. However this technique also works well with high resolution satellite imagery (e.g. QuickBird) as well as with aerial photographs (Leprince et al., 2007).

2.3.3. Aerial Photography

Aerial photography has been a part of research in different earth science applications for decades. Main areas of its use have been stratigrapy, geomorphology, structural geology (faults and folds), ground water and mineralogy.

Although aerial photography has produced good results since its use, however it suffers some limitations such as: high image cost, less area coverage, subjective visual interpretation, long updating time and image geometry variations due aircraft control. Despite these limitations, aerial photography is still a useful tool which can complement useful information to other remote sensing techniques (Ouattara et al., 2004).

As satellite imagery is relatively recent technique as compare to aerial photography, aerial photos available for past earthquakes are of significant importance to get sub-pixel correlation results of surface rupture produced due to earthquakes. There is still a wide scope of the use of aerial photography having sub-metric ground resolution in measuring ground deformation due to earthquakes. However efficiency of this technique depends on the quality of correlation and of co-registration. (Ayoub et al., 2006)

2.3.4. Digital Elevation Model (DEM)

The combined use of remotely sensed data and DEMs can be useful for investigating the morphology of an active tectonic region. DEMs derived from high-resolution imagery will improve our understanding of earthquake surface ruptures in complex tectonic settings. Remote sensing techniques (e.g. DEMs) have potential for picking up displaced geomorphic surfaces, river terraces, drainage channels, alluvial fans, lineaments and topographic ridges which are potential signatures of the appearance of active tectonics (Philip, 2007).

The combination of DEM and 3D cloud points coming from Lidar technologies combined with field analysis is very promising. The main structural features that contribute to rock slope instabilities can be recognized in the analysis of the DEM. The increasing availability of DEMs and their increasing precision will aid in identifying and characterizing geological structures at relatively low cost (Jaboyedoff et al., 2009).

3. Methods and Materials

3.1. Introduction

Terrain modelling through Digital Elevation Models (DEMs) requires knowledge of earth science, mathematics, engineering, computer science and Geographic Information Systems (GIS) for accurate results (Grohmann et al., 2007). Different surface indications like the displaced geomorphic surfaces, lineaments, river terraces, alluvial fans, drainage channels and topographic ridges provide good clues for detecting locations of active faults (Nakata, 1972). Both optical and radar images have potential for extracting lineaments (may be interpreted as faults and joints) and can be characterized by determining strikes and dips (Koike et al., 1998).

The present study "Evaluation of Optical Images Sub-Pixel Correlation for Estimating Ground Deformation" exploits the newly developed technique, embedded in a software package "Co-Registration of Optically Sensed Images and Correlation (COSI-Corr)" (Leprince et al., 2007) for its applicability, sensitivity and robustness in estimating coseismic deformation and fault rupture.

3.2. Overview of Methodology

Sub-Pixel correlation of pre and post earthquake optical imagery gives key information for the investigation of coseismic ground deformation and fault rupture geometry (Crippen and Blom, 1991). However, the uncertainties in the imaging systems and platform attitudes affect the results of correlated images. Therefore co-registration of pre and post earthquake images is a critical step in getting better correlation results (Townshend et al., 1992). The COSI-Corr technique models these uncertainties and limitations due to orbital behaviour of imaging system. Presently the technique is applicable to pushbroom satellite images (e.g. SPOT and ASTER) because in pushbroom imaging, orbital variations of sensors are relatively far less. Images are acquired by the forward motion of the spacecraft keeping optical parts of the sensor system fixed. This makes the correction of viewing parameters in COSI-Corr easier by linearly compensating uncertainties due to attitude drifts and sensor orientation during image acquisition (Leprince et al., 2007).

Automatic and precise orthorectification, co-registration, and sub-pixel correlation of satellite images using COSI-Corr technique gives an opportunity to characterize a fault by estimating the coseismic displacements and surface ruptures (Leprince et al., 2007). The technique does not require external information like GCPs (Ground Control Points) by GPS field campaigns, as procedure is based on topographic knowledge and ancillary data provided with the satellite sensor's platform. Estimating the ground deformation along fault by correlation of optical images depends on the quality of orthorectified images after their precise coregistration.

The processing chain, for adopted methodology, is composed of fundamental steps shown in flowchart below (figure. 3.1)

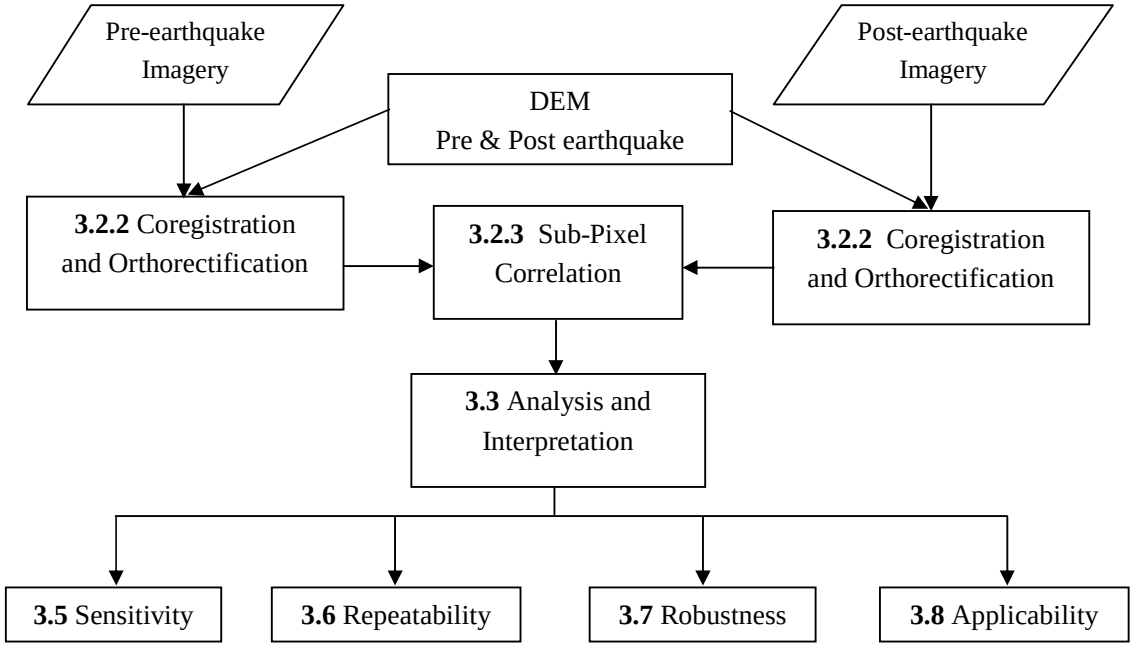

Figure 3-1 Flowchart of Methodology showing basic steps for estimating co-seismic ground deformation

3.2.1. Preprocessing

ASTER Imagery: The imagery level 1A is required for carrying out sub-pixel correlation with COSI-Corr. Radiance of ASTER imagery is automatically done when ASTER imagery is opened with ENVI versions 4.2 and newer. The ASTER .hdf file format is expected as input for COSI-Corr. ASTER band VNIR 3N (nadir viewing) is used (as recommended) for the estimation of ground deformation, however any other band (VNIR, SWIR, TIR) can also be used.

3.2.2. Co-registration

Difficulties in accurate co-registering of satellite images may be due to changing attitude of the spacecraft, digital elevation model (DEM) errors, and inaccurate resampling (Leprince et al., 2007). A UTM (Universal Transfer Mercator) ground projection is used to project the images on common reference system independent of sensor's viewing geometry for coregistration of images.

For precise and accurate co-registration of images, the following orthorectification parameters were determined.

1. **Ancillary File**

   The ancillary file contains the positions, attitudes, and look directions of the satellite while acquiring the image, along with number of lines and columns, nominal ground resolution, and solar azimuth and elevation. This file was prepared from the given ASTER .hdf file for nadir looking VNIR (3N) band using COSI-Corr software.

2. Selection of GCPs

The GCPs generation was made independent of any external data (e.g. GPS or existing map) by using a digital elevation model (DEM) to get pre-earthquake orthoimage and then this image was used as reference to orthorectify post-earthquake image.

More than 30 tie points were generated automatically both from raw and reference images. Points with higher RMS errors were deleted and final points were saved in a text file. In the next step tie points were converted to GCPs and saved as a separate text file. Finally GCPs were optimized through Statistical correlator (as recommended when DEM is used as reference) and Sinc resampling method in order to get better co-registration and ultimately correlation.

3. Orthorectification/Resampling

Inverse mapping matrices were calculated using the optimized GCPs. The resampling method reconstructs the image according to the mapping matrices by selecting one of the available three resampling methods: Bilinear, Bicubic and Sinus Cardinal (Sinc). Bilinear and Bicubic do not accept parameters and are much faster than the Sinc resampling method. However Sinc resampling method is more precise than other two, it accepts parameters like kernel size values (odd). Recommendation is to use the Sinc kernel for an improved resampling quality and ultimate correlation.

The coregistered orthorectified image is produced with an accuracy of 1/50 of the image nominal resolution after accounting for satellite attitude variations without adding any aliasing (Leprince et al., 2007). Similarly the post earthquake is coregistered and orthorectified by using orthorectified pre-earthquake image as reference by following the above mentioned procedure.

Other methodological parameters, summarized in figure 3.2, were used to get the orthorectified images and later for correlation.

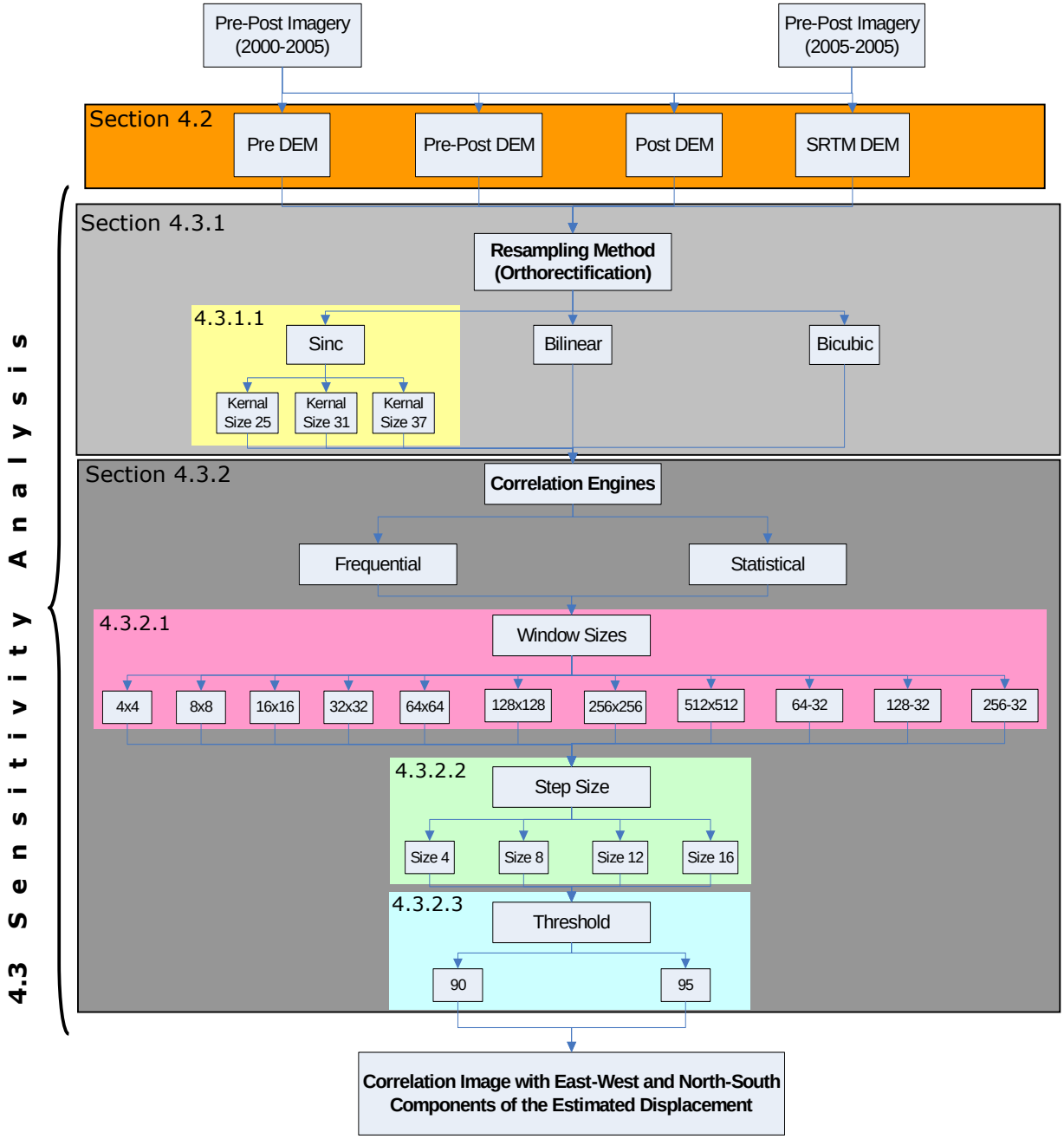

Figure 3-2 Methodological parameters of COSI-Corr technique used to get the different correlated images (results)

3.2.3. Correlation

Sub-Pixel correlation of two orthorectified pre- and post-earthquake optical images gives horizontal ground displacements through an iterative, unbiased process of estimating phase plane in the Fourier domain. This process leads to two correlation images, each representing one of the horizontal ground displacement components (East-West and North-South) with an accuracy of 1/20 of the pixel size (Leprince et al., 2007).

Currently two correlators are available: Frequential and Statistical. The Frequential correlator is Fourier based and is more accurate than the statistical one. Frequential correlator is preferred for sub-pixel correlation of optical images of good quality, due to its sensitivity to noisy images. On the other hand statistical correlator gives coarser results but is more robust than the Frequential correlator as it maximizes the absolute value of the correlation coefficient. So for noisy optical images statistical correlator is recommended for better results (Leprince et al., 2007).

Different methodological options (as show in Fig. 3.2) were applied to get correlated images which later on were compared to check the sensitivity & robustness, repeatability and applicability of the COSI-Corr technique for estimating the ground deformation and surface fault rupture. Main parameters for which different tests were applied are: resampling methods (Sinc (with kernel sizes 25, 31, 37), Bilinear and Bicubic) and correlation methods (Frequential and Statistical), with correlation window sizes, step sizes between two correlating widows, and threshold values.

3.2.4. Measuring Displacements

After getting correlated images using different parameters, some enhancement tools were applied to get rid of procedural errors like striping of the images. The maximum net displacement along the fault was measured as about 7.5 m (Kaneda et al., 2008) in the field. Therefore to keep value range -10m to 10m, other values mostly containing outliers and values with weak SNR were filtered out. Some of the filtered values may be produced by decorrelation which is mainly due to landslide, shadowing difference, vegetation change, or clouds. A mask was applied to the correlated image for cutting out the unnecessary image to minimize the effects of decorrelation and other artefacts.

After applying different enhancement tools a final correlated image, with two bands one giving displacement values in East-West direction and second in North-South, was used to measure displacement along the fault. Before measuring the displacement, the fault rupture was mapped and digitized in a vector file. A fault orientation file was prepared using the mapped fault rupture file. COSI-Corr stacking profiles option was used which takes correlated image and fault orientation file as input for measuring displacement along the fault. Different parameters such as: the number of profiles on the fault, profiles length & width (for stacking number of profiles to get average value at single location) and their location on the fault were set after analyzing by taking different options visually and experimentally. Four locations on the fault were selected based on correlation results and according to the literature reviewed. Profiles, from an area of 15x5 Km perpendicular to fault line, were gathered and stacked to get an average displacement automatically through the use of COSI-Corr software. The displacement values, both from East-West and North-South components, at four selected locations were saved as a text (ASCII) file for further analysis and comparisons.

3.2.5. Vector Field

Sub-pixel Correlation of orthorectified pre- and post-earthquake orthorectified optical images results can be represented in the form of vector field maps. Typically a correlated image or a text file (e.g. field observation by GPS) is the input to construct the vector field map. Multiple files can be added for comparison at or around the fault rupture. Display parameters like title, number of vectors, relative vector ratio, color, line thickness and units can be customized. Vector field parameters, only available for correlated image file, like averaging window and step size between two displayed vectors, can be adjusted for better presentation of vector field results.

3.3. Analysis & Interpretation

The operational methodology adopted for this study exploits the different methodological parameters available in COSI-Corr software which are summarized in the flowchart (figure 3.2). By using these parameters and the two sets of given ASTER images along with their respective and SRTM (Shuttle Radar Topography Mission) DEMs, about 80 correlation image results with their East-West and North-South displacement components were obtained. For analysis and interpretation of the results, different products in ENVI, ArcMap and MS Excel software were prepared. Comparisons were made with the use of different date DEMs, for the purpose of evaluating the co-registration, ortho-rectificaion & ultimate correlation through the resampling methods, kernel sizes of Sinc resampling method and correlators with different correlation window sizes, step sizes between two correlating windows, threshold values etc. The DEM selection options are: pre-earthquake image orthorectification using pre DEM (extracted from the respective pre-earthquake imagery) & post earthquake image orthorectification using post DEM (extracted from the respective post earthquake imagery), second option is the use of pre DEM for both pre & post-earthquake images orthorectification and in third option the pre & post earthquake images were orthorectified using post DEM. At end SRTM DEM was use in order to have a comparison with other DEM selecting options.

After getting the correlation results, their statistical information was generated and exported as text files for further analysis and comparisons in MS Excel software. The histograms were prepared for each correlated image separately both for East-West and North-South displacement components. The mean and standard deviation values for each correlated file were arranged separately both for East-West and North-South components in order to get their graphs for comparisons.

Vector field results for each correlated image were also exported as jpeg and text files for further processing in MS Excel software. From exported vector-field text files different calculations were made for getting resultant displacement values and their directions (angles in degrees) from East-West & North-South displacement components. Scatter plots of the resultant displacements and their directional angles for different methodological parameters were prepared separately in order to check their relation (or dependency). For each correlated result, the displacement values were averaged & counted for different defined intervals and then were plotted for comparing the results of using different parameters. The same process was repeated in order to get the comparisons for angles (direction of displacement).

Similarly the exported text files of measured displacements at selected locations on the fault rupture were arranged and graphed in MS Excel for analysis and comparisons in order to evaluate the results for different options of using parameters given in the technique.

3.4. Quantification of Results

In order to have a quantitative assessment a very subjective interpretation of the results was made and given in table 4.1. Different weights were assigned after the visual and comparative analysis of the images and graphs. Results were analyzed in the grouping of four categories based on DEMs option, Resampling method, Correlation method and another dataset. For each category results were investigated for seven attributes given as correlation image, histograms mean & Standard deviation, vector field, resultant vector magnitude, direction of displacement, and the displacement measurement. The correlation results were judged based on the amount of decorrelation patches, smoothness or noise level both for E-W and N-S displacement components. Then comparative judgment of their respective histograms and mean & variance was made. The vectors along the detected fault line were investigated in vector fields for their magnitude and direction. The effects of vector magnitude and direction were also taken under consideration besides around the deducted fault. Finally the visual comparisons of the measured displacement values at specified locations were made. For each attribute, a weight between 0 and 1 was assigned according to its performance or quality. These weights were then averaged and scaled in the range of 0 to 1.

3.5. Sensitivity Analysis

Out of the 80 correlation results, about 25 were selected to check the sensitivity of methodological parameters in measuring the horizontal displacement both in East-West and North-South components at selected locations along the earthquake causative Balakot-Bagh Fault (BBF) of 2005 Kashmir earthquake. Comparisons were prepared in Excel graphs and overlay maps in ArcMap to check the response of changing methodological parameters.

3.6. Repeatability

In continuation of evaluation of the technique for sub-pixel correlation of optical images, one of the objectives was met by testing its repeatability using different pair of ASTER images bracketing the earthquake event of the same area. Repeatability of the technique can be checked by applying it with different sensor data of another area for measuring possible ground deformation. Due to non availability of data and time limitation it could not be possible to carry out the test for another area. So the repeatability test was limited to only repeating the correlation process for the same area with different date data sets and then comparing its results with previously calculated results.

3.7. Robustness

Robustness can be defined as the capability of system or technique to remain stable against variations in operating environment. The present study tests the robustness of the technique by checking its applicability, sensitivity and repeatability for different data sets. Results can be varied due to noise in the images, different features like clouds, shadows, atmospheric effects, snow coverage, seasonal variations, different topography, landslides, change in vegetation cover, man-made activities or applying different methodological parameters

3.8. Applicability

The possible application areas of sub-pixel correlation of optical imagery e.g. COSI-Corr are: terrain change detection and estimation caused due to earthquakes, glacier movements, sand dunes migration, volcanic activity, urban growth monitoring, subsidence due different reasons etc. Although this technique is not yet used for all above mentioned applications, in the present study one of the objectives is to check its applicability specifically for estimating the ground deformation induced by an earthquake. After correlating the optical images using different correlating parameters along with other resampling and DEMs options results were prepared in the form of graphs for comparison and analysis.

3.9. Materials

Materials used to accomplish this study are given below.

3.9.1. Satellite Data

ASTER Image and DEMs derived from ASTER images were provided. Three different dates ASTER data, bracketing the seismic event (earthquake), along with their respective DEMs were provided:

i. AST_L1A_0031027200505 52 29_20080731073352_9434.hdf
ii. AST_L1A_0031114200006 06 42_20080731073352_9443.hdf
iii. AST_L1A_0030909200505 52 23_20080910034835_2768.hdf

Process. Level	Acq_date	Acq-time (GMT)	Gen-date	File format
AST_L1A_003	10 27 2005	05 52 29	07 31 2008	.hdf
AST_L1A_003	11 14 2000	06 06 42	07 31 2008	.hdf
AST_L1A_003	09 09 2005	05 52 23	09 10 2008	.hdf

Table 3-1. Provided ASTER imagery description

DEMs

i. Post DEM: DEM extracted from post-earthquake imagery of date November 27, 2000.
ii. Pre DEM: DEM extracted from pre-earthquake imagery of date November 14, 2000.
iii. Pre DEM: DEM extracted from pre-earthquake imagery of date September 09, 2005.
iv. SRTM DEM (Shuttle Radar Topography Mission - DEM).

ASTER Characteristics

The ASTER uses pushbroom sensors which contain linear array of detectors oriented normal to the satellite flight path for image acquisition (Abrams et al., 2002). Three subsystems are integrated in ASTER instrument which are: 15m spatial resolution of visible & near-infrared (VNIR), 30m spatial resolution of shortwave infrared (SWIR) and 90m spatial resolution of thermal infrared (TIR). The VNIR subsystem has two telescopes of focal length 329 mm with solid state focal plane which record data in 60 Km wide strip as one line on the Earth surface. VNIR subsystem of ASTER gives a capability of extracting digital elevation models (DEM) due to the one telescope viewing 27.60 off-nadir and other viewing nadir (straight down) (Abrams et al., 2002). ASTER data, due to low cost,

comparable spatial resolution; particularly ASTER VNIR because of its capability of generating DEMs, has advantages to other sensors' data for terrain change detection.

3.9.2. Software

i. COSI-Cor (Leprince et al., 2007) module embedded in ENVI 4.5 for processing, analyzing and preparing results using provided data.
ii. ArcGIS (ArcMap) version 9.3 for preparing map composition and overlays.
iii. MS Excel for calculations and preparing graphs of results.

4. Results

4.1. Introduction

Sub-pixel correlation of ASTER optical images has been achieved through the described methodology using multi-date data sets, DEMs and different parameters (figure 3.2) given in the COSI-Corr technique. A correlation image gives horizontal displacement values in two bands; band1 is East-West displacement component while band2 describes North-South displacements. After adequate post processing different correlated images were obtained using the above mentioned options. Using these correlated images different products were derived in the form of maps and graphs for their comparisons. Here I will explain some basic figures which are used in comparisons and interpretation of the results.

Correlation image, as described above, gives the horizontal values of displacement. Figure 4.1 is a North-South component of horizontal displacement; positive values show displacement towards the North while negative values give displacement in the South direction.

The figure shows a clear discontinuity due to displacements along the existing fault caused by an earthquake. This discontinuity was traced, showing fault line along which the movement of blocks occurred. The white areas in the image are decorrelation patches due to landslides, shadows, seasonal variations or snow cover changes. Correlation images were exported as text (ASCII) files in order to make the histograms for interpreting and comparing the results. The standard deviations and mean values of for each correlated images were also plotted for the same purpose.

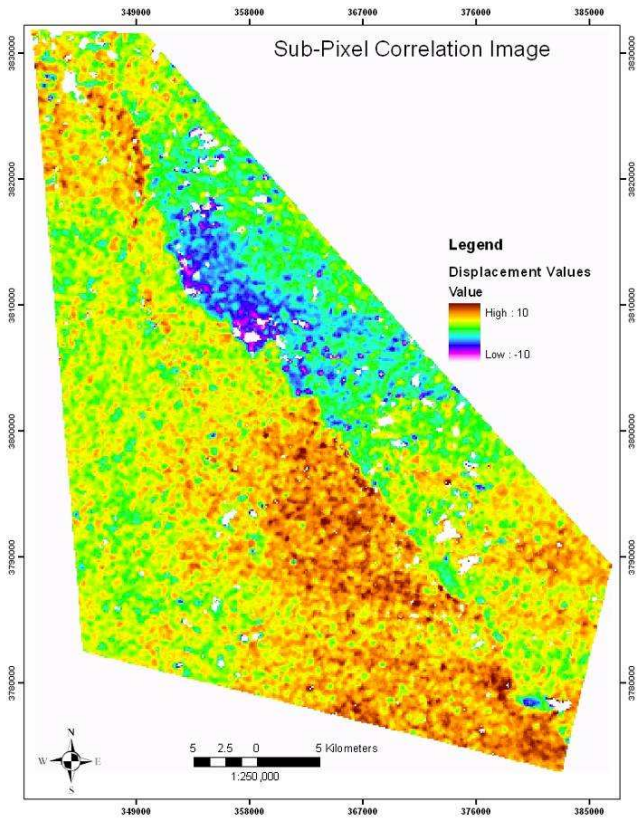

Figure 4-1 Sub-pixel correlation of optical images result showing horizontal displacement values in North-South direction

.

A vector field map was prepared (figure 4.2) from the correlation image using both displacement components. This represents the displacement values in form of vectors. The magnitude of a vector in vector field map is the measurement of displacement and its orientation is the direction of displacement. From the figure we can see the displacements are mostly along the marked fault line showing the relative movement of different blocks. Vector field images were exported as shape files for comparing different results in order to evaluate the performance of the COSI-Corr technique. Vector field images were also exported as text (ASCII) files containing East-West and North-South displacement components then, by using these, the resultant displacements and angles were calculated. The calculated resultant displacements and angles were plotted separately for comparing different results. From the calculated angles rose diagrams were prepared in order to have a comparison of displacement directions for different correlated images.

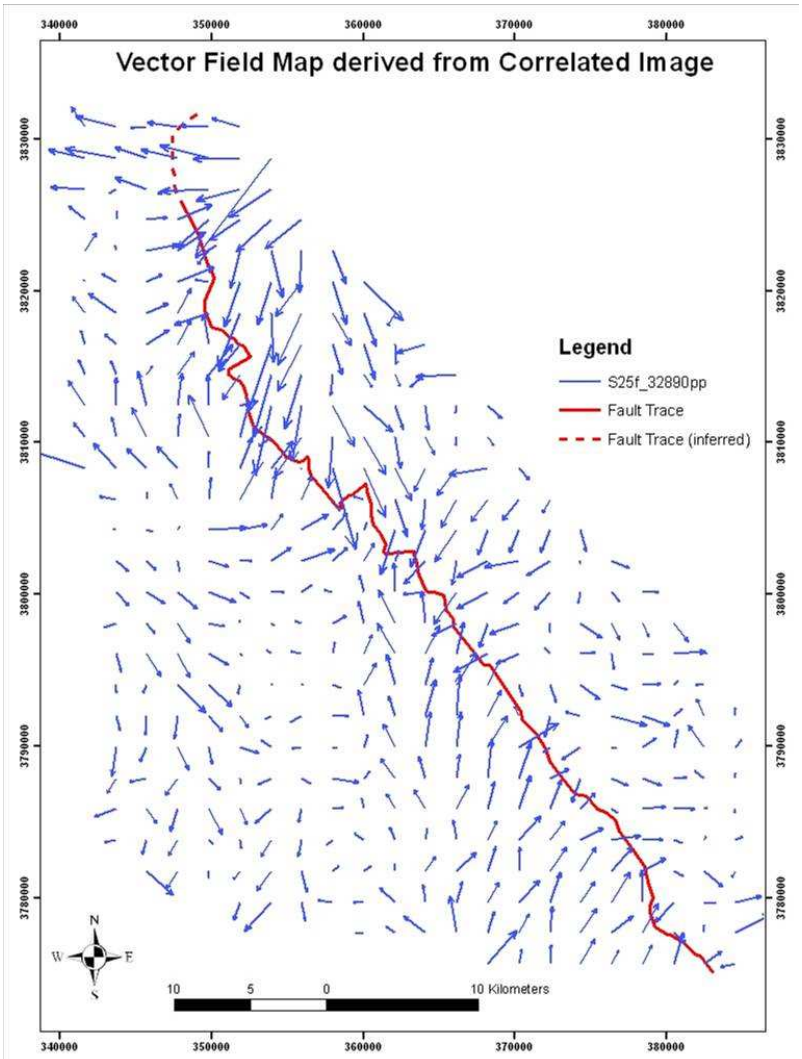

Figure 4-2 Vector field map, from a correlation image, showing displacement directions and magnitudes in the form of vectors

The sub-pixel correlation of pre- and post-earthquake ASTER images provided an image of displacements (shifts) due to earthquake (figure 4.3). Displacement values at four specified locations (blue boxes) on the digitized fault line (red line) were measured (figure 4.3).

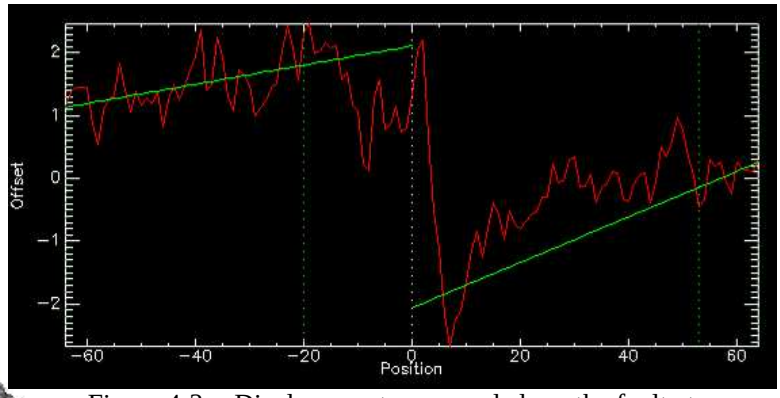

Figure 4-3 Displacement measured along the fault at a specified location

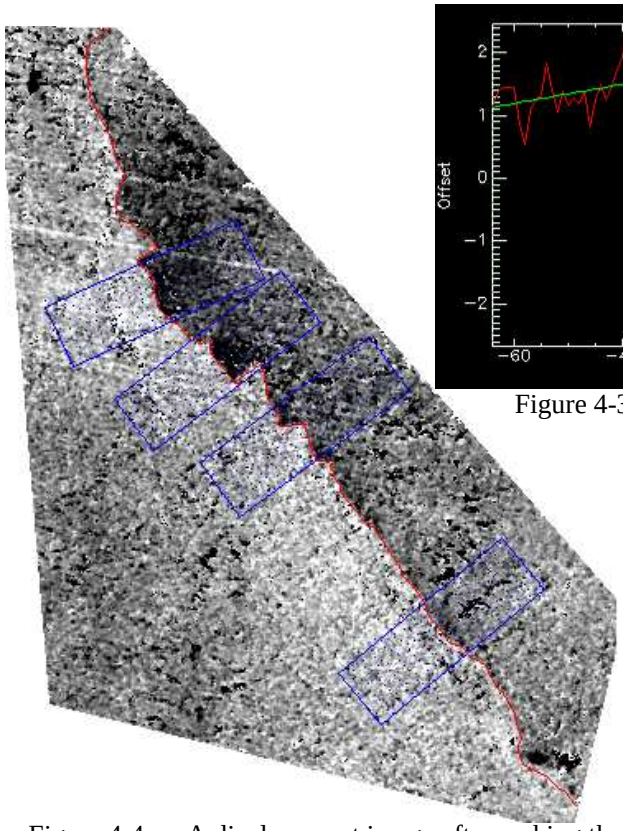

Figure 4-4 A displacement image after making the sub-pixel correlation of pre- and post-earthquake ASTER images

An example of measuring displacement along the fault is shown in the figure 4.4. The displacement measurements at selected locations were exported as text (ASCII) files for each correlated image. These displacement values were plotted for evaluating different results obtained by using different DEM options, resampling methods and correlation methods with their different methodological parameters (all are described in figure 3.2) in estimating the ground displacement.

Quantification of Results

A very subjective quantification of results was carried out after assigning different weights based on the visual comparisons & interpretation of results and the criteria defined in the methodology (Section 3.4). The averaged and scaled results were obtained for the categories like DEM options, resampling methods, correlation methods and displacement measurements are shown in table 4.1. The best values for each category are highlighted showing its performance relative to others. According to the table results, the pre-post DEM option, Sinc 25 resampling method, Frequential correlator with window size 32, step size 8 and threshold value 90 are found to be the best among the results. At the end two different dataset results were compared and found that the first pair gives better results. While doing the comparisons of different correlated images, graphs, vector field maps and the measured displacements, the above mentioned case of best result was taken as a partial reference along with the generic quality or performance of different results and some evidences from the literature.

	DEMs				Res. Methods					Correlator													Image Pairs	
	Pre-Post	Pre	Post	srtm	Sinc			Bili-near	Bic-ubic	Freq:	Stat:	Window Size					Step Size				Threshold		1st	2nd
					25	31	37					4	8	16	32	64	4	8	12	16	90	95		
S25f_32890pp (DEM Options)	**0.69**																							
S25f_32890pre (DEM Options)		0.49																						
S25f_32890post (DEM Options)			0.50																					
S25f_32890srtm (DEM Options)				0.40																				
S25f_32890pp					**0.68**																			
S31f_32890pp (Res. Methods)						0.47																		
S37f_32890pp (Res. Methods)							0.56																	
Bil-f_32890pp (Res. Methods)								0.49																
Bic-f_32890pp (Res. Methods)									0.17															
S25f_32890pp										**0.64**														
S25s_32890pp (Correlator)											0.49													
S25f_4890pp												0.23												
S25f_8890pp (Window Size)													0.23											
S25f_16890pp (Window Size)														0.39										
S25f_32890pp (Window Size)															**0.70**									
S25f_64890pp (Window Size)																0.44								
S25f_32490pp (Step Size)																	0.41							
S25f_32890pp (Step Size)																		**0.66**						
S25f_321290pp (Step Size)																			0.53					
S25f_321690pp (Step Size)																				0.49				
S25f_32890pp (Threshold)																					**0.66**			
S25f_32895pp (Threshold)																						0.54		
S25f_32890pp_img1 (Image 2)																							**0.64**	
S25f_32890pp_img2 (Image 2)																								0.37

Table 4-1 The quantification of results based on visual comparison and interpretation of results

4.2. DEM based Analysis

Digital Elevation Model has important role in orthorectification and coregistration process of pre- and post-earthquake images. There are different DEMs available such as pre-post DEM, pre-DEM, post-DEM and SRTM DEM (description is given in Appendix B and also in figure 3.2). Comparisons of the results were made using different DEM selection options, Sinc25 resampling method with Frequential correlator keeping the window size 32, step size 8 and threshold value 90 as constant.

Figure 4.5 investigates the average displacement for different defined intervals, variations are seen for four DEM options (given above and also in figure 3.2) in measuring the smaller values. The pre-post DEM option gives almost average values in between the other two ASTER DEM options. The SRTM DEM gives higher resultant displacement values. After selecting different DEM options for coregistration of the images, the histograms of correlated images both for E-W and N-S displacement components were compared in figures A-1 & A-2. The visual comparison of the histograms shows that there is no significant difference in N-S component of the displacement. Only pre-DEM option gives low frequency for small displacement values and it is more sensitive in measuring positive higher displacement values. The E-W displacement component results for different DEM options are varying. The post-DEM option gives more measurements for small displacements as compared to the other three options which seem to be more sensitive in calculating the higher measurements.

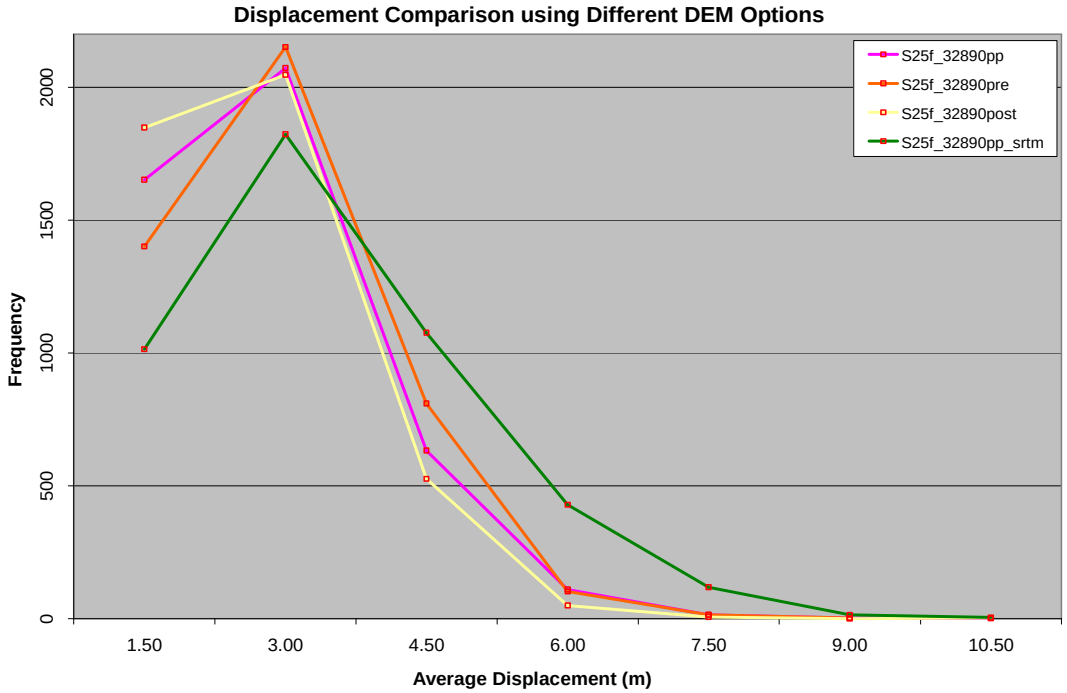

Figure 4-5 Average resultant displacement of defined intervals for different Options of selecting DEM

The vector field comparison (figure 4.6) of three ASTER DEM options differs at different portions of the image. The direction and magnitude of the displacement differs significantly, however around the indicated fault line the attitude of displacement vectors marks the movement of different blocks towards each other above and below the fault line. The post-DEM option gives low magnitude of

resultant vector along the indicated fault line in the lower part of the image. The pre-DEM option also gives low magnitude of resultant vectors in the middle of the image below the fault line.

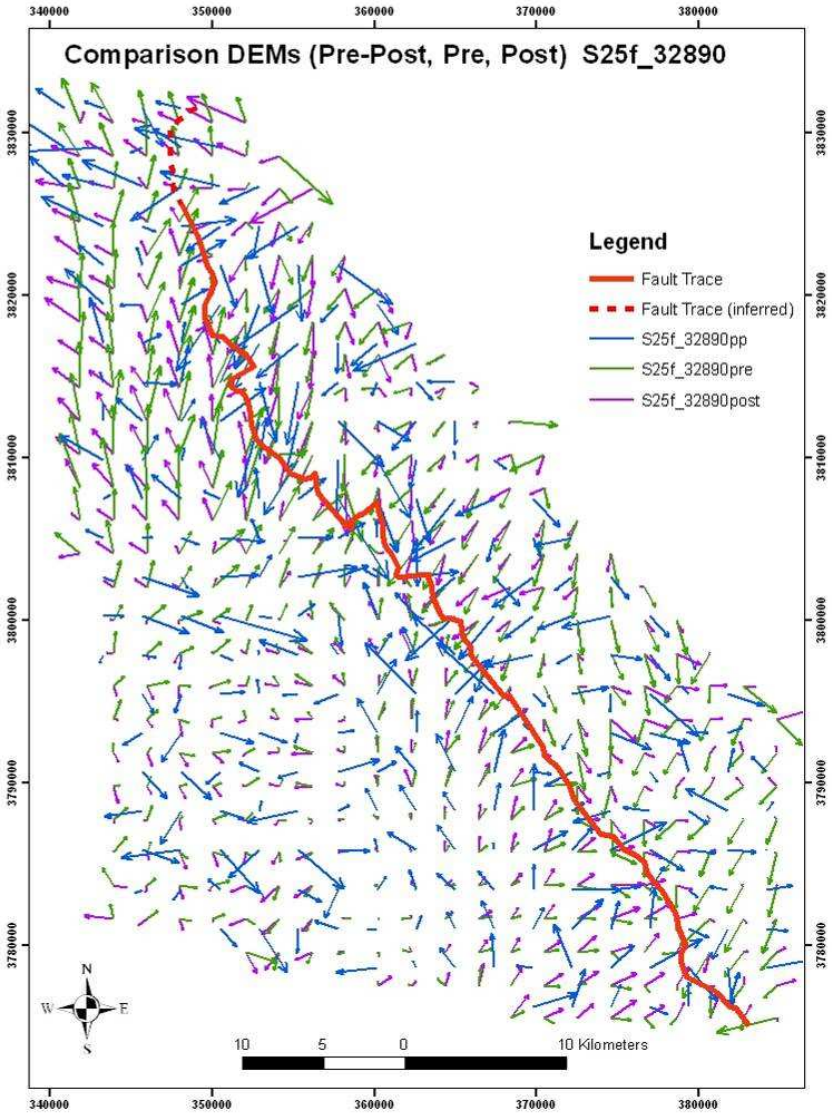

Figure 4-6 Vector Field comparisons of displacement for different-date-DEMs used to orthorectify the images

In figure A-3 the mean values for four DEM options are almost the same, there is minor difference with the use of post DEM option only. The standard deviation of E-W displacement components differs significantly but for N-S displacement component there is minor disparity. Use of pre-DEM option gives more variability in correlation image result for measuring E-W displacement component, the variability is high in N-S displacement component as well; while for SRTM DEM option, variability in measuring the E-W displacement component is the highest.

Results of displacement angle measurements (figure A-4) are quite different for different DEM options and hence are not comparable, as can also be seen in figure A-5 of their respective rose diagrams. Pre-DEM option gives NE-SW direction of displacement, post-DEM gives NW and pre-post-DEM does not give any clear indication of the direction of displacements. The SRTM DEM option provides clear direction of displacement in NW-SE direction.

From the above discussion, conclusion can be made that the use of pre-post DEM is suitable for the purpose of getting correlation results. Logically also the respective pre-DEM for pre-earthquake imagery and post-DEM for post-earthquake imagery will rectify the raw images accordingly. The SRTM DEM option gives different results in E-W displacement component and are not consistent with ASTER derived DEMs.

4.3. Sensitivity Analysis

Sensitivity analysis for the “Evaluation of Optical Imagery Sub-pixel Correlation for Estimating the Ground Deformation” gives an overview of how the change in different methodological parameters affects the change in results. The summary of these parameters are given in figure 3.2 and their comparison along with the interpretation of results are given below.

4.3.1. Resampling Methods

Resampling methods reconstruct the image based on mathematical algorithms. Three resampling methods Sinc, Bilinear & Bicubic are available for orthorectification and coregistration of optical images. To check the sensitivity of resampling methods, comparisons of these were made through vector field diagrams and different graphs while keeping the correlation parameters (Frequential, window size 32, step size 8, threshold 90) constant and using pre-post DEM (pre-DEM for pre-earthquake image and post-DEM for post-earthquake image orthorectification).

Figure 4.7 shows that the average values of resultant displacements for different defined intervals are almost the same for Sinc and Bilinear methods. Bilinear method gives less number of low displacement values than the Sinc but higher displacement values are calculated more in Bilinear method. However Bicubic gives very different results showing comparatively less number of pixels with small displacement and much larger values of the resultant displacements for most of the pixels.

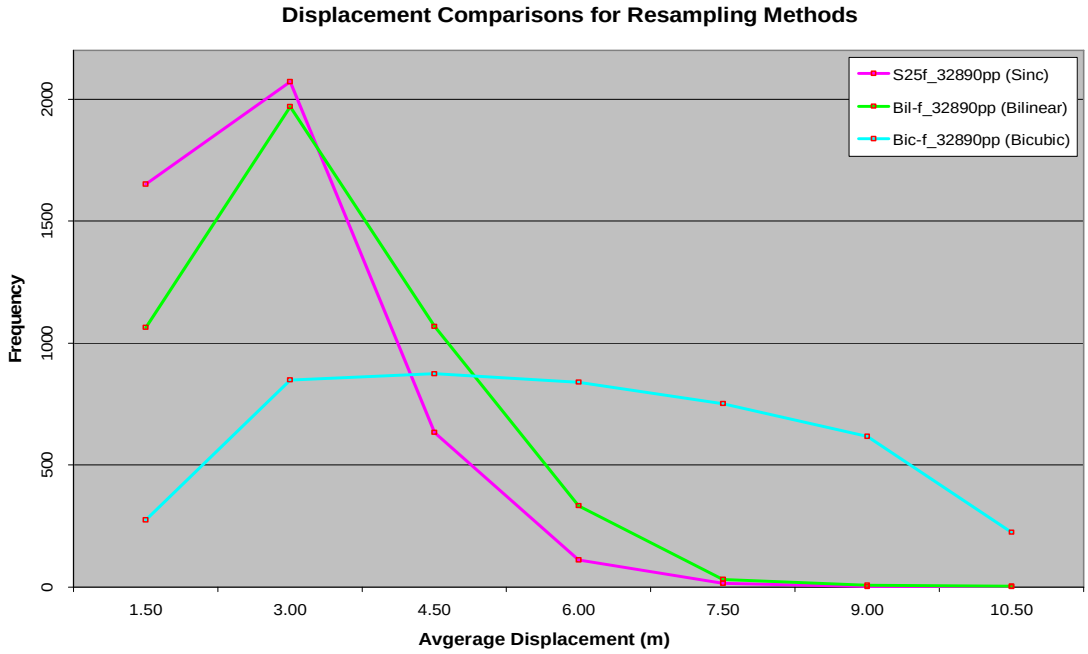

Figure 4-7. Average resultant displacement of different intervals for resampling methods

Visual inspection of the histograms (figures A-6 & A-7) of correlated images reveals that the Sinc method gives the displacement values closely concentrated around the average value of no displacement in N-S & E-W directions, while Bilinear and Bicubic methods are almost the same in N-S displacement with comparatively less number of displaced pixels around mean values. However their variability in E-W direction is higher than the Sinc method, particularly the Bicubic curve shows a strange behaviour of the method in measuring the displacement.

Figure A-8 gives mean and standard deviation (variance) both of N-S and E-W displacement components for three resampling methods. The mean/average displacement values in N-S and E-W directions are almost the same for all three methods, only Bicubic gives slightly different result in E-W direction. The displacement values variance in N-S direction is also almost the same for three methods but in E-W direction variance changes significantly, Bicubic being with the highest variance. The scatter plot of the Sinc method (figure A-9) shows no relationship of Sinc25 and Bilinear resampling methods in measuring the displacement. So both methods work independently for calculating the ground displacement.

Vector field (figure A-11) observation indicates that the vectors calculated by Sinc and Bilinear methods are comparable and around the detected fault both show displacement towards the fault. However the vectors calculated by Bicubic method show the displacement from NW and SE to be converging towards the center of the image which is unrealistic and quite contrary to the other two methods. At both edges of the image their magnitude is much higher and decreasing towards the center of the image. More close examination at pixel level shows variations in the directions of displacement vectors for both (Sinc & Bilinear) methods.

Figure A-10 (comparison of displacement directions) shows average angles plotted vs defined intervals for three resampling methods. Figure A-12, consisting of respective rose diagrams, shows

angles counts for different directions of the measured displacement. From these two figures we can see that the Bicubic resampling method provides a specific displacement direction (NNW to SSE) for all the pixels in the correlation image. The Bilinear gives displacement direction in almost N-S direction, while the Sinc method shows almost equal distribution in all directions. However histograms, resultant displacement and vector field images prove that Bicubic resampling method do not give accurate results.

Bilinear and Bicubic resampling methods are mathematically based on higher order polynomials and may alter original image values introducing some aliasing/biasing to the results. Bicubic being based on even higher order polynomial than Bilinear, its use requires some specific conditions regarding area or datasets. In present case its results are quite odd, may be due to its complexity. The roll of platform describes attitude variations in East-West direction which is higher as compared to other attitude variations like pitch and yaw. The roll variations are not modelled properly from ancillary data for all three resampling methods in general. The roll effect is particularly higher for Bilinear method; and for Bicubic method it is the highest.

4.3.1.1. Kernel size of Sinc resampling method

The resampling method Sinc accepts further parameters like kernel size. Kernel size can be defined as odd value starting from 11. To test the effect of kernel size three values (25, 31 & 37) were tried using Sinc resampling method with pre-post DEM and Frequential correlator with window size 32, step 8 and threshold 90 as constant. The lower values of kernel size give results of coarser quality.

From figure 4.8 we can see that the kernel size 31 gives N-S displacement direction while the other two options (kernel size 25 & 37) do not give any specific displacement direction. The same results can also be observed from the angles comparison figure A-13.

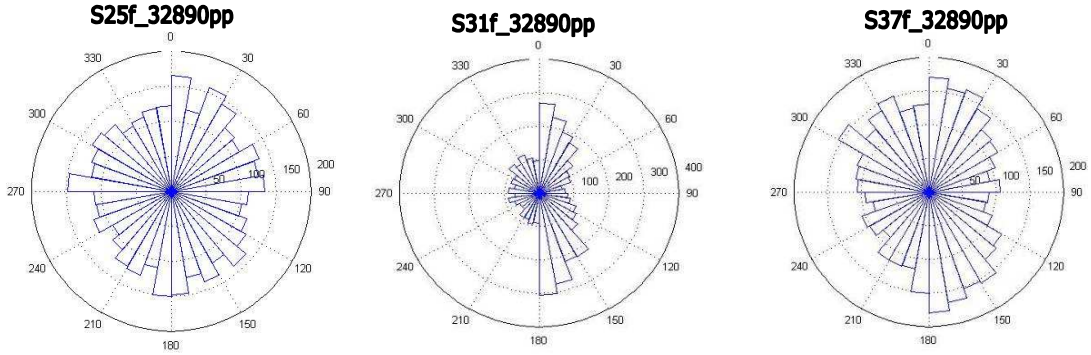

Figure 4-8. Rose diagrams showing displacement directions for three kernel sizes (25, 31, 37) of Sinc resampling method

Visual inspection of histograms (figures A-14 & A-15) shows that there is no considerable effect of kernel size in measuring N-S displacement component while in E-W direction they show variability. Kernel size 31 shows more variability than the kernel size 25 & 37 which can also be seen from the figures A-16 and A-17 (show average resultant magnitude and mean-&-variance respectively). Vector

field image (figure A-18) shows that vectors calculated with kernel size 25 are significantly different than the other two options. However upper left portion of the image above the detected fault gives comparable results for the three kernel sizes.

The above discussion shows that there is inconsistency in using three kernel sizes. The histograms, resultant displacement and angle diagrams show that kernel size 31 gives different results than the other two, while the vector field image shows that kernel size 25 is different.

4.3.2. Correlation Methods

Two correlation methods are available for sub-pixel correlation of optical imagery which are: Frequential and Statistical. Frequential method works in Fourier domain while Statistical is based on statistical methods. For comparison of the performance of correlation methods in measuring ground displacement, Bilinear and Sinc25 resampling methods were chosen while keeping the other correlation parameters (window size 32, step size 8, threshold 90) constant and using pre-post-DEM (pre-DEM for pre-earthquake image and post-DEM for post-earthquake image orthorectification).

Figure 4.9 shows the comparison of Frequential and Statistical correlator for Sinc25, Bilinear and Bicubic resampling methods. The figure indicates that the mean value for N-S displacement component is almost same and variance differs slightly. However in E-W direction the displacement component has considerable change in mean value while the variance differs drastically. The Bilinear resampling method shows variability in E-W direction decreasing from Frequential to Statistical correlator while other two methods (Sinc25 & Bicubic) give opposite results.

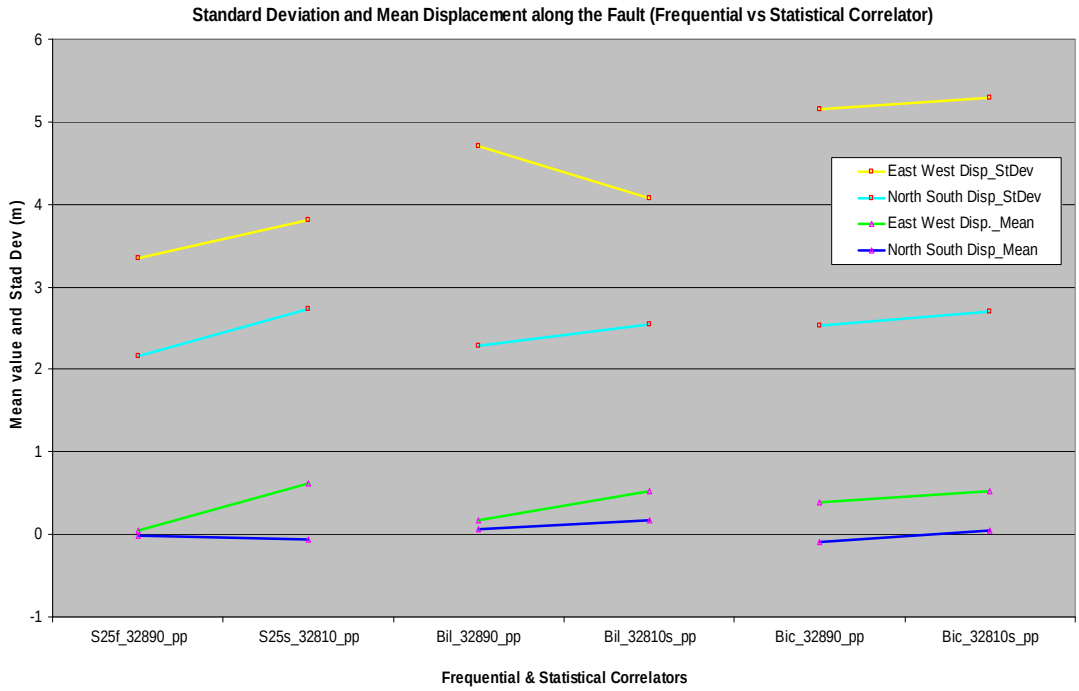

Figure 4-9. Mean and standard deviation of North-South and East-West components of displacement for correlation methods

The Frequential and Statistical correlator histograms comparison for Sinc and Bilinear resampling methods is shown in figures A-19 & A-20. Both correlators for Bilinear method give almost similar

results in N-S direction whereas they differ in measuring the displacement in E-W direction. The histogram of E-W displacement component describes that the Frequential method shows higher frequency of displaced pixels around mean value while the Statistical shows more variability. Average resultant displacement magnitude figures (A-21 & A-22) show that the Sinc resampling method is more sensitive for both correlators in measuring the ground displacement. Statistical correlation method for Sinc and Bilinear resampling methods gives approximately same results showing its robustness

The vector field image of both correlators for Bilinear resampling method (figure A-23) shows that there is no significant difference in measuring the ground displacement except at a few locations. The angle diagrams along with their respective rose diagrams (figures A-24 & A-25) reveal that both correlators, using Bilinear resampling method, give displacement direction in almost North-South, while in the case of Sinc25 there is no dependency in measuring displacement for both the correlators. Frequential correlator (for Sinc25) does not provide any specific direction of displacement while Statistical correlator shows approximate North-South direction. Although both correlators for different resampling methods do not give coherent or clear results when only using angle information, however this information can be used in relation to other figures (e.g. vector field or resultant displacement) for interpreting the Correlator behaviour.

Therefore it can be inferred that the application of correlation methods is consistent in measuring displacement in N-S direction, but not so good for E-W displacement component. This again may be due to the roll effect in E-W direction. Also Frequential is more sensitive in estimating the small displacement values while Statistical seems more robust against the change of parameters

4.3.2.1. Window Size

Correlation window defines the area (in pixels) on both orthorectified coregistered images to check the correlation (e.g. shift in pre & post earthquake imagery). To check the effect of window size on correlation, different comparisons of window sizes were made keeping the resampling method (Sinc) with pre-post DEM and other correlation parameters (step 8, threshold 90) as constant.

The different window sizes selected for the purpose of comparison are 4, 8, 16, 32 & 64. Figures 4.10 & 4.11 show that the window sizes 4, 8 & 16 provide excellent direction of displacement in E-W direction, however it is contrary to the reality. On the other hand while comparing window size 32 and 64 results of displacement direction, the window size 64 gives N-S direction of displacement and window size 32 does not show any prominent direction of displacement. However as earlier said, the angel (direction of displacement) results should be seen in relation to the resultant displacement and vector field results.

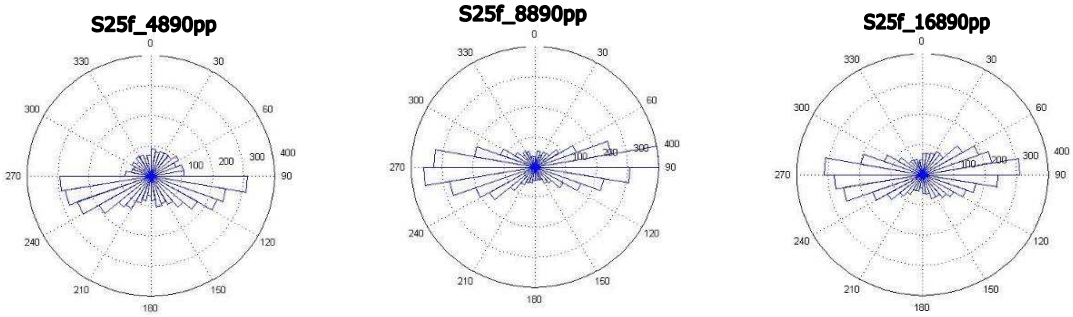

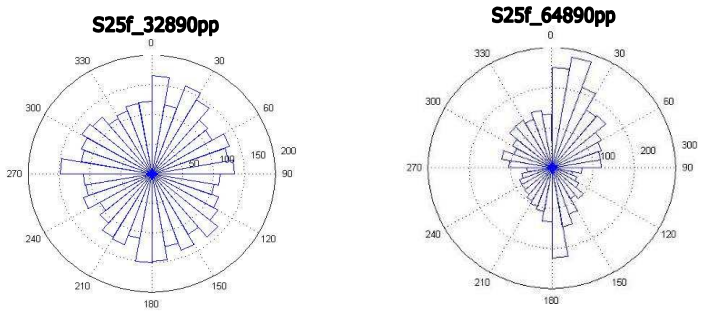

Figure 4-10. Rose diagrams showing the displacement direction distribution for window sizes of Frequential correlation method

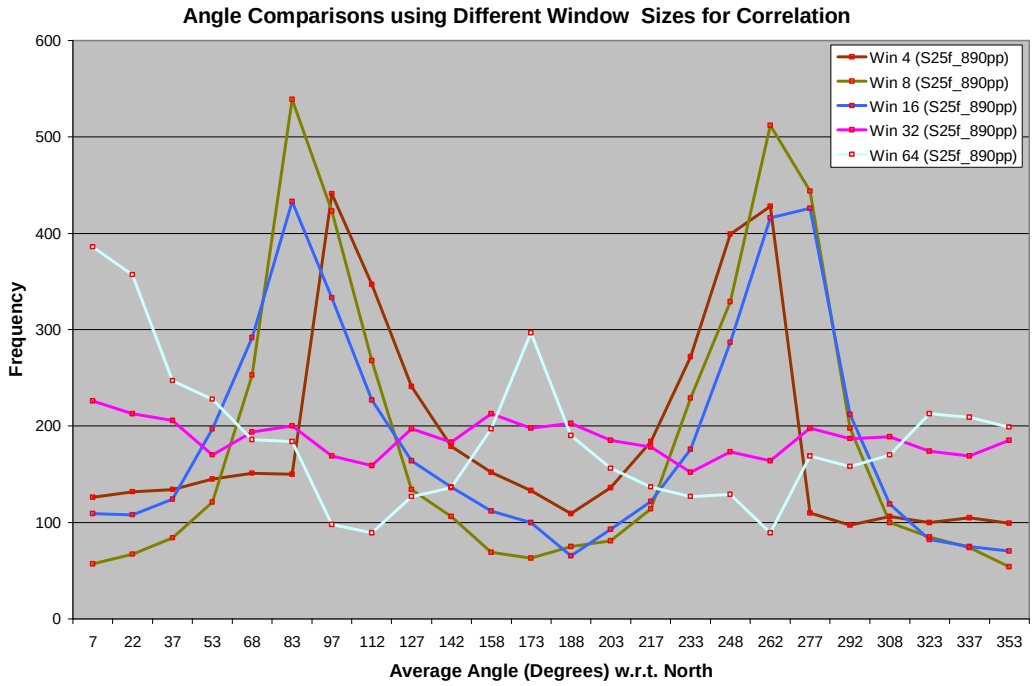

Figure 4-11. Average angle (direction of displacement) of different intervals for window sizes of Frequential correlation method

The effect of using different window sizes for correlation is examined (figures A-26 to A30). From these figures we can see that results of window sizes 4, 8 & 16 are conspicuously different and window sizes lower than 32 give mostly noisy correlation images. There is not any specific correlation pattern for these three window sizes as compared to the window size 32 and 64. Unlikely they show more variations in N-S displacement component than E-W (figure A-29). The window size 8 has even more strange results among window sizes lower than 32. The histogram of N-S displacement component (figure A-26) of window size 64 shows that most of the smaller measurements are around higher mean value as opposed to the window size 32 histogram. Figure A-28 gives similar observations of odd behaviour of window size 4, 8 & 16 while window sizes 32 & 64 give comparable results. Window size 32 is more sensitive in measuring smaller measurements than the window size 64. The figure A-29 shows that the mean value for window size 8 is drastically different from the other window sizes. Figure A-30 (vector field comparison of window size 16, 32 & 64) depicts that at most of the locations results for window size 32 & 64 are comparable.

Above discussion provides basis of concluding that the use of window size 32 or 64 to be considered more optimal as compared to others. The use of window sizes smaller than 32 gives mostly noisy results.

4.3.2.2. Step Size

Step size defines how many pixels will shift between the two sliding windows for measuring correlation. To check the effect of step size on correlation, comparisons of different step sizes (4, 8, 12, 16) were made keeping the resampling method (Sinc25) with pre-post DEM and other correlation parameters (Frequential correlator, window size 32 and threshold 90) as constant. The use of step size defines the number of pixels (resolution) in the correlated image, such as with step size 4 the image has more frequency of pixels (resolution 60 m in this case) as compared to others e.g. step size 16 gives 240 m resolution (less number of pixels).

From figures (4.12, A-31, A-32 and A-33) we get a clear perception about the performance of different step sizes used in the correlation method. According to the figures, average and variability of the displacement distances is almost the same in N-S and E-W directions. The only exception is the use of step size 16 (figure 4.12), which gives different result in calculating the mean displacement of the pixels in E-W direction as compared to the other step sizes.

Small step size like 4 is more susceptible for giving decorrelation patches in the correlation image. On the other hand large step size produces average and smoothing effect in the correlation image which might produce biasing in the quality of the results. So the step size 8 is optimal and chosen for most of the correlation processes of optical images.

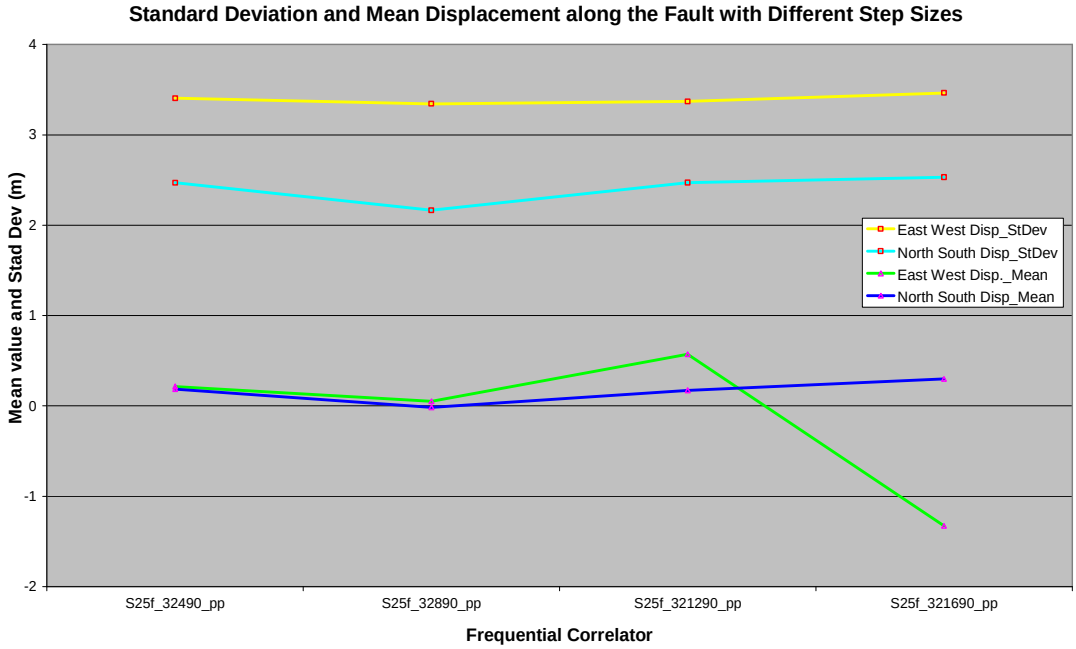

Figure 4-12. Mean and standard deviation, both N-S and E-W displacement components, for different step sizes of Frequential correlation method

According to the vector map (Figure A-34) of the study area, most of the vectors in the upper right side of the indicated fault line take downward (SSW-S) direction. Similarly most of the pixels in the lower right area below the fault line seem to be displaced in NNW direction as indicated by the vectors with the selection of step size 8 and 16. Step size 4 and 16 show vectors of minor magnitudes in the upper left portion below the indicated fault line which is inconsistent with the reality.

Figure A-35 shows the direction of displacement (angles) for whole of the image to get an indication of the effect of selecting different step sizes. Step size 4 shows the highest frequency of pixels displaced at about 0 and 180 degrees (N-S direction). Also the rose diagrams (figure A-36) illustrate that step size 12 and 16 give opposite displacement directions while the step size 4 gives prominent N-S direction of displacement.

From the above discussion it can be inferred that the step size 8 is reasonable in performing the correlation of optical imagery. Its results are the least biased by the decorrelation or smoothing of image.

4.3.2.3. Threshold

This subsection will describe the effect of threshold values in doing the sub-pixel correlation of optical images. Two threshold values (90 & 95) were tried for Sinc and Bilinear resampling methods in order to test the use of threshold values. The figures 4.14 & 4.15 depict that Sinc25 method is sensitive to the change of threshold value in measuring the displacement in E-W direction, where as the Bilinear method gives the same results for whatever threshold (90 or 95) is selected.

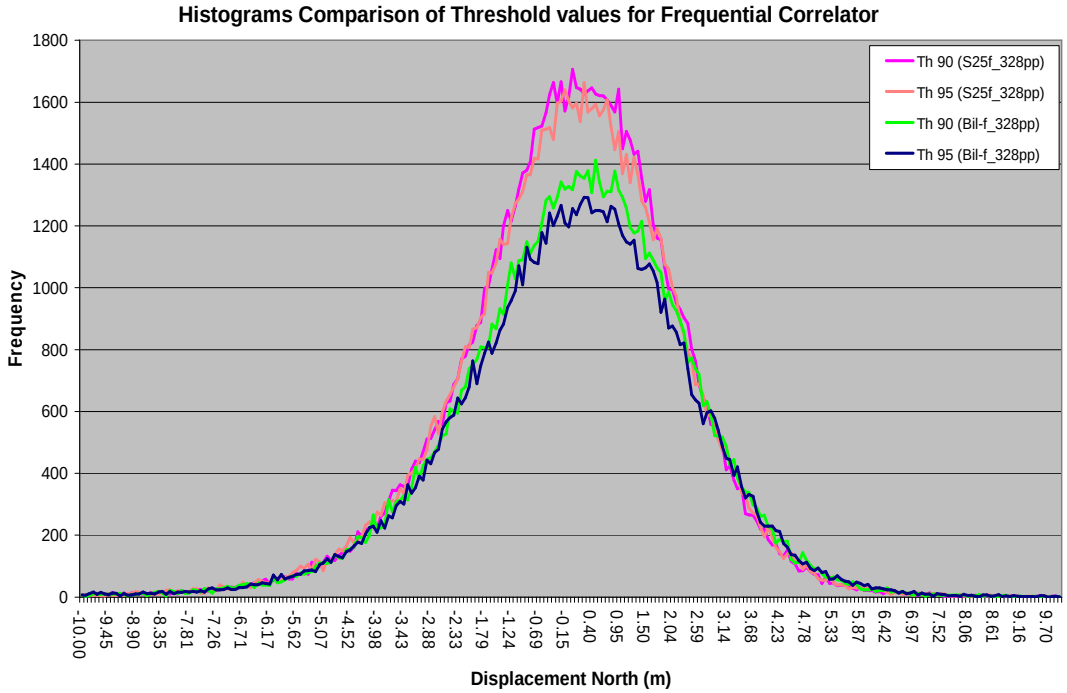

Figure 4-13. Histograms of displacement in North-South direction for different Threshold values of Frequential correlation method

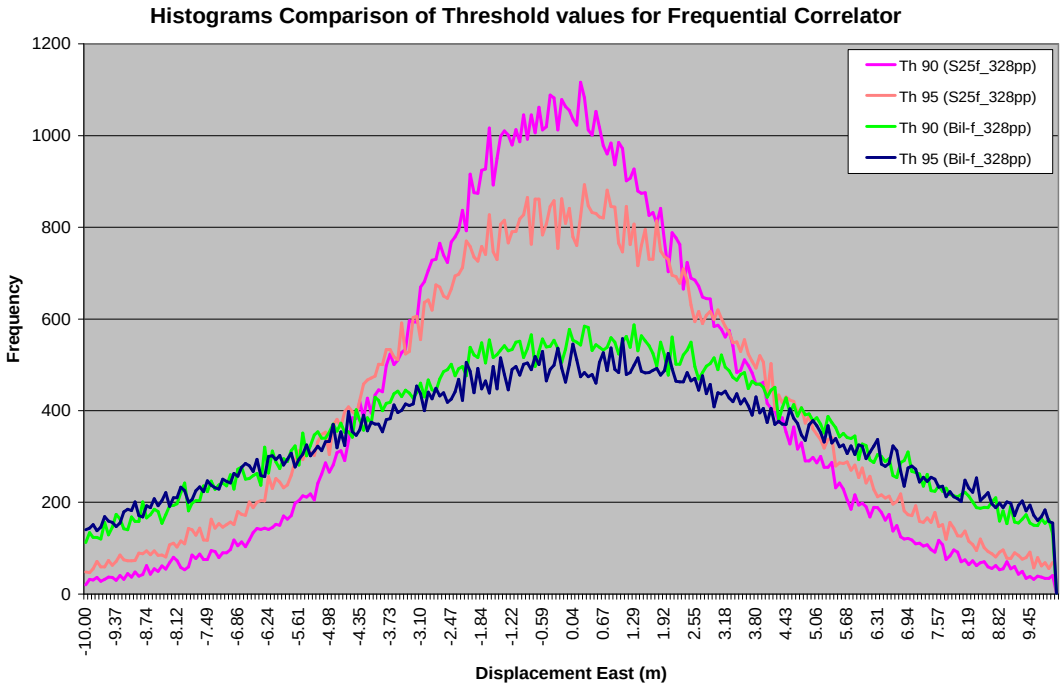

Figure 4-14. Histograms of displacement in East-West direction for different Threshold values of Frequential correlation method

Threshold values Comparison for Sinc25 and Bilinear methods shown in figures (A-37 & A-38) again emphasizes the above mentioned results about the sensitivity of Sinc method for the selection of different threshold values whereas the results of Bilinear method are stable for both threshold values.

The vector field image (figure A-39) of Bilinear method for different threshold values shows that there is no significant effect of the change of threshold value. However the change of threshold values for Sinc25 resampling method shows some differences in the direction of displacement while the magnitude is almost unaffected (figure A-40). This can also be verified from the graph (figure A-41) of angles and rose diagrams (figure A-42) that Sinc25 method with threshold value 95 gives SE direction while the threshold value 90 for Sinc method does not give any prominent direction of displacement. The Bilinear resampling method gives N-S direction of displacement for both threshold values. Therefore Sinc 25 method is sensitive to the selection of threshold values.

4.4. Measuring Displacements along the Fault

Displacements were measured along the fault at specified four (profile) locations (shown in figure 4.3 A) using the correlated images separately and then were exported as text (ASCII) files. These measurements were then plotted for comparing and interpreting different results. Estimation of displacements along the fault is generally decreasing from profile 1 to profile 4 at selected locations. Different comparisons were given below for the purpose of evaluating the COSI-Corr technique in its various aspects.

4.4.1. DEMs Selection Effects

Effect of using different options of selecting DEMs (figure 3.2 shows these options) is investigated in figure 4.15. The graph shows that in E-W direction the effect is significant, SRTM DEM being the highest. ASTER DEM options show negligible difference of measurements at stack 2 and 3. In N-S direction the ASTER pre-DEM shows higher displacement values at stack 2 & 3 and SRTM DEM gives low displacement values at stack 3 & 4.

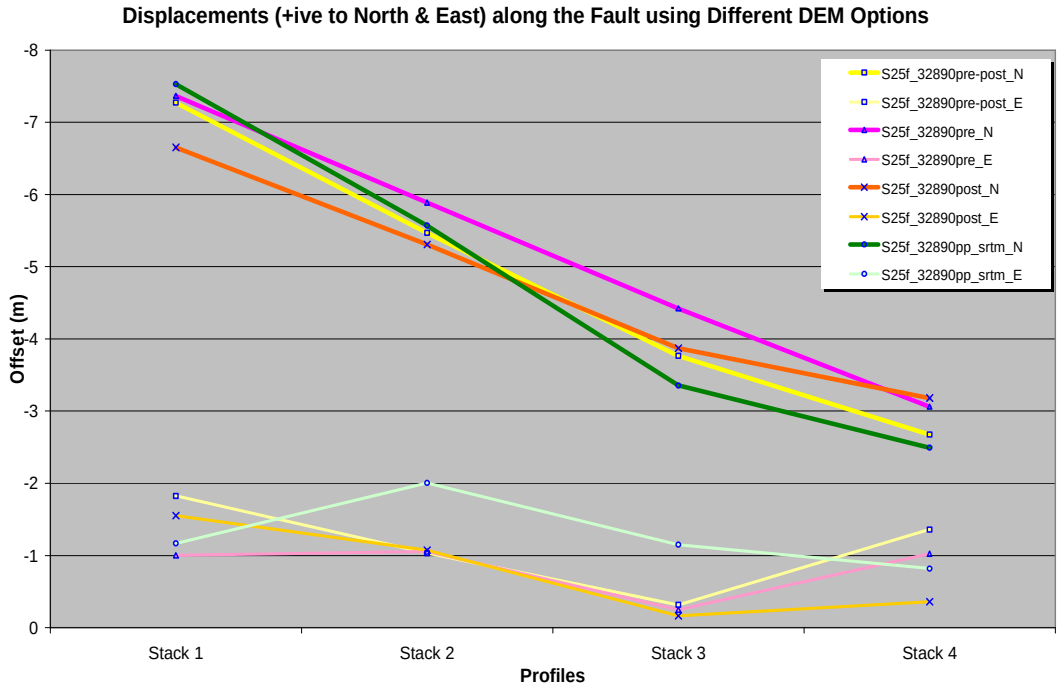

Figure 4-15. Displacement measurements along the fault at selected locations using different options of selecting DEMs

4.4.2. Resampling Methods

The displacement measurements along the faults at four selected locations are affected by the use of three resampling methods (Sinc, Bilinear & Bicubic). Figure A-43 indicates that Sinc and Bilinear resampling methods are almost the same in measuring N-S and E-W displacement components whereas performance of Bicubic method is quite different in both directions. As discussed earlier in sensitivity analysis the Bicubic resampling method response to different parameter is contradictory.

4.4.2.1. Kernel Size

Selecting different kernel sizes (25, 31, 37) for Sinc resampling method do not affect the displacement values largely (figure A-44). Only minor differences are observable at stack3 for N-S displacement component and at stack1 & 2 for E-W displacement component.

4.4.3. Correlation Method

Figure A-46 describes the effect of using different correlation methods. Frequential and Statistical correlators using Sinc 25 with pre-post DEM and correlation parameters like window size 32, step size 8 were investigated (see figure 3.2 for the description of all the parameters and datasets). Both correlators give almost the same results at stack 2 & 3 while at stack 1 & 4 they differ significantly in

measuring N-S displacement component. Statistical correlator gives higher values for E-W displacement component than Frequential correlator while in N-S displacement component the result is opposite. One more noticeable difference for Statistical correlator is that it gives higher displacement value in E-W, even higher from N-S component at stack 4 which is not realistic.

4.4.3.1. Window Size

Selection of window size shows considerable influence in measuring the displacement as can be seen in figure 4.16. Smaller window size like 4, 8 results are inconsistent and do not give reliable results. Their results for E-W displacement component are even higher than for N-S displacement component which is not true. Window size 16, 32 & 64 give comparable results in N-S displacement component and window size 64 results are higher at stack 2, 3 & 4. In E-W direction window sizes 64 give very inconsistent measurements of displacement than the other window sizes and hence its graph shows very strange behaviour.

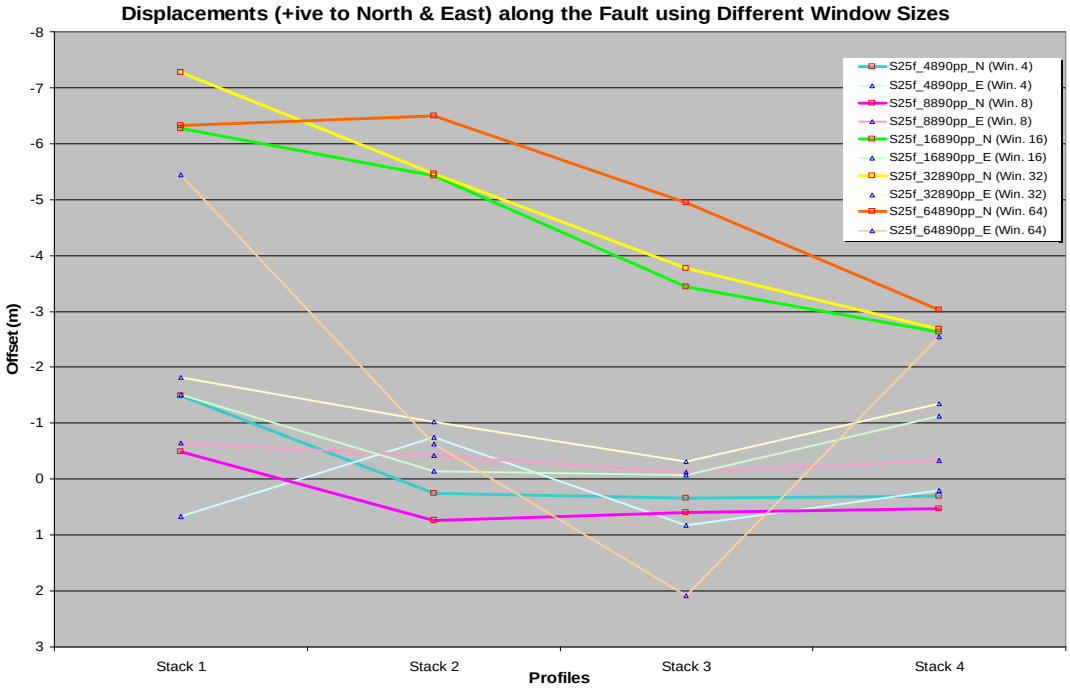

Figure 4-16. Displacement measurement along the fault at selected locations using different window sizes for Sinc 25 resampling method

In order to investigate the effect of window size for other two resampling methods, a comparison was made for window size 16, 32 & 64 (figure A-46). Window size 16 in Bilinear and window sizes 32 & 64 in Bicubic give opposite results at stack 2 & 3 in measuring the N-S displacement component. In E-W component the results of all window sizes for two resampling methods are incompatible and differ considerably. The results of Sinc 25 (figure A-46) are comparable to Bilinear (figure A-47) for window size 32 in measuring both E-W and N-S displacement components.

4.4.3.2. Step Size

The behaviour of different step sizes (4, 8, 16) in measuring the displacement is shown in figure A-47 using Sinc 25 resampling method and Frequential correlator having window size 32 & threshold value 90. Step size 4, 8 & 16 show almost same results at stack 1 & 4 and at stack 2 & 3 step size 16 gives higher values of N-S displacement component. In E-W displacement component the figure does not show any consistency of results of the three step sizes in measuring displacement. Step size 4 and 16 in E-W displacement component give positive displacement values which might not be the case actually.

4.4.3.3. Threshold

Figure A-48 investigates the effect of choice of different threshold values (90, 95) using the Sinc 25 resampling method and Frequential correlator with window size 32 and step 8. It shows that the N-S displacement values are almost same for both threshold values except at stack 3 with minor differences. In E-W displacement component the threshold value has considerable effect in measuring the displacement values particularly at stack 3 & 4.

4.5. Repeatability

In order to check the repeatability of the technique, a second pair of images (pre-earthquake image of September 2005 and post-earthquake image of October 2005) was selected to perform the sub-pixel correlation. Same mask was used to the 2nd pair of images for getting the same spatial subset like of previous 1st pair of images in order to have their comparison. September 2005 image has slightly less overlap to October 2005 image due to the small shift of first image, so there is small gap on upper left side of the image because the correlation process only accounts for overlapped area (figure A-49). The September 2005 pre earthquake image is very cloudy, although most of the cloud patches are out of masked area, some are in the selected spatial area. The masking process also excludes this data from the image that is why we have a difference of about 28110 pixels of two correlated images. Comparison of both correlated images (from 1st and 2nd pairs) using Sinc 25 resampling method and Frequential correlator with window size 32, step size 8 and threshold 90 were made.

Histograms (figures A-50 & A-51) besides the change of pixel frequencies show difference in measuring the ground displacement. The 2nd pair of images shows more variability and gives more pixels at larger displacement values. The distribution of pixel frequencies differs even more in E-W displacement component, similar to the earlier comparisons of two directions, due to more attitude variations in E-W direction of the platform. Figures A-52 and A-53 show their comparisons in terms of resultant displacement and mean & standard deviation respectively, these show similar kind of results as stated above.

Figure A-54 shows the comparison of average angle (direction of resultant displacement) and their respective rose diagrams. The comparison describes that there is no any similarity for both of image pairs in giving the direction of displacement. At some places it is even in opposite directions.

The vector field comparison (figure A-55) depicts that there is considerable difference in measuring the magnitude and direction of the displacement. However at some places direction is same with different magnitude of displacement.

Displacement measured by the two pairs of images at four different locations is compared in figure 4.16. Results of two correlated images are drastically different at all locations except at location 2 both in N-S and E-W direction. The second pair of images gives mostly higher displacement values in N-S direction, while in E-W direction results are opposite at locations 3 & 4.

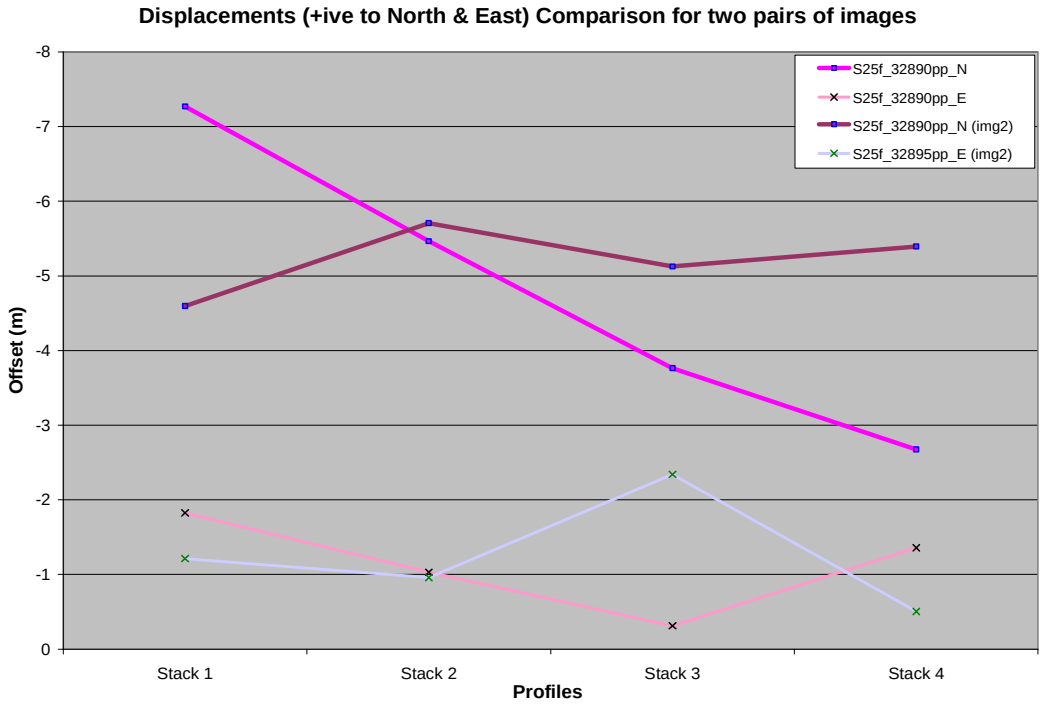

Figure 4-17. Displacement measurements along the fault at selected locations for two pairs of images bracketing the earthquake

From the above discussion it can be concluded that the repetition of sub-pixel correlation technique, for different-date image pair of the same area, did not give comparable results. This difference might be due to clouds and associated shadows and also small gap in the masked area. Due to noise in the image, the sub-pixel correlation produces large decorrelation patches which biased the estimation of ground displacement along the fault at four specified locations.

4.6. Robustness

Robustness of the technique can be evaluated by checking its sensitivity for methodological parameters applied to various types of data sets having different qualities, areas of specific characteristics. The degree of robustness increases when the results are similar (or comparable) relatively after applying above mentioned options. In the present case study, the COSI-Corr technique was evaluated by applying different parameters (figure 3.2) of the technique to two pairs of datasets bracketing the earthquake. By comparing and interpreting the results it was found that the overall performance does not show its robustness for various applied parameters, selection of DEMs, and different-date datasets of the same area. The results do not have consistency for applied parameters of

resampling and correlation methods. The measurements of displacement along the fault give drastically different results in E-W displacement component while in N-S direction results are comparable besides some exceptions.

4.7. Mapping and Analysis of Fault Rupture

The sub-pixel correlation of optical imagery provided a two band resultant image; band1 gives E-W displacement component while the band 2 gives N-S displacement component.

The figure 4.18A shows a N-S displacement component with clear discontinuity occurred due to ground movement caused by 2005 Kashmir earthquake. Positive values (yellow to dark red) show movement towards North while negative values (cyan, blue to magenta) to South. The white areas in the image are decorrelation patches or outliers (where the displacement value exceeds 10m), these were filtered. Decorrleation is mainly due to landslides or man-made changes whereas the outliers are due to the effects of shadows or seasonal variations.

The sharp discontinuity in the correlated image was traced precisely and termed as fault rupture produced due to 2005 Kashmir earthquake. This fault rupture is about 75 Km mainly along the previously mapped Muzaffarabad and Tanda faults now collectively called Balakot Bagh Fault BBF (figure 2.2). From the figure 2.2 we can see the fault rupture mainly follows the contact between two geological formations. In the upper Jehlum valley the fault trace is linear, except at the south-east it abruptly changes and forms “V” due to the topographic ridge (figure 4.18B), showing the effect of topography on fault rupture.

Fault trace becomes irregular where it joins the Muzaffarabad fault and cuts across the Kunhar valley. This irregularity is due to roughness of the topography on eastern side of the Kunhar valley shown in figure 4.18B. The irregularity of the fault trace starts at the confluence of Neelum and Jhelum rivers, it is also a junction of Muzaffarabad and Tanda faults. This point is also relatively closer to the 2005 Kashmir earthquake’s epicenter.

At north-western side, fault rupture disappears abruptly near the hairpin turn of MBT (Main Boundary Thrust) called Hazara–Kashmir Syntaxis. A small portion of marked fault trace was inferred where the correlation result was not so clear, it follows the pattern of the turn of MBT showing its structural control. The fault trace is also parallel to the western flank of the Syntaxis.

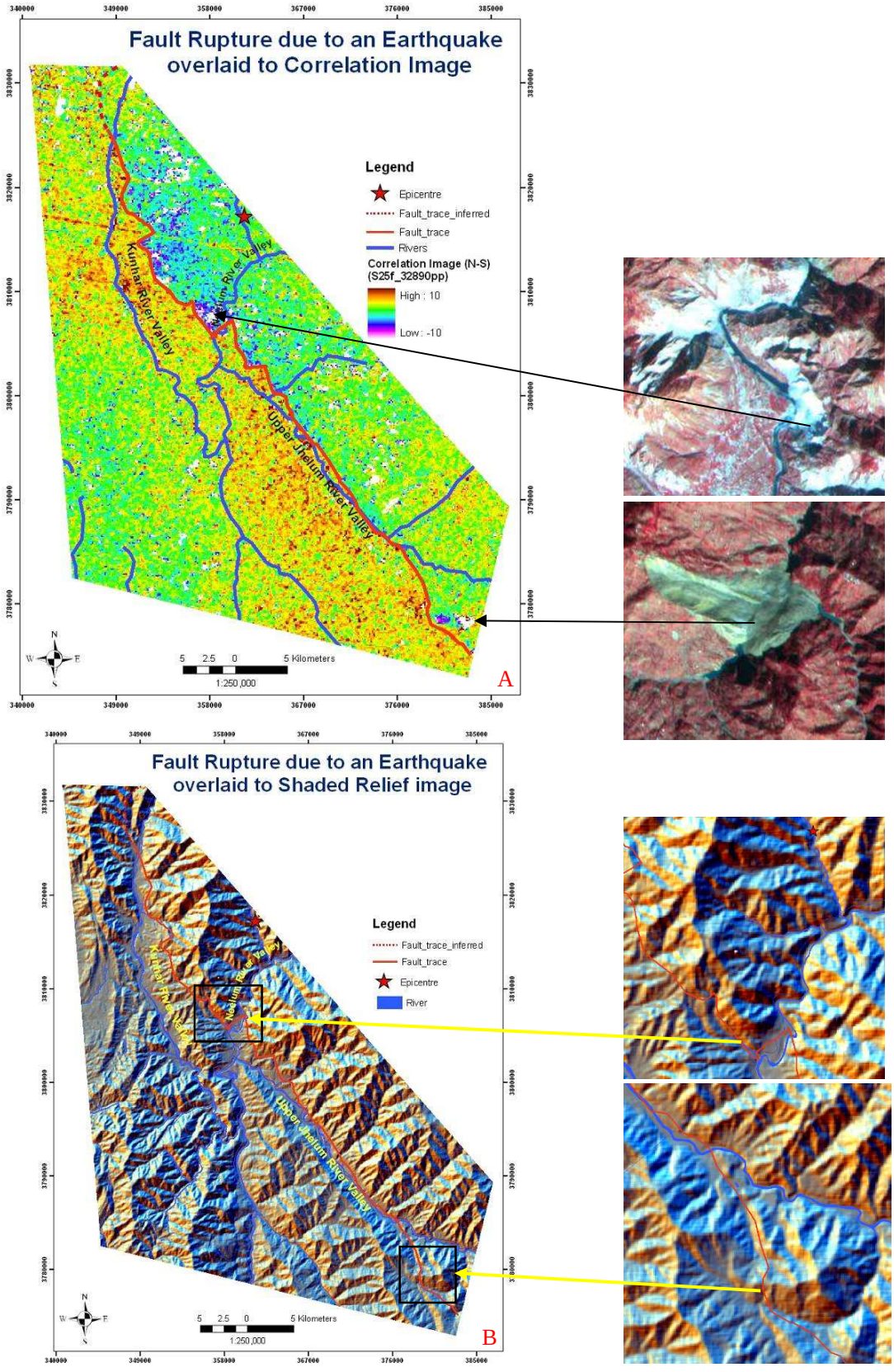

Figure 4-18. A) Correlation Image (N-S displacements) B) Shaded Relief Image

Applicability

The COSI-Corr (Co-Registration of Optically Sensed Images and Correlation) technique was developed for various change detection applications. Presently its applicability is limited to pushbroom sensor datasets and specific correlation methods (Frequential or Statistical). It was also applied to aerial images successfully for monitoring surface changes. In present study its applicability was evaluated for detecting the ground displacements due to earthquake. By comparing results of using different options (described in figure 3.2), it was found that its applicability is reasonable for qualitative analysis. In terms of using the technique it has simple & smooth function for getting correlated images with the provision of tools for their post processing and deriving different products. It provides both automatic and manual options in setting different parameters in order to have desired results. In the case of earthquake induced changes this technique can help in getting early damage assessment of the area and further investigations of various geological aspects.

5. Discussion and Conclusions

5.1. Discussion

This chapter provides a discussion of the results given in chapter 4 obtained by using different DEM options, datasets and methodological parameters of the COSI-Corr technique (all described in figure 3.2) in detecting and measuring ground displacements. The answers of the research questions will be given in light of the results and discussed in order to meet the objectives of the research.

The selection of DEM affects the results significantly. Various DEM options (pre-post pre-DEM, post-DEM, SRTM-DEM described in figure 3.2 and Appendix B) were tried; the SRTM DEM did not give promising results, pre-DEM option was relatively better but it did not cope with the surface changes which occurred after the earthquake. Post-DEM results were reasonably good as it accounts for the surface changes occurred after earthquake. The pre-post DEM option was found to be the best of all, as logically the orthorectification of pre-earthquake (post-earthquake) image should be better for using pre-DEM (post-DEM) option of the same-date image because it rectifies the elevation and positional variations accordingly.

The resampling methods (Sinc, Bilinear & Bicubic) reconstruct the image based on mathematical algorithm. Due to complex formulation the original image values can be altered by the selection of resampling method. The Sinc resampling method was found to be reasonably good in the process of orthorectification and coregistration. The use of the kernel size did not affect the results significantly. Bilinear resampling method results are moderate; it is not sensitive in measuring the small displacement values. However for noisy images its results are better than the Sinc resampling method. Bicubic resampling method does not prove to be a reliable method in measuring the ground displacements caused by an earthquake. Its use may require some specific conditions regarding the area or dataset characteristics.

The correlation method selection is related to the choice of dataset characteristics, spatial resolution or quality of dataset and also to the investigated area with some seasonal preferences. Frequential correlator gives more accurate results; however it requires a data of good quality and takes longer processing time. On the other hand the Statistical method is comparatively robust and fast but less accurate, however its performance for noisy images is better.

The use of different correlation parameters enable to get the results according to the set requirements. The window size for correlation of two optical images is sensitive in giving the displacement results. A window size lower than 32 does not give good result, particularly the window sizes 4 and 8 results are too noisy and unreliable. The sensitivity of the window size is more with Sinc resampling method. Step size defines shift number of pixel between two correlating windows and gives the pixel size in the output correlated image. The step size 4 is more susceptible to decorrelation patches where as step size 8 and 16 give comparable results. The step size 16 did not provide accurate results of

displacement measurements in East-West direction. Therefore the use of step size 8 gives promising and comparable results in measuring the ground displacements. The use of threshold value is sensitive to Sinc resampling method. For other two methods the results are almost similar. The threshold value 90 with Sinc 25 resampling method was found to be good in producing the correlated results.

Finally the performance of the COSI-Corr technique was evaluated with different datasets and methodological parameters (figure 3.2). The quantified table of averaged and scaled weights describes that the Sinc resampling method with kernel size 25, and Frequential correlator with window size 32, step size 8 and threshold value 90 is the most suitable option to get ground displacement measurements along the fault.

After detection and mapping of fault, different characteristics found of the fault rupture are: it has approximate length of about 75 Km running mostly in a rugged topography. It runs through the contact of geological formations along the previously mapped active Muzaffarabad and Tanda faults. The fault rupture shows the influence of other structural features in the region.

The following section provides the answers of the research questions formulated in chapter one in order to meet the research objectives.

1. *How are the different parameters of the adopted methodology sensitive in measuring displacement along an active fault?*

In order to check the sensitivity of the COSI-Corr technique using different DEM options, datasets and parameters of the technique (all are given in figure 3.2) various comparisons were made in the form of images, map overlays, or graphs. At the end a table of quantification was produced by assigning different weights to the results attributes. The parameters of the technique are found to be sensitive in measuring the displacements along the fault in one way or another. Sinc resampling method proves to be more sensitive than the other two methods and among correlators; the Frequential method seems to be more sensitive. However their results are not consistent in measuring the ground displacements.

2. *Are the results affected when the sub-pixel correlation process is repeated using different pre-earthquake remote sensing dataset?*

When the technique was applied to another dataset of the same area, the results were drastically different. This might be due to the noise or clouds in the second image which produce more decorrelation patches. This might be one of the reasons for not giving comparable results in measuring the ground displacements.

3. *Does the technique prove to be robust after sensitivity and repeatability analysis?*

From the results obtained after the comparative interpretation for sensitivity and repeatability analysis, it was found that the performance of COSI-Corr technique can not be termed as robust. It is because of the reason that it gives variations in the results with the change of methodological parameters and with the use of another dataset of the same area.

Is the technique suitably applicable for the purpose of estimating the ground deformation caused by an earthquake?

After the analysis it was found that applicability of the technique to monitor the terrain change is reasonable and its results can compliment to other techniques. As it gives horizontal displacement components and its results near field are more accurate so this can be combined with other technique (e.g. InSAR or GPS field measurements) whose performance is not good near field but gives accurate results in far & vertical fields in order to have complete information for the characterization of terrain changes.

4. *How does the selection of Digital Elevation Models (DEMs) from different dates affect the sub-pixel correlation?*

Selection of DEM options (figure 3.2) affected the correlation and measurement of the ground displacement along the fault. The pre-post DEM (means pre-DEM for pre-earthquake image orthorectification and vice versa) gave reasonably accurate results as compared to other choices like pre-DEM or post-DEM only. The use of SRTM DEM did not provide accurate correlation results particularly in East-West direction.

5. *How do different features along a fault rupture affect the correlation of images and measurement of displacement?*

Different features affect the propagation of fault rupture in the ground, the major effect being the topography. The rugged topography of the area made the rupture of the fault very zigzag and it is in mostly upper half of the image, while in lower half the fault line is almost linear along the upper Jhelum river valley except at the end (SE) where it turns abruptly due to the hill in its way. Secondly, the fault rupture mainly follows the pre-existing active faults (Muzaffarabad & Tanda) and runs along the contact of different geological formations. The middle of the image where two previously active faults join by an abrupt step is the continuity of the same fault rupture. This join of two faults is close to the epicentral location of 2005 Kashmir earthquake. Due to earthquake there were lots of landslides in the area which are major source of decorrelation in the image. Other causes of correlation lost may be clouds, shadows, snow or land cover change and/or any infrastructural change.

5.2. Conclusion

Based on the interpretation and sensitivity analysis different conclusions were drawn about the developed methodology in terms of its sensitivity, repeatability, robustness, applicability potential for mapping the fault rupture and measuring co-seismic (2005 Kashmir earthquake) surface deformation along the fault.

- Sinc resampling method and Frequential correlator are sensitive in the use of technique's parameters (given in figure 3.2). Its results are more accurate as compared to Bilinear resampling method and Statistical correlator which give moderate accuracy but are more robust than the Sinc method. However the Bicubic resampling method is not accurate and sometimes it is even unrealistic.

- The COSI-Corr technique did not give promising results for another dataset of the same area in measuring the ground displacements. Therefore the technique does not prove to be robust for different methodological parameters and different datasets.

- The technique still can be applied for change detection and terrain monitoring although its results by the use of different parameters and datasets are varying for measuring ground displacements.

- The use of different DEM selection options is prone to biasing the displacement estimations due to the errors of DEM and it ultimately affects the correlation & estimation of the ground deformation.

- Sub-pixel correlation of optical images is greatly affected due to landslides, shadowing effect, topography, snow or land cover changes and infrastructural changes.

5.3. Recommendations

Recommendations for the future work are as follows:

- The technique should be applied to a flat area, in order to avoid the use of DEM because high relief of rugged terrain affects the measurement of ground displacements.

- Field visits and validation data is necessary for complete evaluation of the technique.

- For a better evaluation of the technique different types and dates datasets, particularly of high spatial resolution, should be used e.g. SPOT, QuickBird or Ariel photos etc.

- Aid of other ancillary datasets e.g. geological or geophysical can be beneficiary in context of estimating the ground deformation due to an earthquake.

References

Abrams, M., Hook, S. and Ramachandran, B., 2002. Aster User Handbook. Nasa Jet Propulsion Laboratory, vol 2.

Avouac, J.P., Ayoub F., Leprince S., Ozgun K. and D.V., H., 2006. The 2005, Mw 7.6 Kashmir Earthquake: Sub-Pixel Correlation of ASTER Images and Seismic Waveforms Analysis. Earth and Planetary Science Letters, Vol. 249(No. 3-4): pp 514-528.

Ayoub, F., Leprince S. and J.P., A., 2006. Aerial Photography for Seismic Ground Deformation Measurement. ISPRS Journal of Photogrammetry and Remote Sensing.

Bilham, R. and Ambraseys, N., 2004. Apparent Himalayan Slip Deficit from the Summation of Seismic Moments for Himalayan Earthquakes, 1500-2000. Current Science.

Bossart, P., Dietrich, D., Greco, A., Ottiger, R. and Ramsay, J.G., 1988. The Tectonic Structure of the Hazara-Kashmir Syntaxis, Southern Himalayas, Pakistan. Tectonics, 7(2): 273-297.

Burgmann, R., Rosen P. A. and J., F.E., 2000. Synthetic Aperture Radar Interferometry to Measure Earth's Surface Topography and Its Deformation. Annu. Rev. Earth Planet. Sci., Vol. 28: pp.169–209.

Calkins, J.A. et al., 2004. Geological Map of the Garhi Habibullah Area, District Mansehra and Parts of Muzaffarabad District, AJK: Geological Survey of Pakistan, Geol Map Series v. Geological Survey of Pakistan, pp. VI, no. 13, Sheet No. 43 F/7, 1:50,000.

Cara, G.S., 2004. Terrain Change Detection using ASTER Optical Satellite Imagery along the Kunlun Fault, Tibet, The University of Texas at El Paso.

Chung-Pai Chang, Kun-Shan Chen, Chih-Tien Wang and Yen, J.-Y., Application of Space-borne Radar Interferometry on the Crustal Deformation in Taiwan: Perspective from the Nature of Events.

Crippen, R.E., 1992. Measurement of Subresolution Terrain Displacement using SPOT Panchromatic Imagery. Episodes, Vol. 15(No. 1).

Crippen, R.E. and Blom, R.G., 1991. Measurement of Subresolution Terrain Displacements using SPOT Panchromatic Imagery. IEEE Transactions: 1667- 1670.

Dellow, G.D., Ali Q., Hussain S., Khazai B. and A., N., 2006. Preliminary Reconnaissance Report For The Kashmir Earthquake Of 8 October 2005, NZSEE Conference.

Durrani, A.J., Elnashai A. S, Hashash Y.M.A, Kim S. J. and Masud A., 2005. The Kashmir Earthquake of October 8 2005.

EERI_Report., 2005. First Report on the Kashmir Earthquake of October 8, 2005.

Grohmann, C.H., Riccomini, C. and Alves, F.M., 2007. SRTM-based morphotectonic analysis of the Poços de Caldas Alkaline Massif, southeastern Brazil. Computers & Geosciences, 33(1): 10-19.

Jaboyedoff, M., Couture, R. and Locat, P., 2009. Structural Analysis of Turtle Mountain (Alberta) using Digital Elevation Model: Toward a Progressive Failure. Geomorphology, 103(1): 5-16.

Jayangondaperumal, R. and Thakur, V.C., 2008. Co-Seismic Secondary Surface Fractures on Southeastward Extension of the Rupture Zone of the 2005 Kashmir Earthquake. Tectonophysics, Vol. 446(No. 1-4): pp.61-76.

Kaneda, H. et al., 2008. Surface Rupture of the 2005 Kashmir, Pakistan, Earthquake and Its Active Tectonic Implications. Bulletin of the Seismological Society of America, Vol. 98(No. 2): pp. 521-557.

Kazmi, A.K. and Qasim Jan, M., 1997. Geology of Pakistan. 554 pp.

Kervyn, F., 2001. Modelling Topography with SAR Interferometry: Illustrations of a Favourable and Less Favourable Environment. Computers & Geosciences, Vol. 27(No. 9): pp. 1039-1050.

Koike, K., Nagano, S. and Kawaba, K., 1998. Construction and analysis of interpreted fracture planes through combination of satellite-image derived lineaments and digital elevation model data. Computers & Geosciences, 24(6): 573-583.

Leprince, S., Barbot S., Ayoub F. and Avouac J.P., 2007. Automatic and Precise Orthorectification, Co-Registration and Sub-Pixel Correlation of Satellite Images, Application to Ground Deformation Measurements. IEEE Transactions on Geoscience and Remote Sensing, Vol. 45(No. 6): pp. 1529-1558.

Liu, J.G. and Ma, J., Imageodesy on MPI & GRID for Co-seismic Shift Study using Satellite Optical Imagery Department of Earth Science and Engineering, Imperial College London, SW7 2AZ

Massonnet, D. and Feigl, K.L., 1998. Radar Interferometry and Its Application to Changes in the Earth's Surface. Reviews of Geophysics, Vol. 36(No. 4): pp. 441-500.

Michel, R., Avouac J. P. and J.., T., 1999. Measuring Ground Displacements from SAR Amplitude Images: Application to the Landers Earthquake. Geophysical Research Letters, Vol. 26(No. 7): pp 875-878.

Nakata, T., 1972. Geomorphic history and crustal movements of foothills of the Himalaya. Report, Tohoku University, Japan: pg.77.

Ouattara, T., Couture R., Bobrowsky P. T. and Moore A., 2004. Remote Sensing and Geosciences.

Pavez, A. et al., 2006. Insight into ground deformations at Lascar volcano (Chile) from SAR interferometry, photogrammetry and GPS data: Implications on volcano dynamics and future space monitoring. Remote Sensing of Environment, 100(3): 307-320.

Philip, G., 2007. Remote Sensing Data Analysis for Mapping Active Faults in the Northwestern Part of Kangra Valley, NW Himalaya, India. International Journal of Remote Sensing, Vol. 28(No. 21): pp. 4745-4761.

Rubin, C., 1996. Systematic underestimation of earthquake magnitudes from large intracontinental reverse faults: historical ruptures break across segment boundaries. Geology 24: 989–992.

Strang, G. a. N. and Truong., 1997. Wavelets and Filter Banks: Wellesley. Wellesley-Cambridge Press, 22(28): 183 p.

Townshend, J.R.G., Justice, C.O., Gurney, C. and McManus, J., 1992. The Impact of Misregistration on Change Detection. IEEE Transactions on Geoscience and Remote Sensing, 30(5): 1054-1060.

Tralli, D.M., Blom R. G., Zlotnicki V., Andrea D. and Evans D. L., 2005. Satellite Remote Sensing of Earthquake, Volcano, Flood, Landslide and Coastal Inundation Hazards. ISPRS Journal of Photogrammetry and Remote Sensing, Vol. 59(No. 4): pp. 185-198.

Tronin, A.A., 2006. Remote sensing and earthquakes: A review. Physics and Chemistry of the Earth, Parts A/B/C, 31(4-9): 138-142.

Van Puymbroeck, N., Miche, l.R., Binet, R., Avouac, J.P. and Taboury, J., 2000. Measuring Earthquakes from Optical Satellite Images. Applied Optics, vol. 39(no. 20): pp 3486- 3494.

Walker, R.T., 2006. A Remote Sensing Study of Active Folding and Faulting in Southern Kerman province, S.E. Iran. Journal of Structural Geology, Vol. 28(No. 4): pp. 654-668.

Appendix A

Appendix-A contains comparison figures of the results

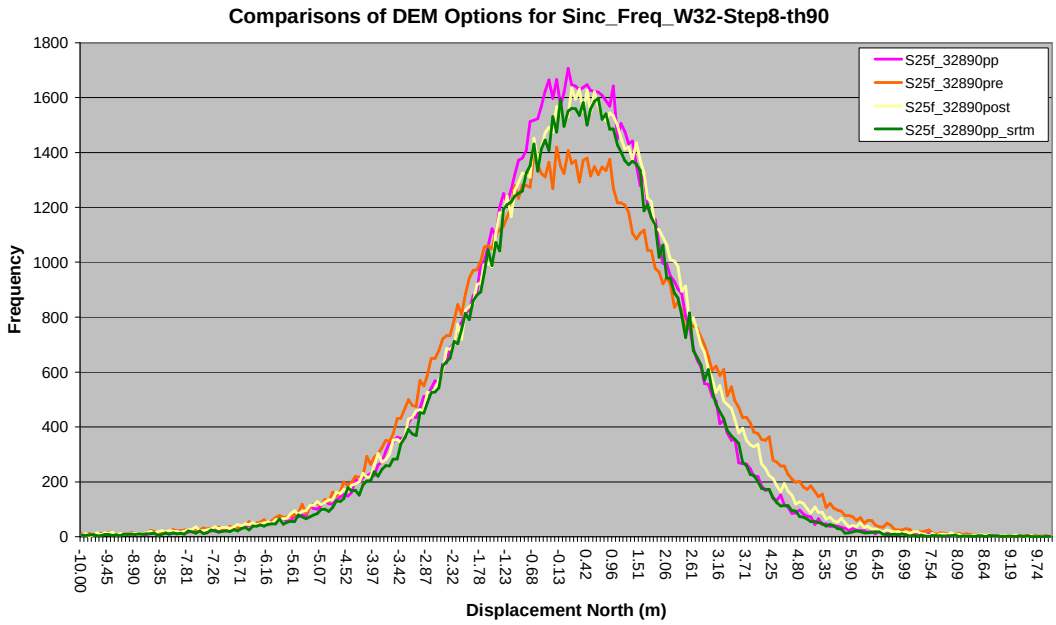

Figure A- 1. Histograms of displacement in North-South direction for different date DEMs used to orthorectify the images

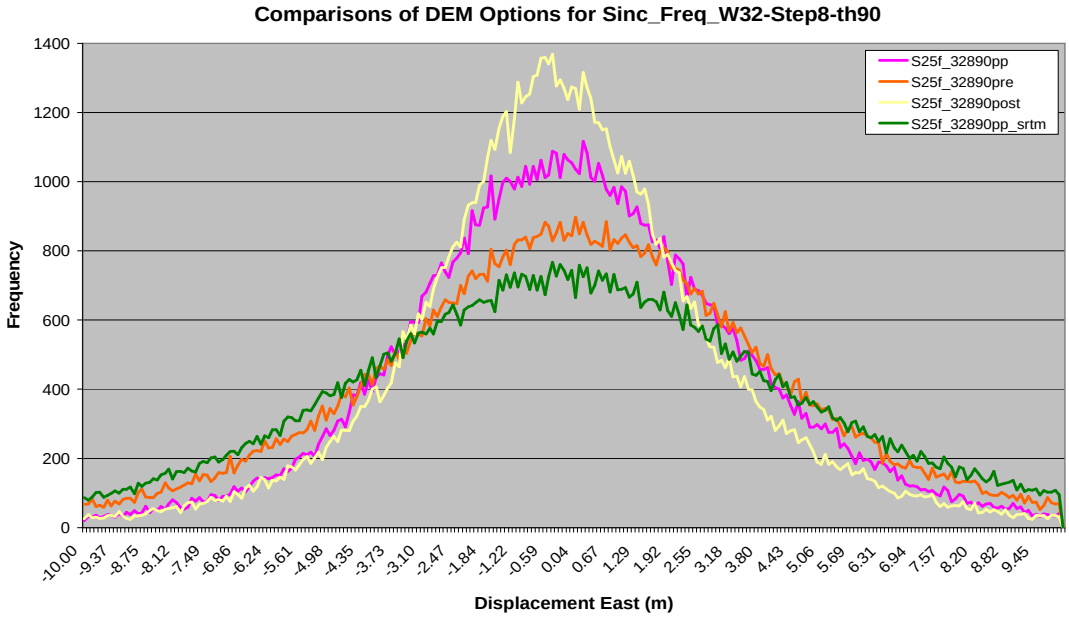

Figure A- 2. Histograms of displacement in East-West direction for different date DEMs used to orthorectify the images

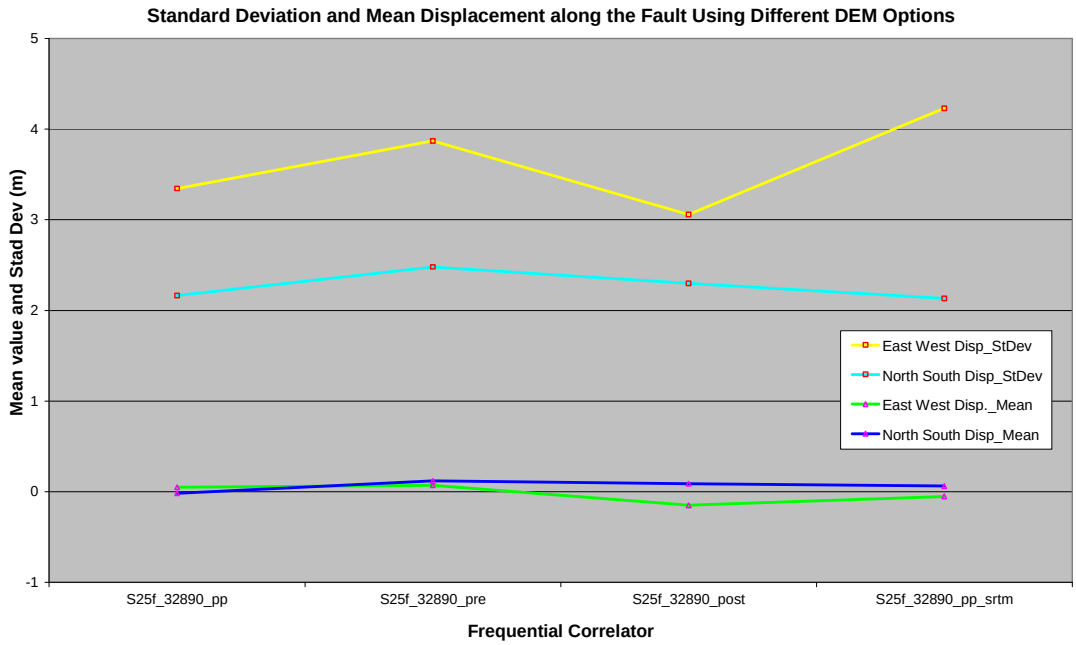

Figure A- 3. Mean and standard deviation both for North-South and East-West components of displacement for different date DEMs used to orthorectify the images

.

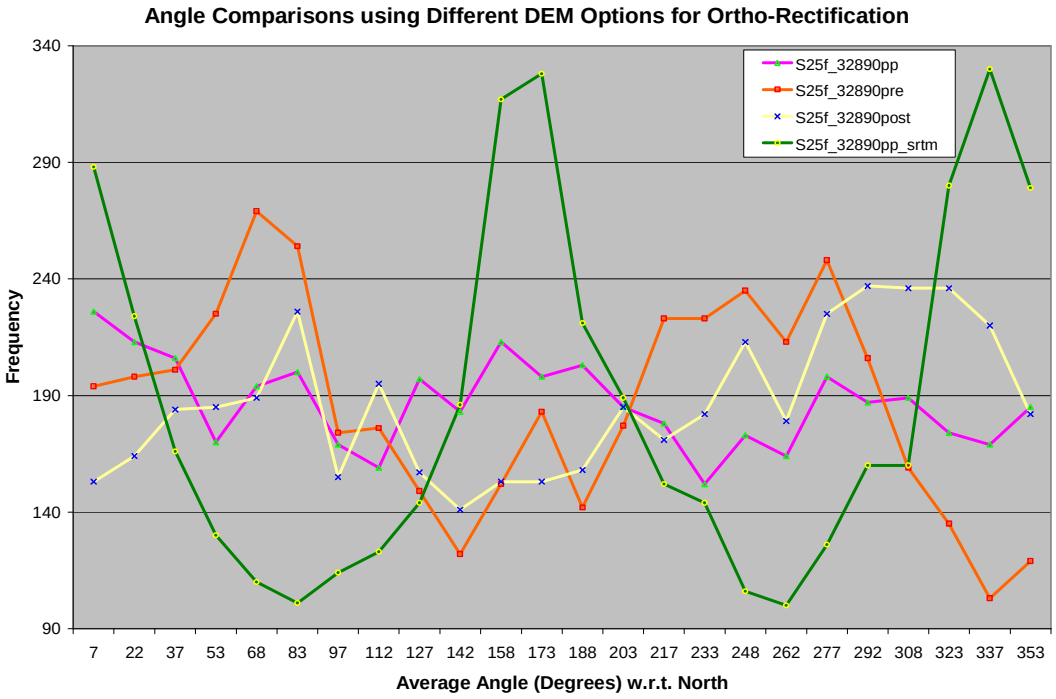

Figure A- 4. Average angle (direction of displacement) of different intervals for different date DEMs used to orthorectify the images

.

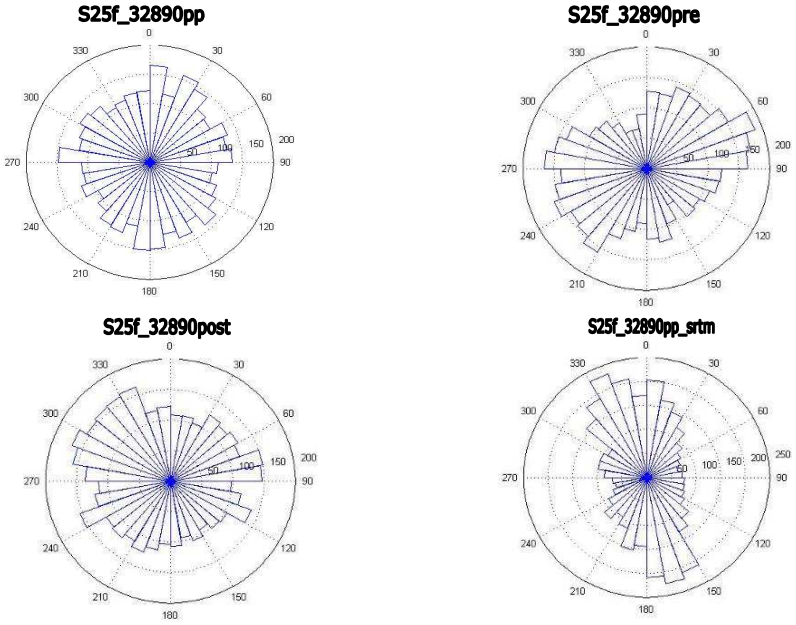

Figure A- 5. Rose diagrams showing displacement directions for different DEM options using Sinc25 resampling method and Frequential correlator

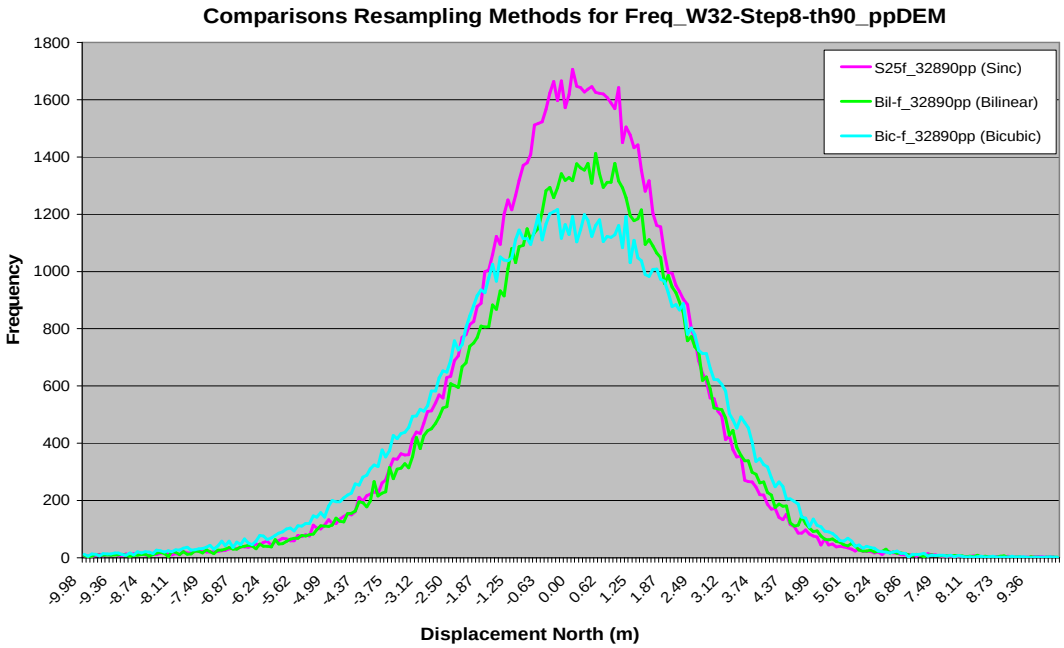

Figure A- 6. Histograms of displacement in North-South direction for different resampling methods

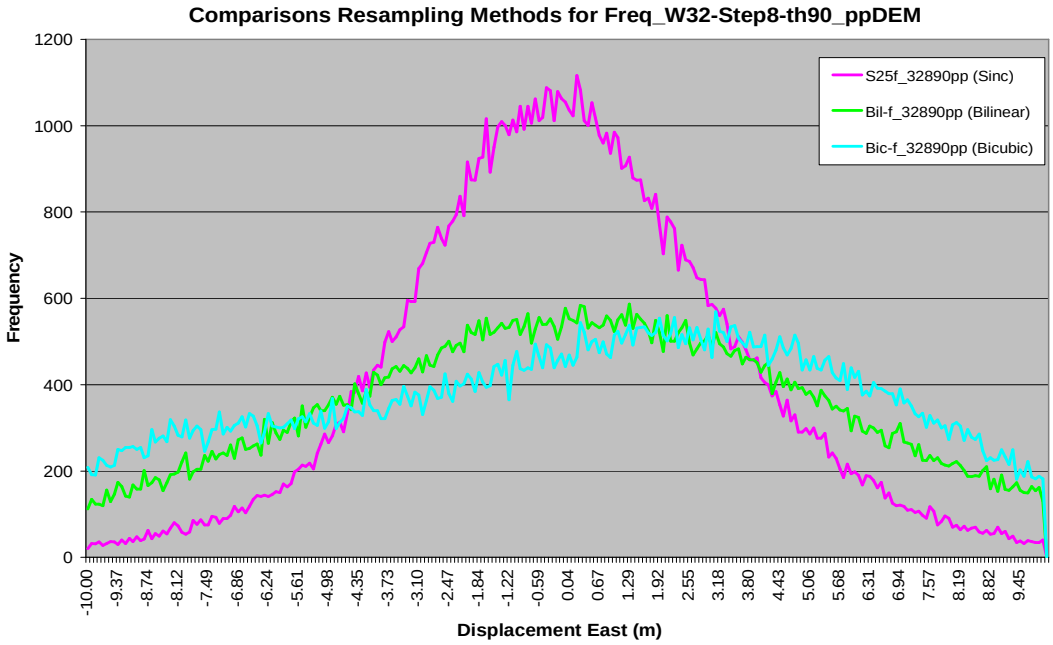

Figure A- 7. Histograms of displacement in East-West direction for different resampling methods

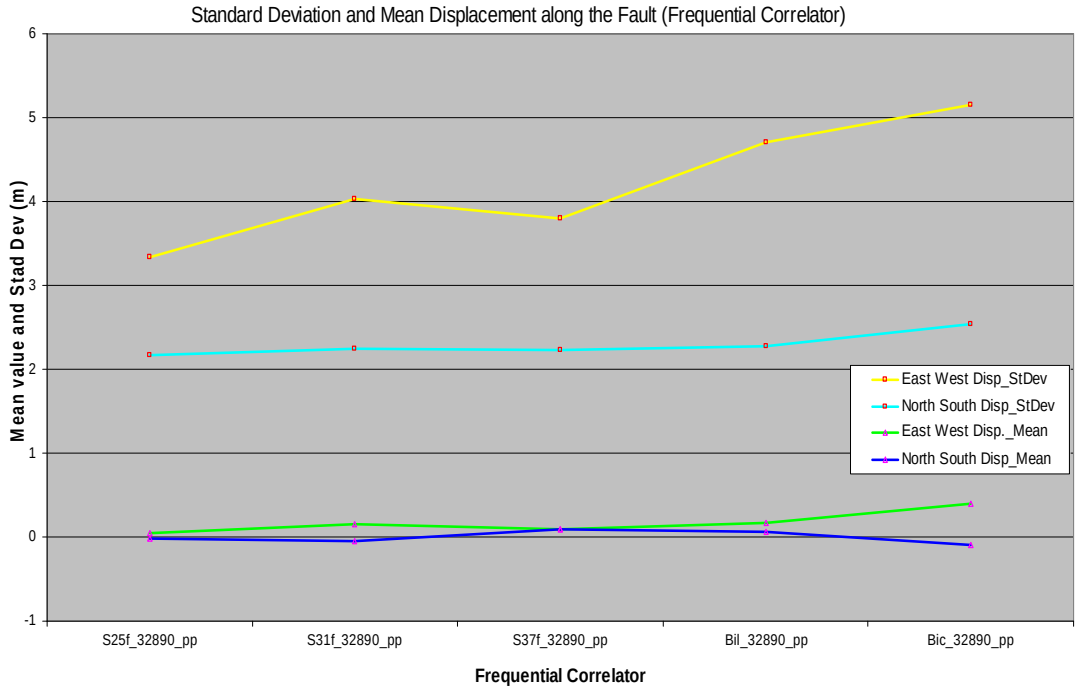

Figure A- 8. Mean and standard deviation both for North-South and East-West components of displacement for resampling methods

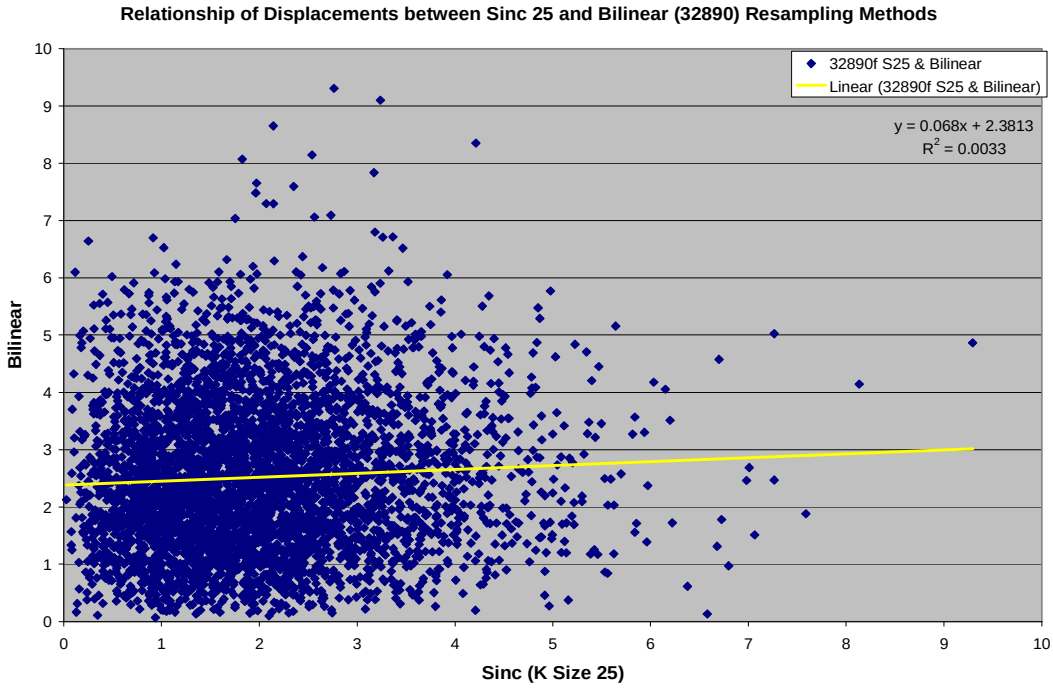

Figure A- 9. Scatter plot for comparison of resultant displacement for Sinc 25 & Bilinear resampling methods

.

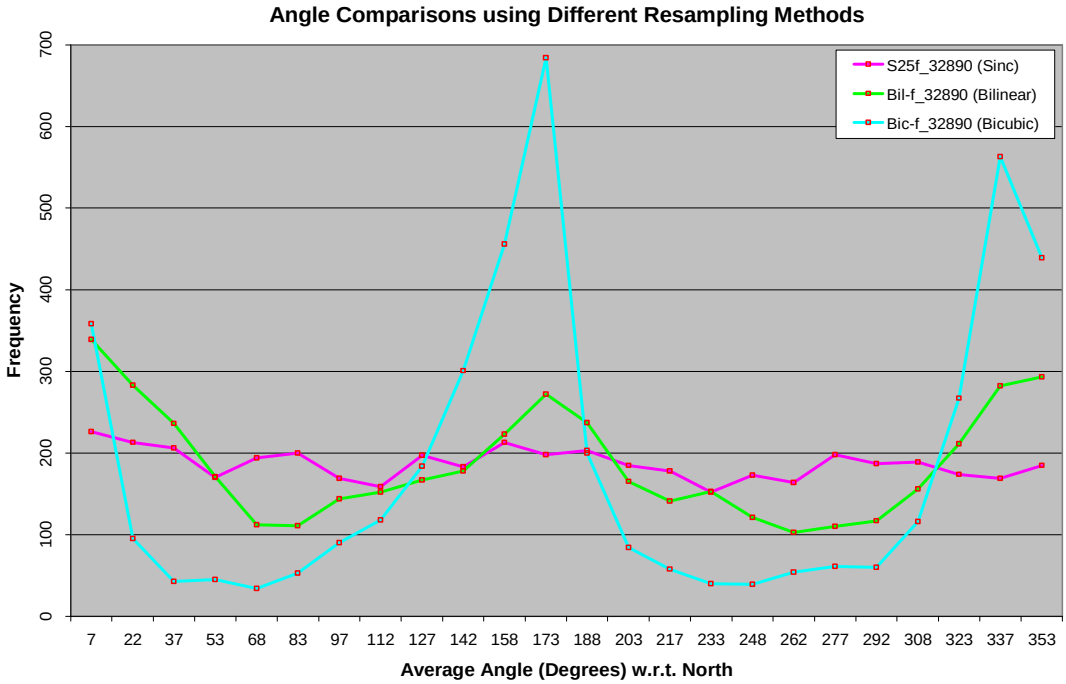

Figure A- 10. Average angle (direction of displacement) of different intervals for resampling methods

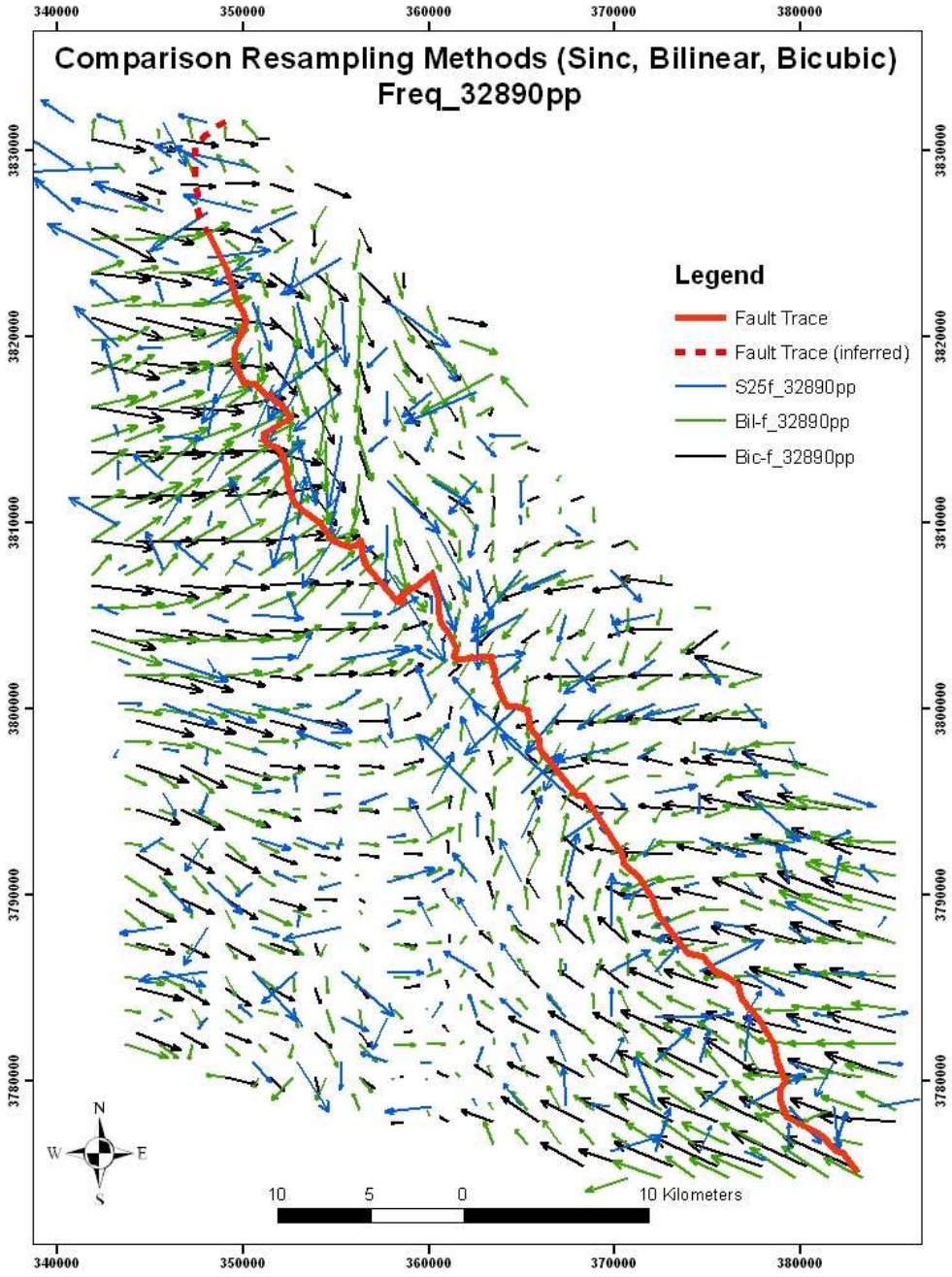

Figure A- 11. Vector Field comparisons of displacement for resampling methods

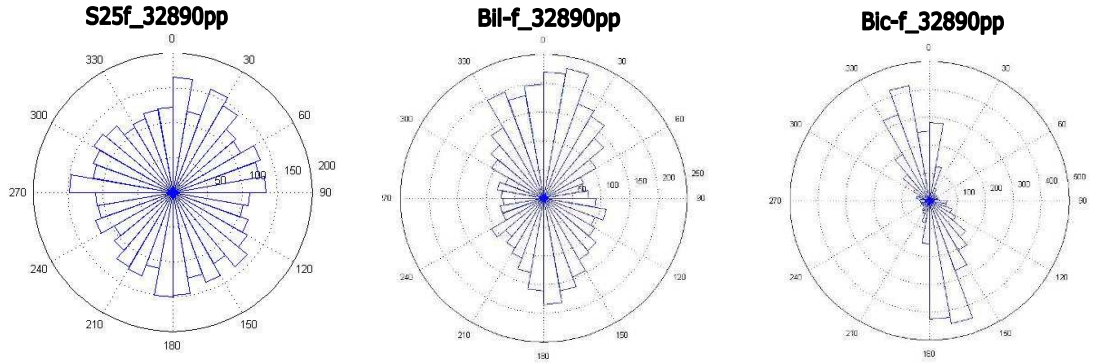

Figure A- 12. Rose diagrams showing displacement directions for three resampling methods

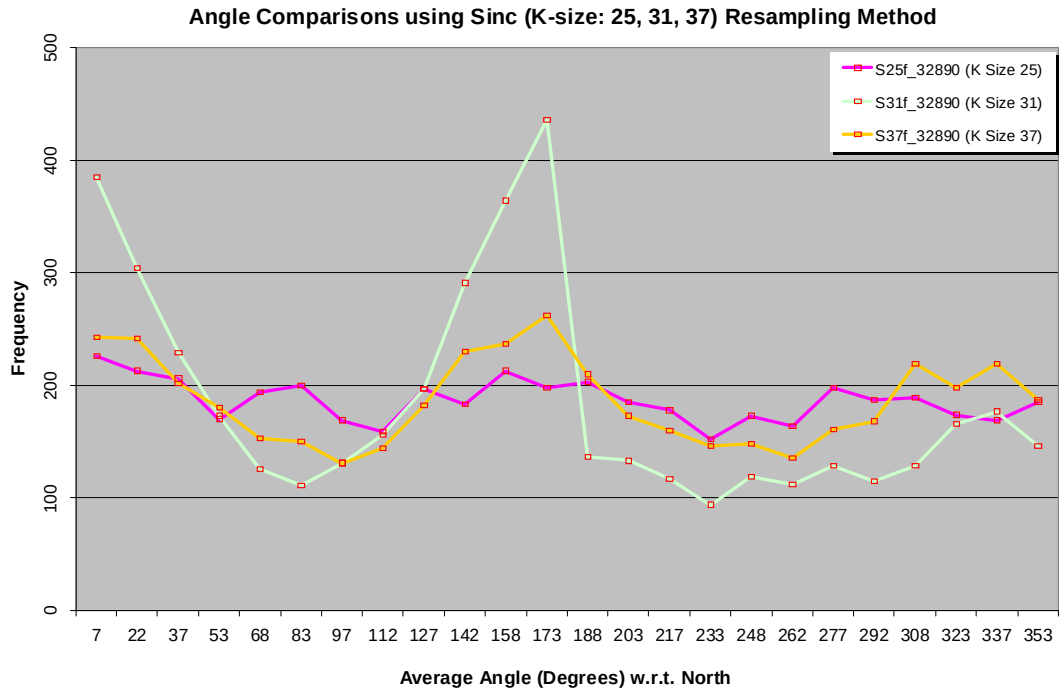

Figure A- 13. Average angle (direction of displacement) at defined different intervals for resampling methods

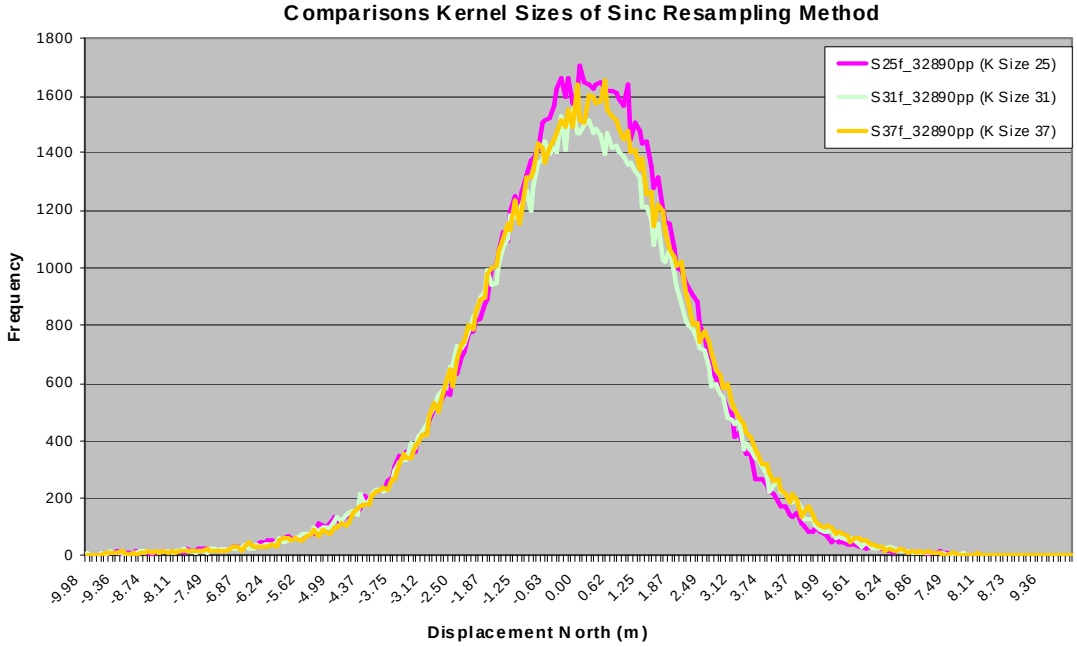

Figure A- 14. Histograms of displacement in North-South direction for kernel sizes of Sinc resampling method

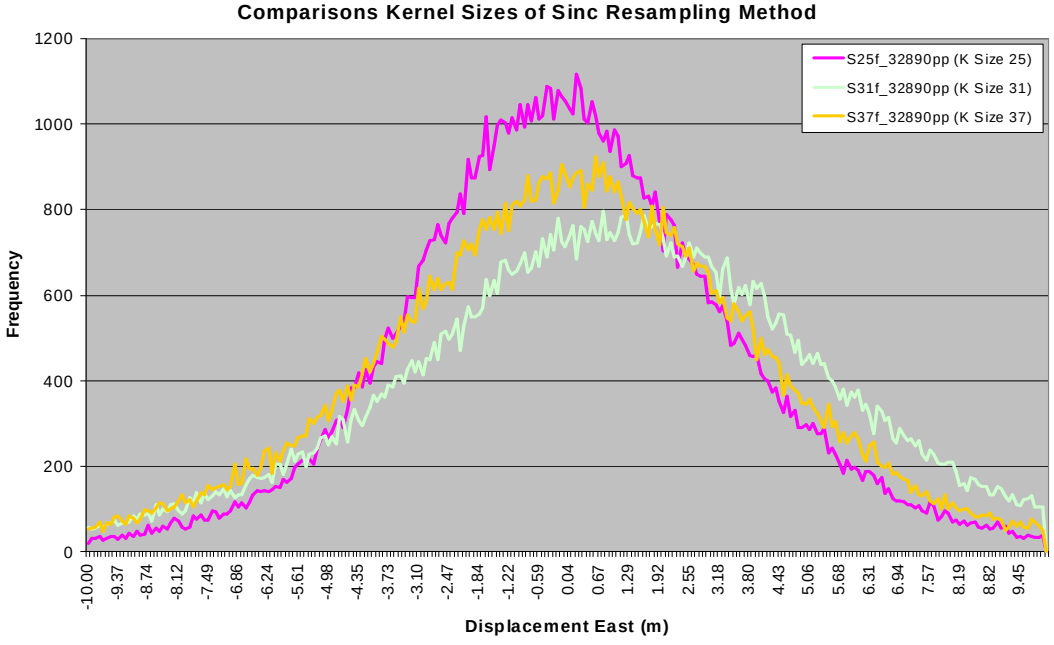

Figure A- 15. Histograms of displacement in East-West direction for kernel sizes of Sinc resampling method

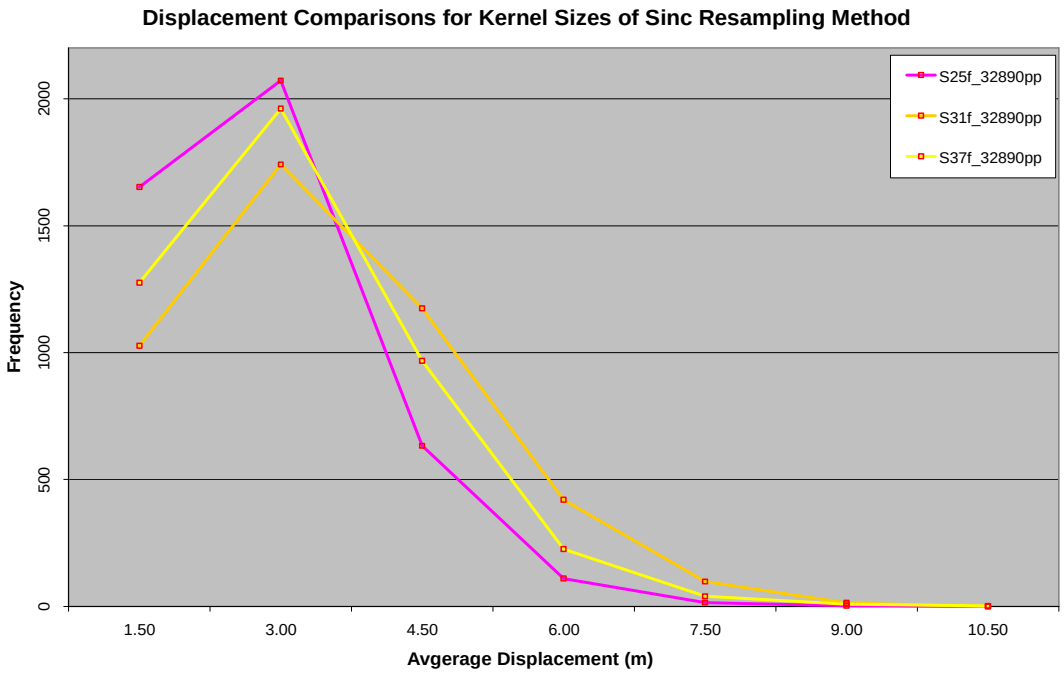

Figure A- 16. Average resultant displacement of different kernel sizes of Sinc resampling method

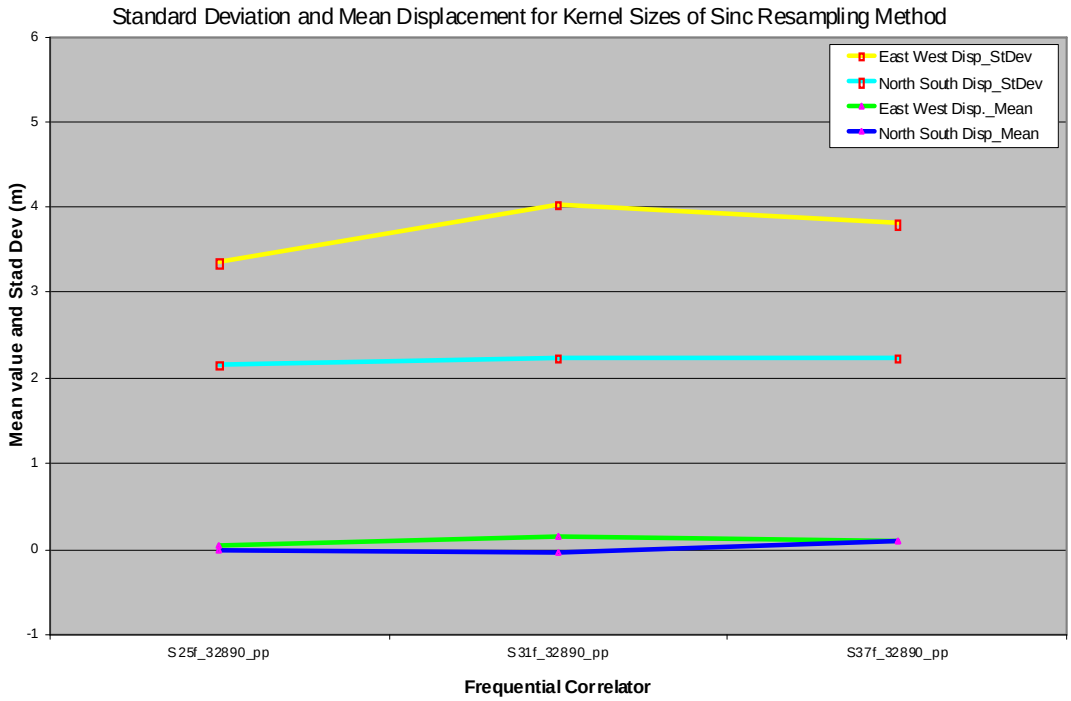

Figure A- 17. Mean and standard deviation both for North-South and East-West components of displacement for kernel sizes of Sinc resampling method

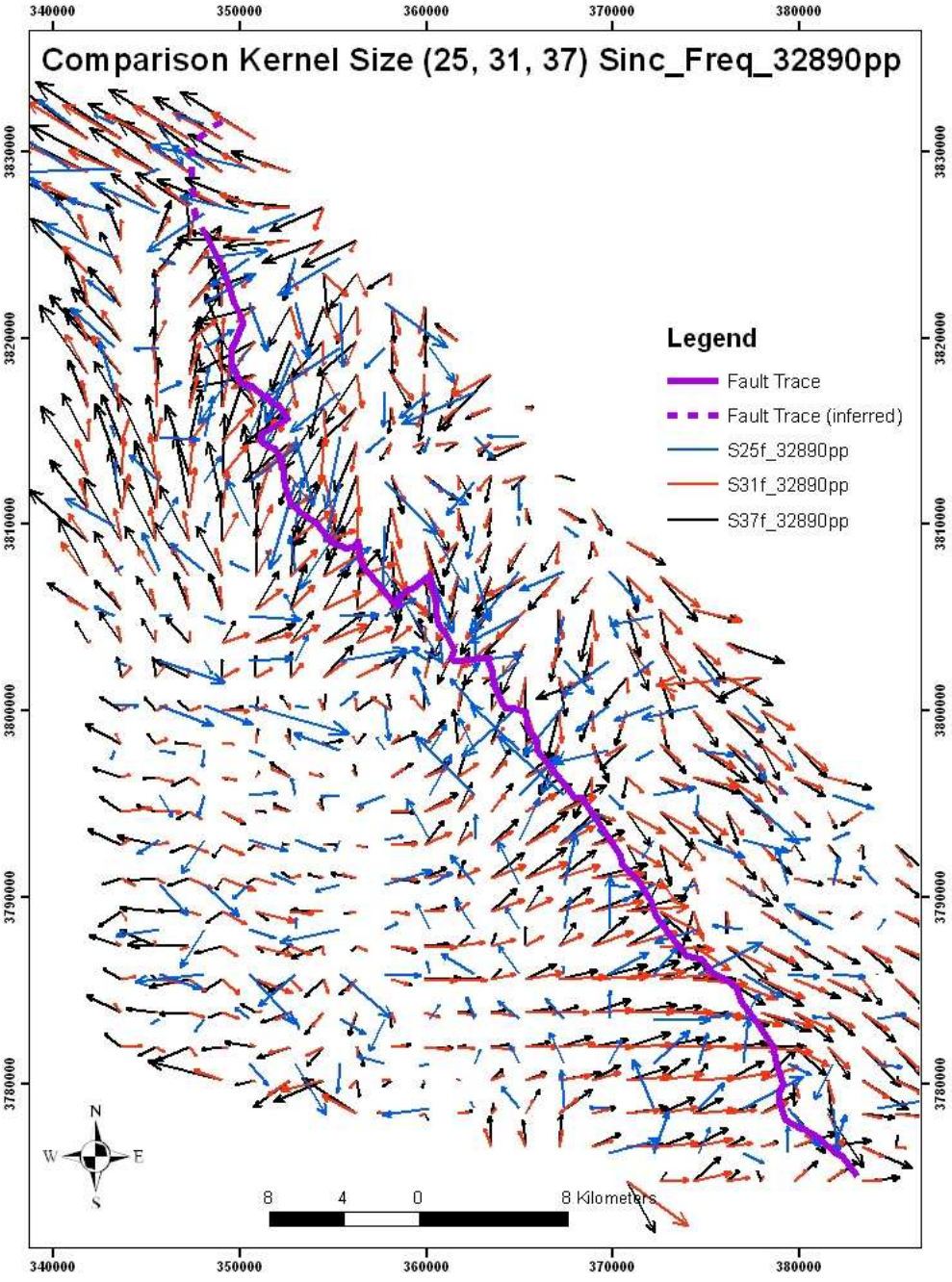

Figure A- 18. Vector Field comparisons of displacement for Kernel Size of Sinc resampling method

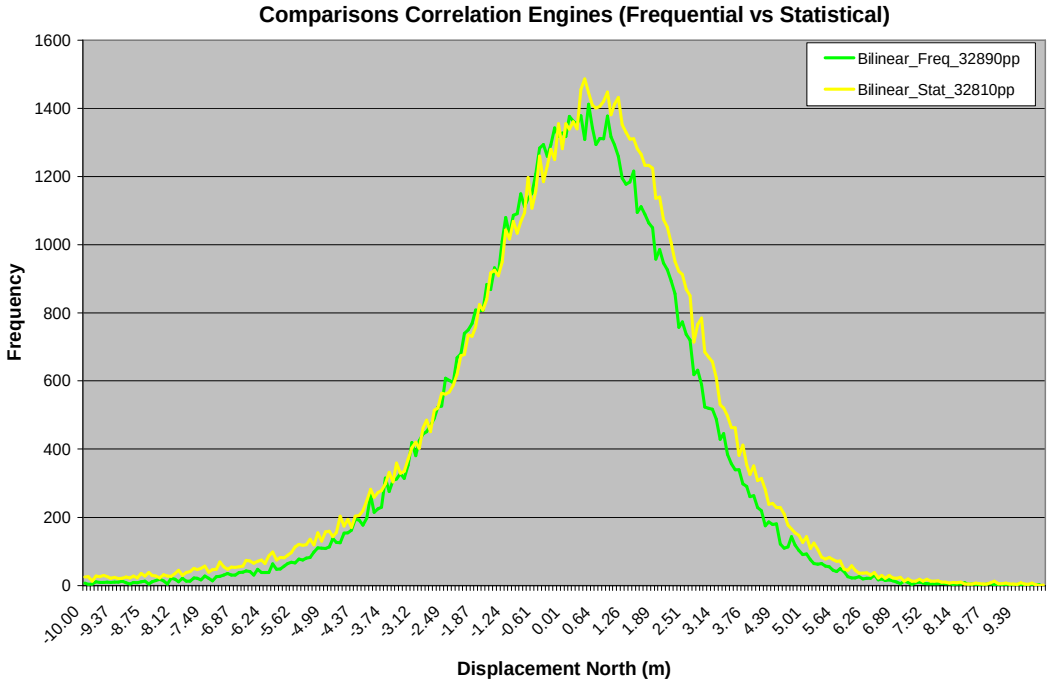

Figure A- 19. Histograms of displacement in North-South direction for different correlation methods

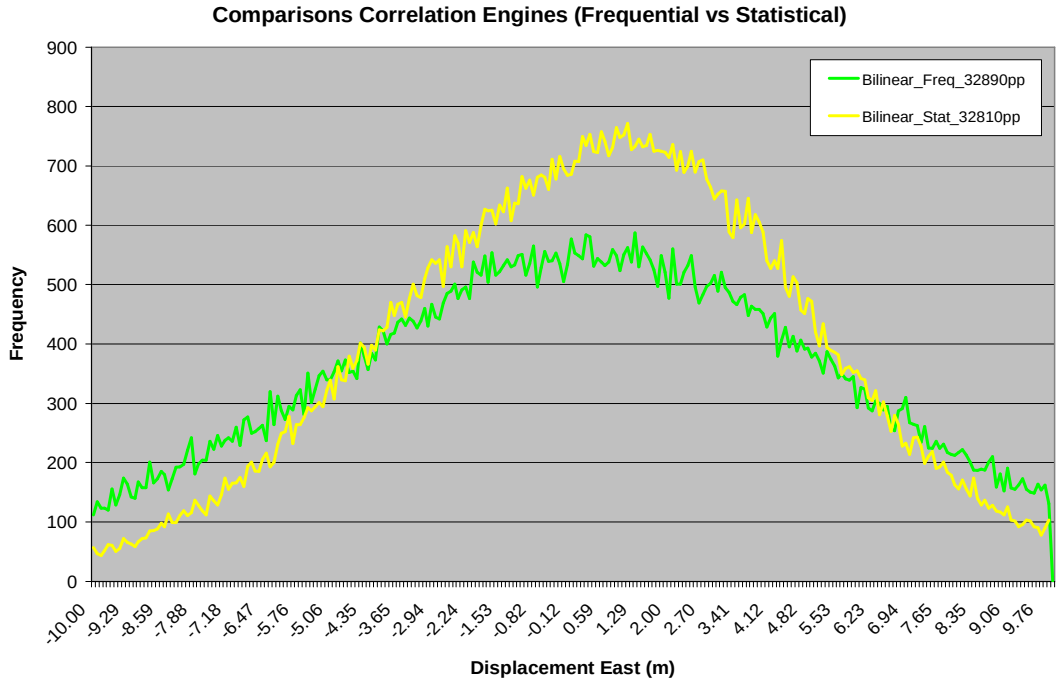

Figure A- 20. Histograms of displacement in East-West direction for different correlation methods

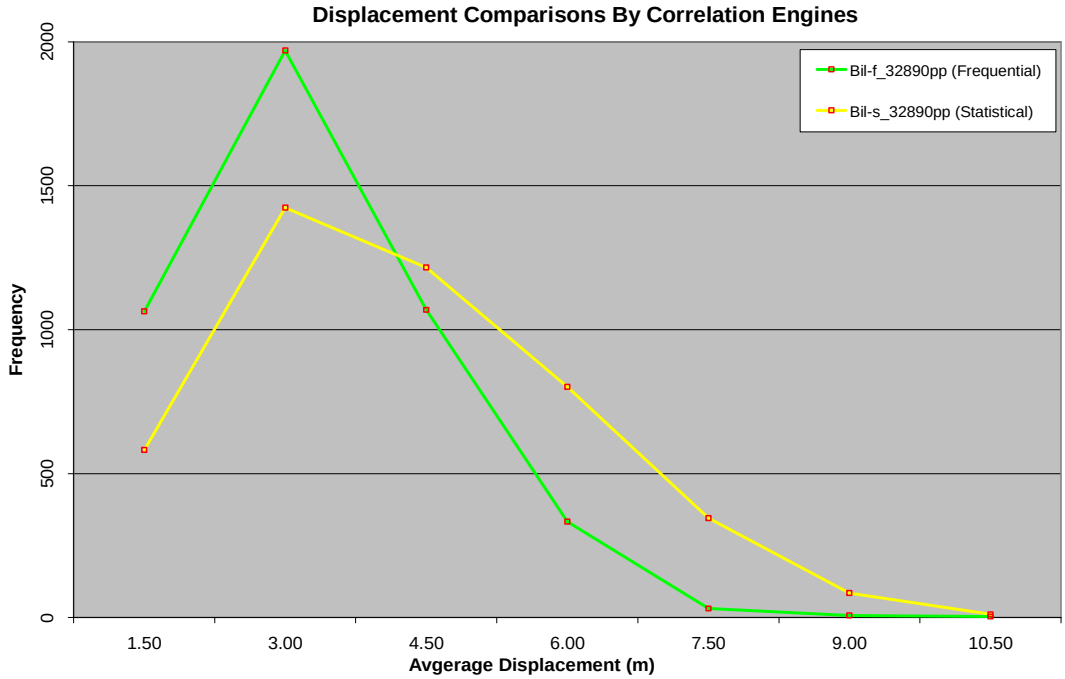

Figure A- 21. Average resultant displacement of different intervals for correlation methods using Bilinear resampling method

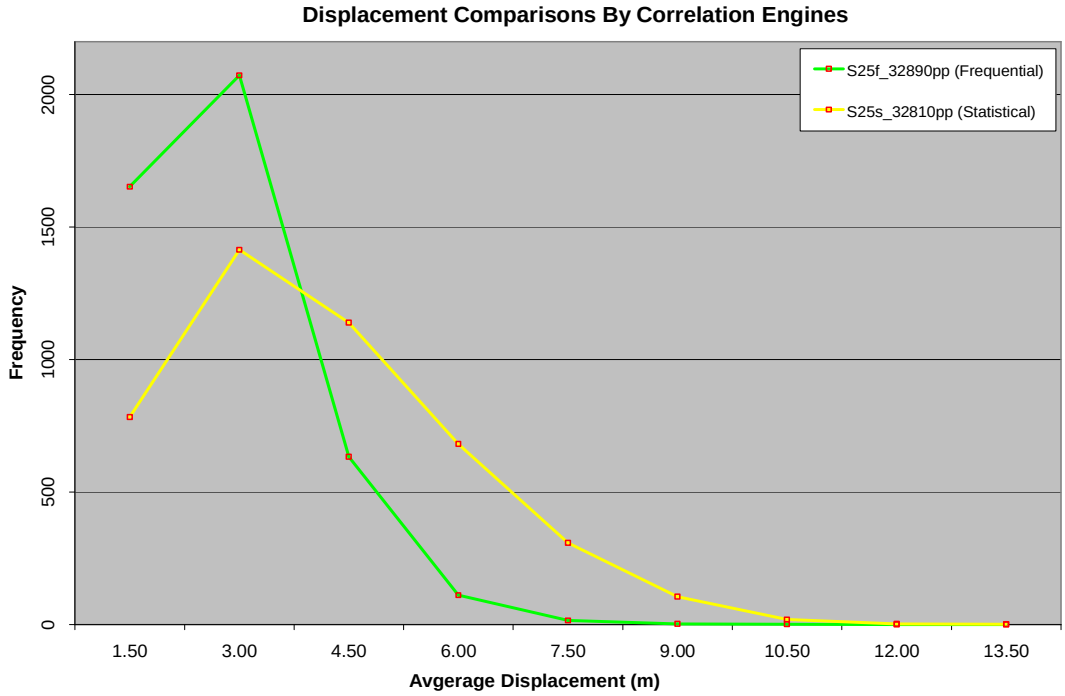

Figure A- 22. Average resultant displacement of different intervals for correlation methods using Sinc25 resampling method

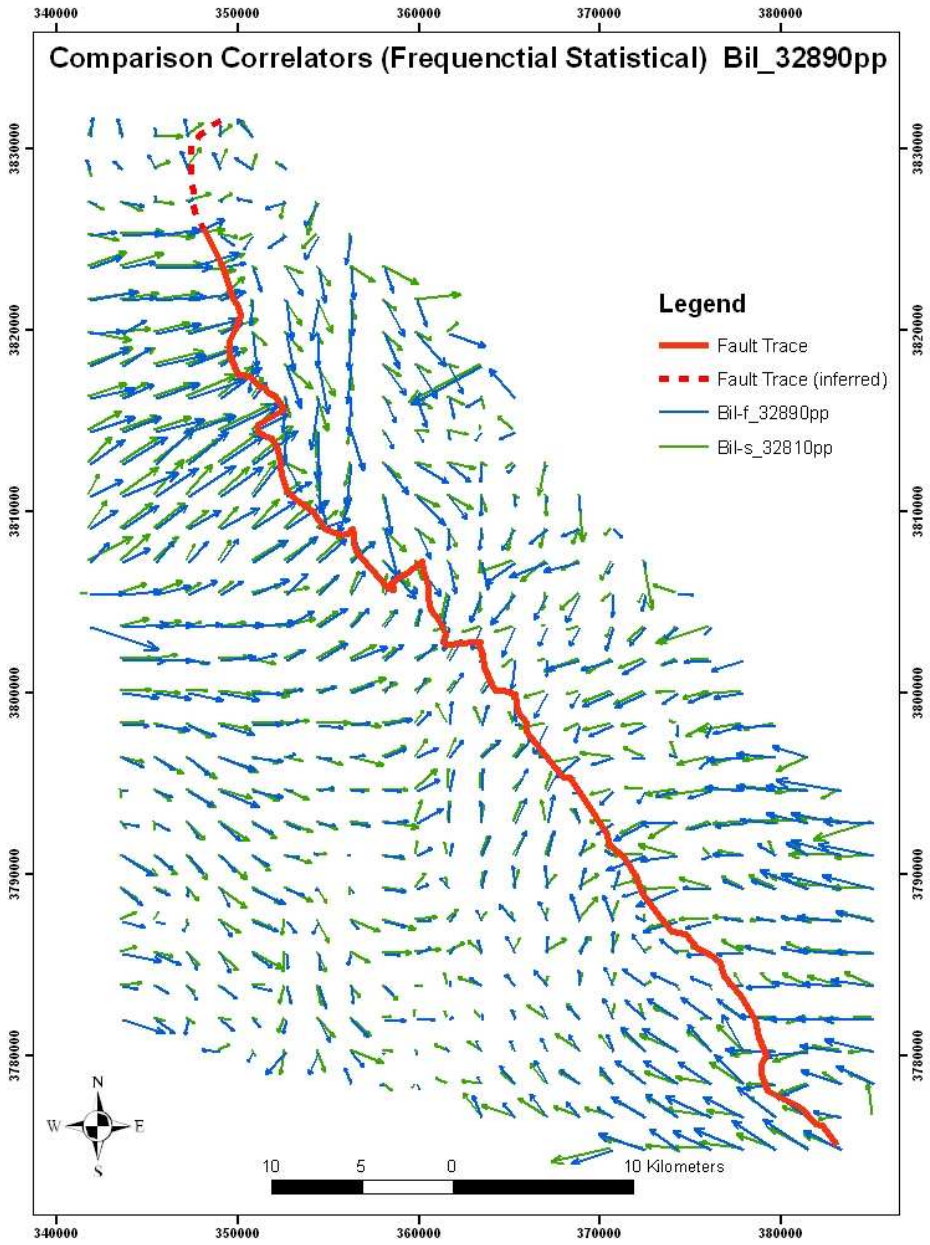

Figure A- 23. Vector Field comparisons of displacement for correlation methods

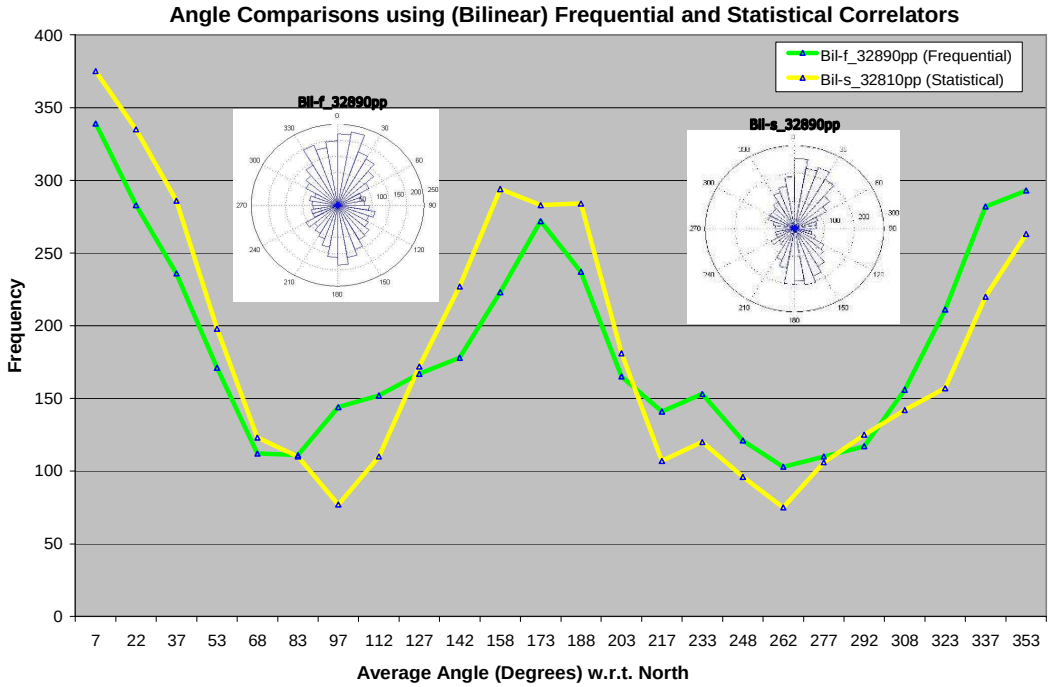

Figure A- 24. Average angle (direction of displacement) of different intervals for correlation methods using Bilinear resampling method

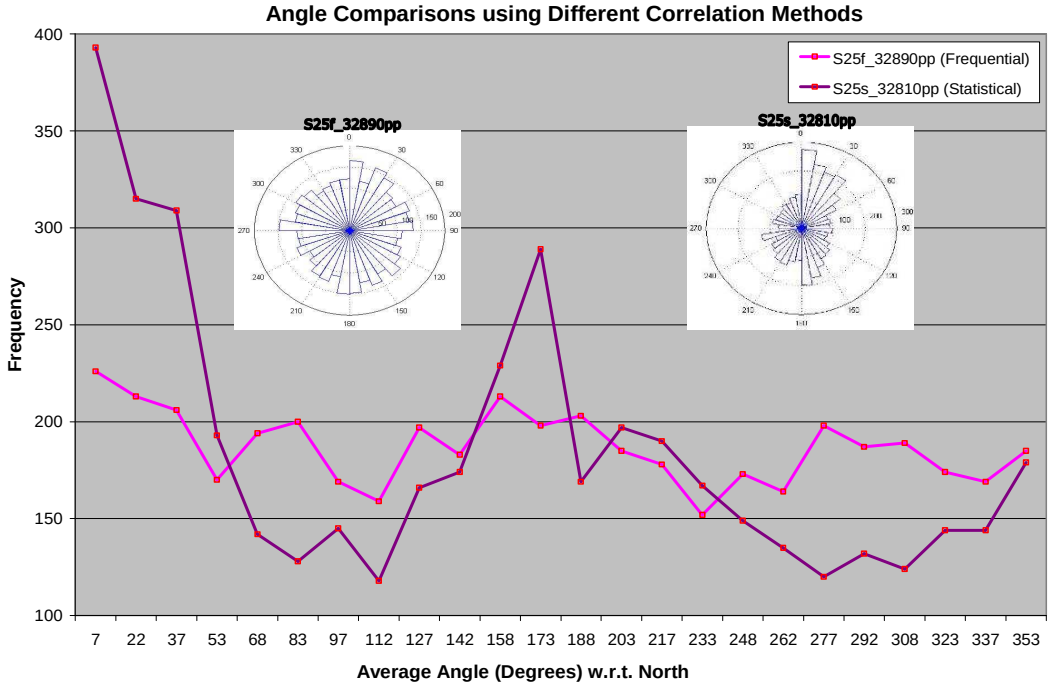

Figure A- 25. Average angle (direction of displacement) of different intervals for correlation methods using Sinc25 resampling method

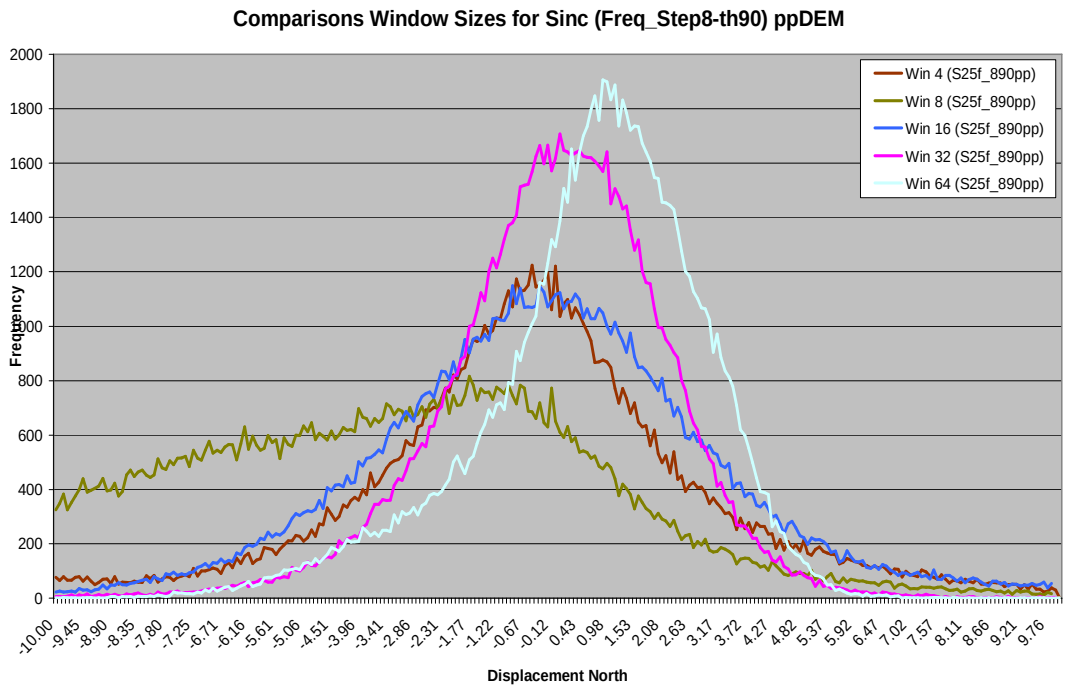

Figure A- 26. Histograms of displacement in North-South direction for different window sizes of Frequential correlation method

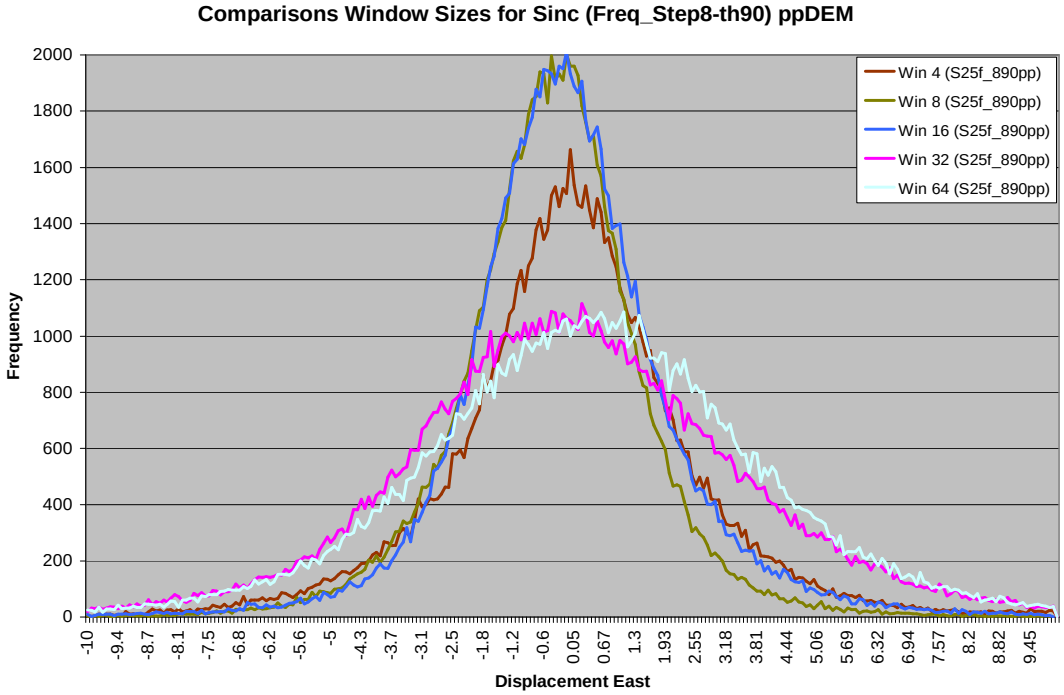

Figure A- 27. Histograms of displacement in East-West direction for different window sizes of Frequential correlation method

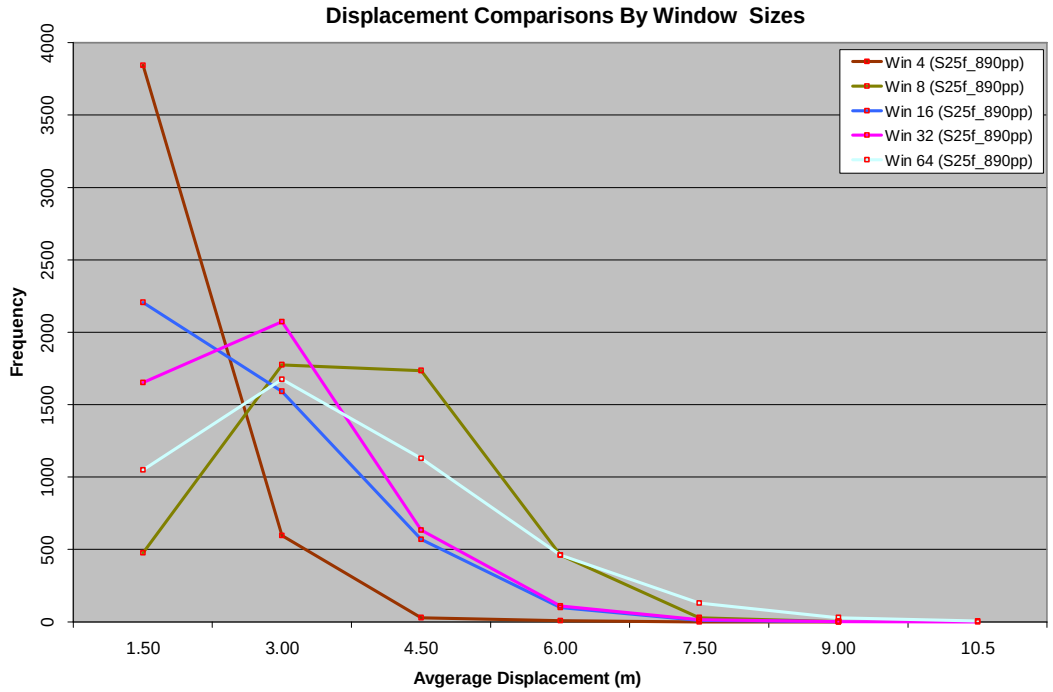

Figure A- 28. Average resultant displacement of different intervals for window sizes of Frequential correlation method

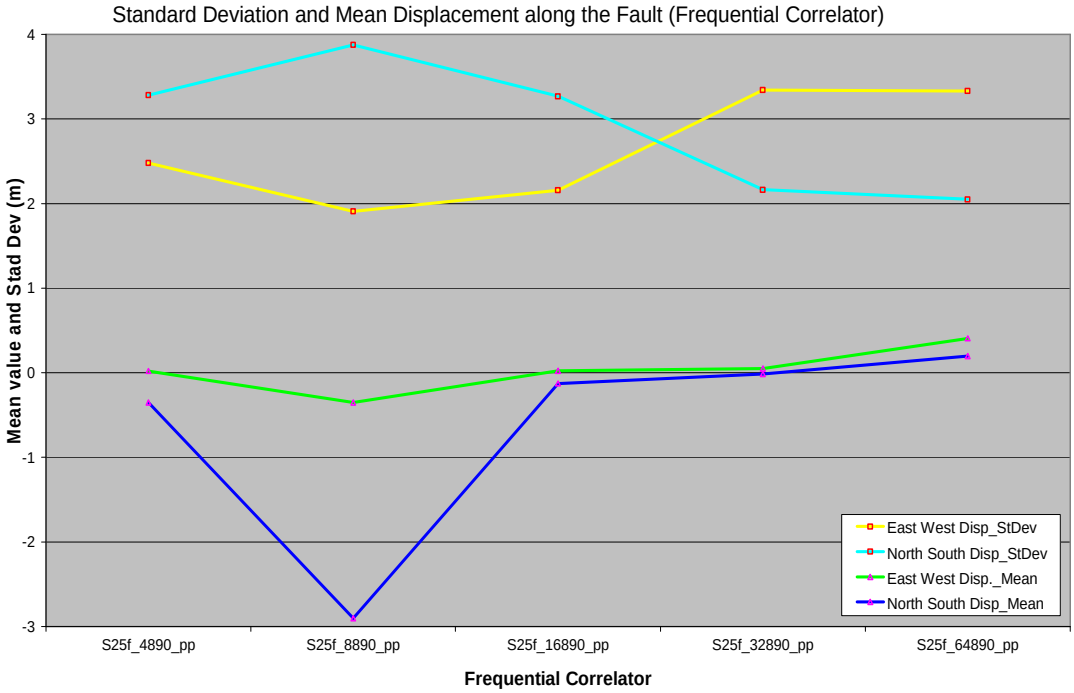

Figure A- 29. Mean and standard deviation both for North-South and East-West components of displacement for window sizes of Frequential correlation method

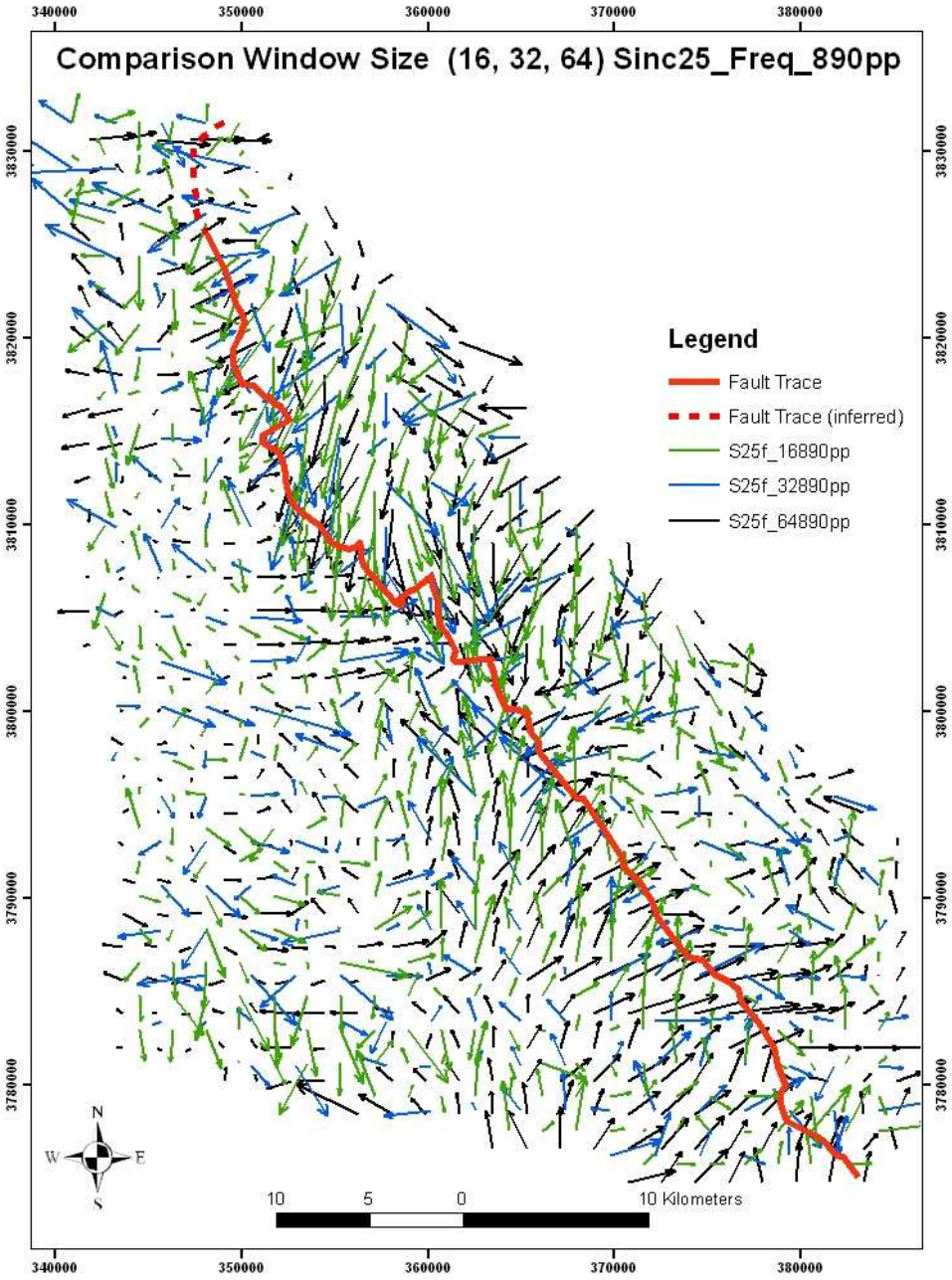

Figure A- 30. Vector Field comparisons of displacement for window sizes of Frequential correlation method

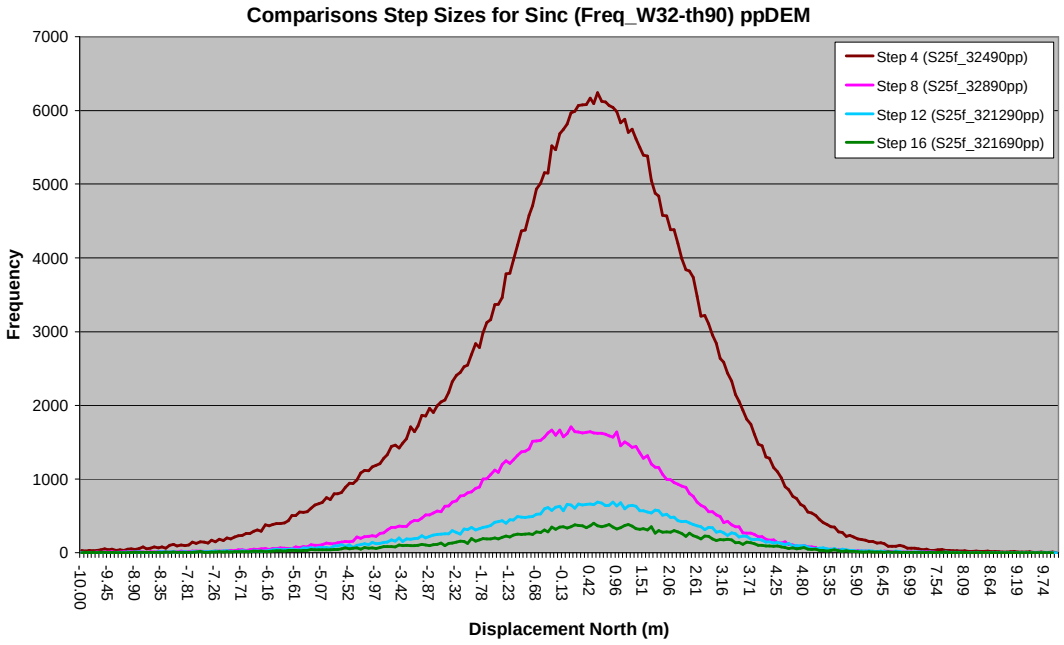

Figure A- 31. Histograms of displacement in North-South direction for different step sizes of Frequential correlation method

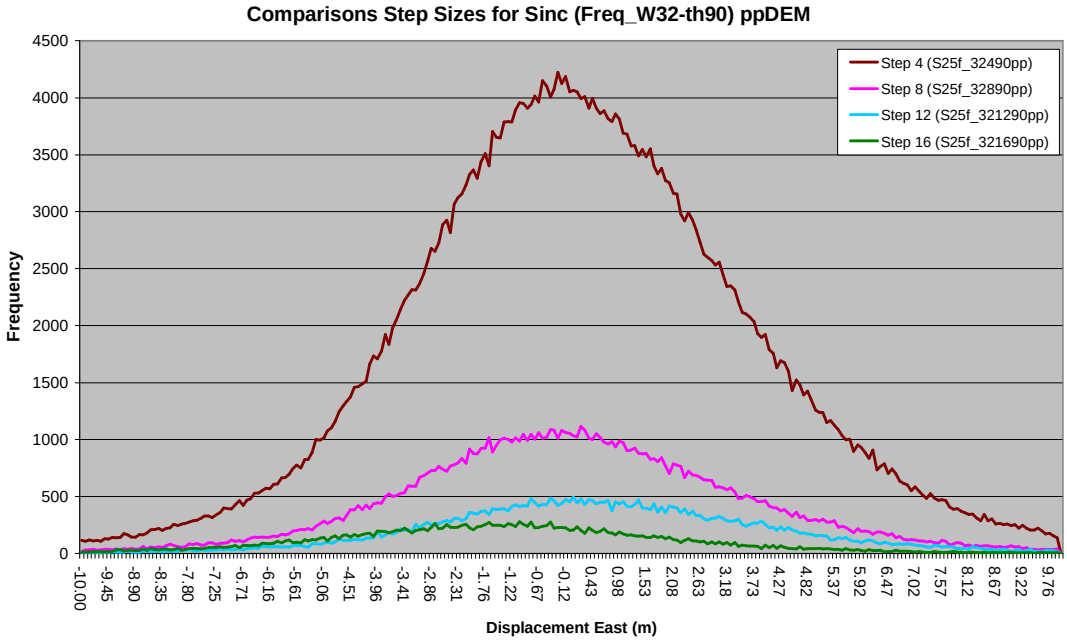

Figure A- 32. Histograms of displacement in East-West direction for different step sizes of Frequential correlation method

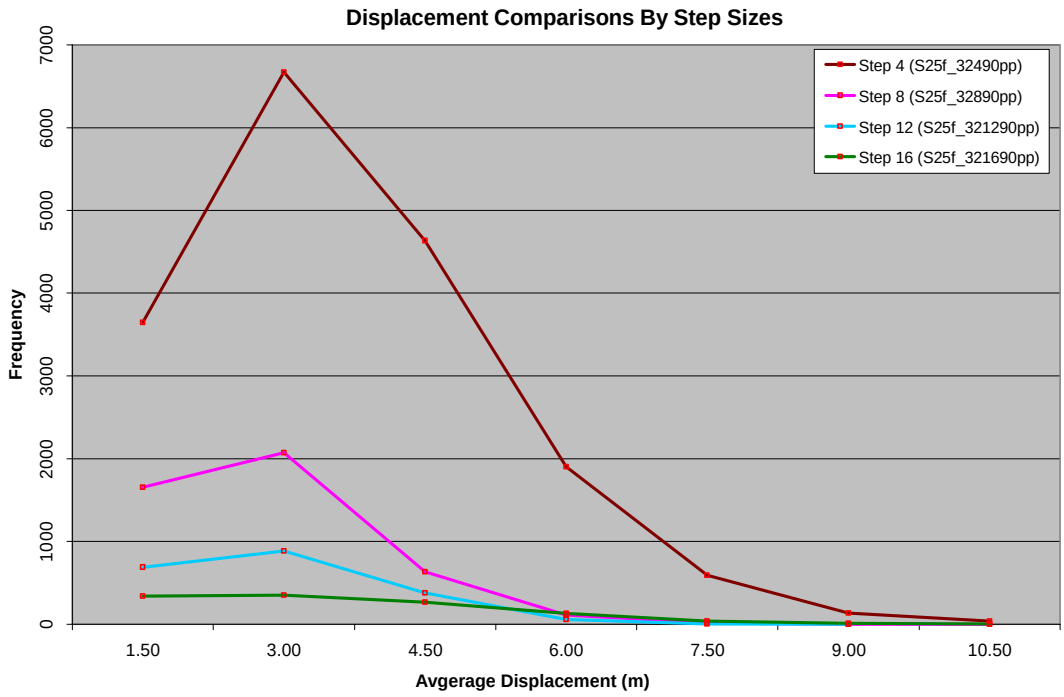

Figure A- 33. Average resultant displacement of different intervals for step sizes of Frequential correlation method

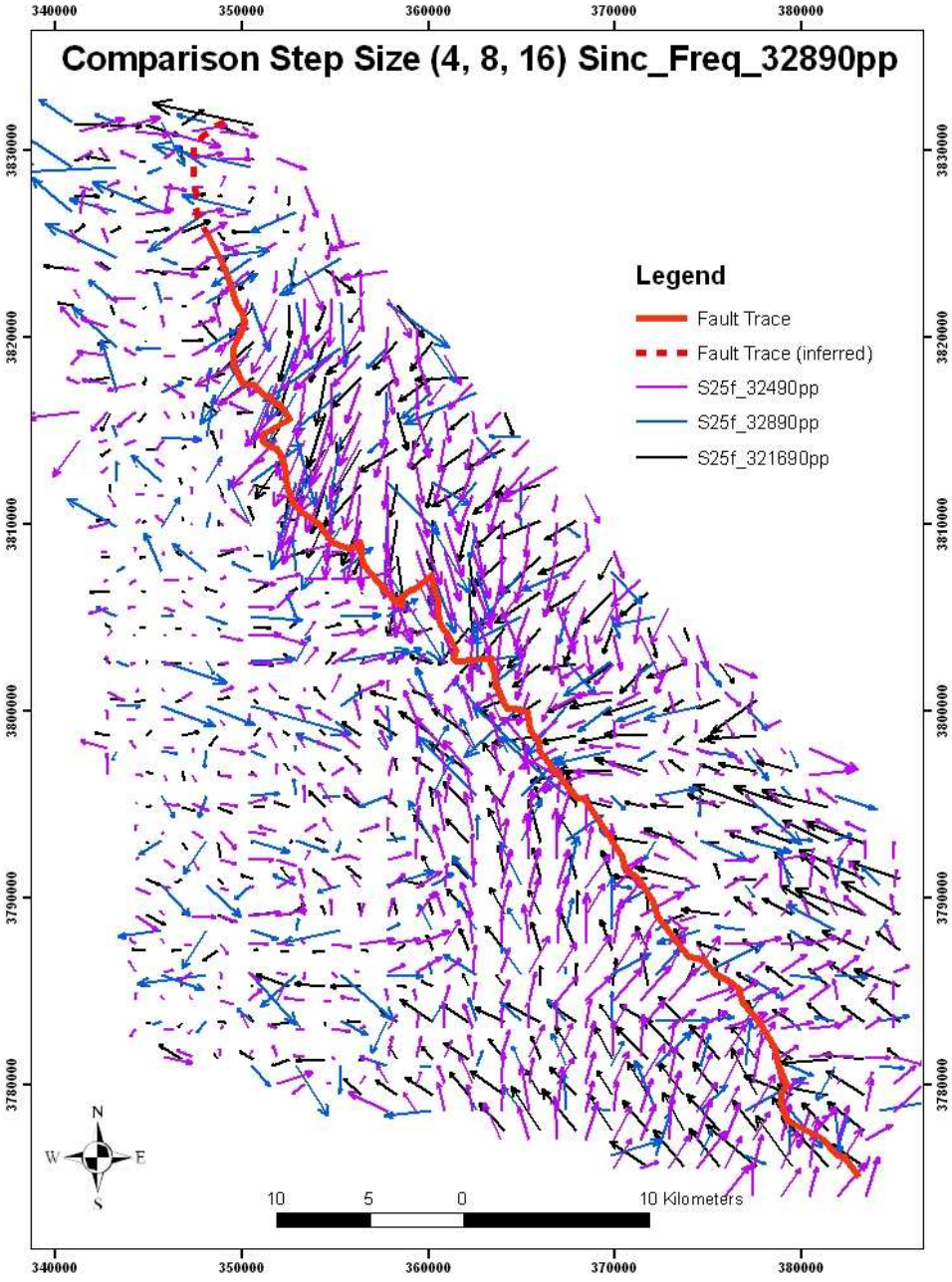

Figure A- 34. Vector Field comparisons of displacement for step sizes of Frequential correlation method

.

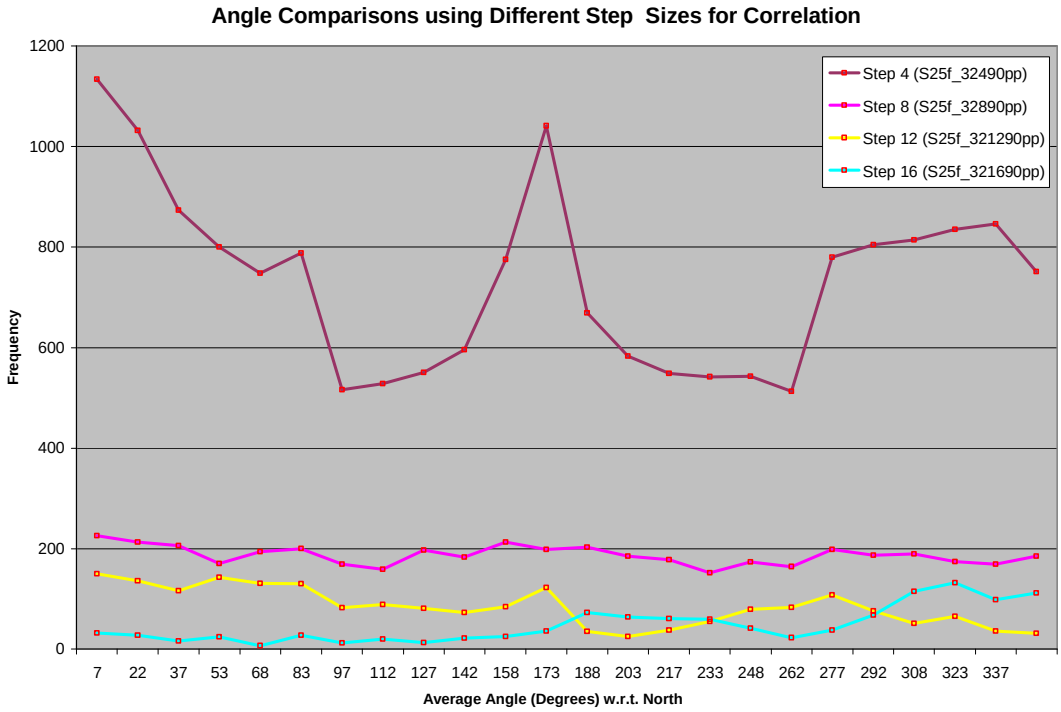

Figure A- 35. Average angle (direction of displacement) of different intervals for Step sizes of Frequential correlation method

.

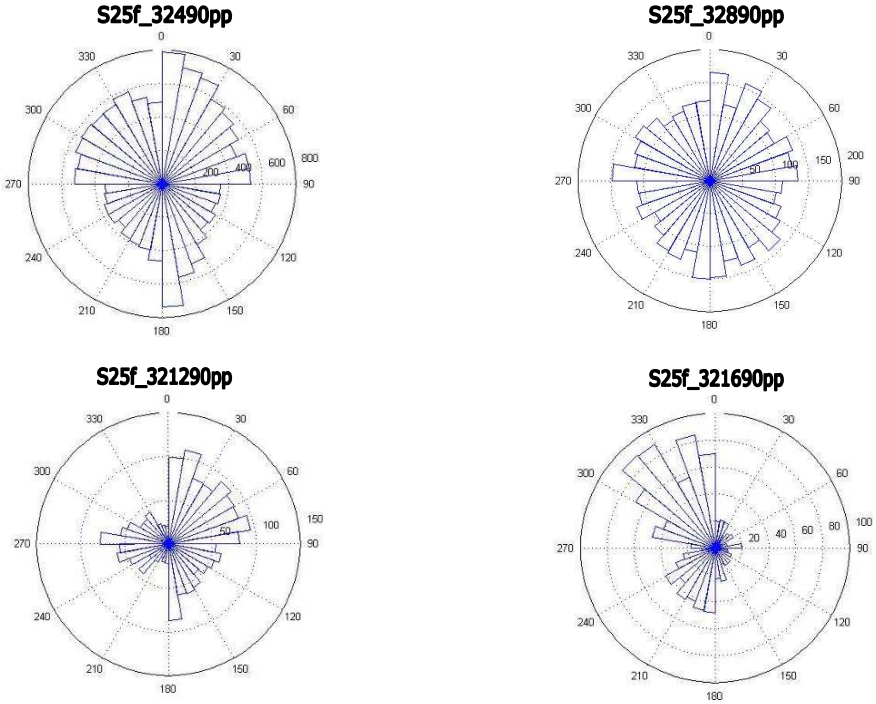

Figure A- 36. Rose diagrams showing displacement directions for different step sizes of Sinc resampling method

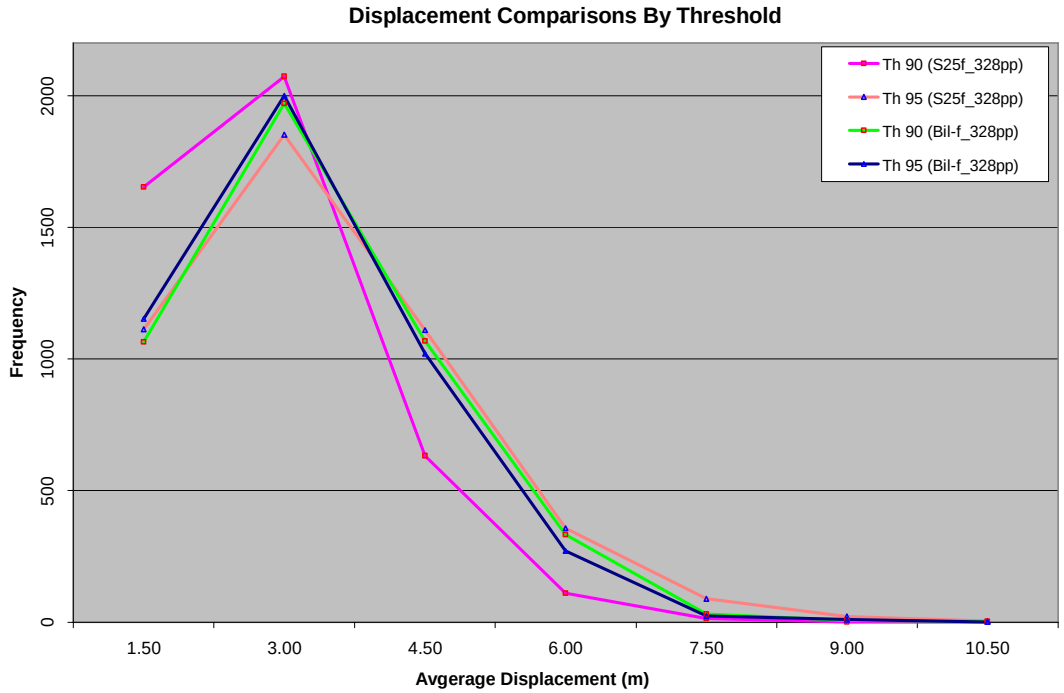

Figure A- 37. Average resultant displacement of different intervals for Threshold of Frequential correlation method

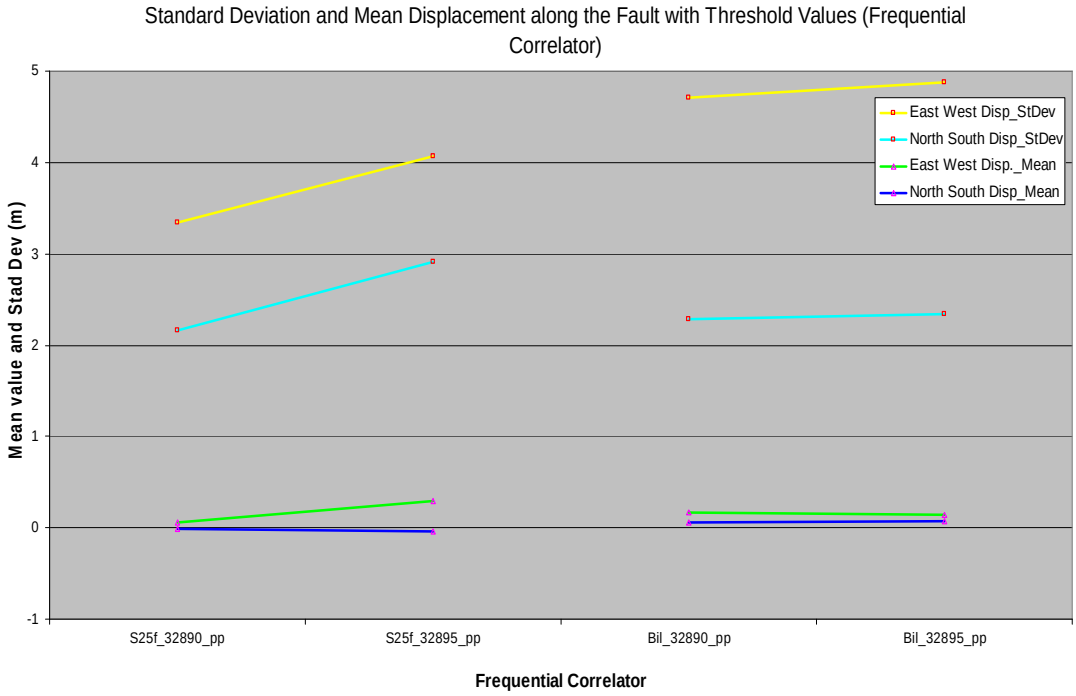

Figure A- 38. Mean and standard deviation both for North-South and East-West components of displacement for Threshold of Frequential correlation method

.

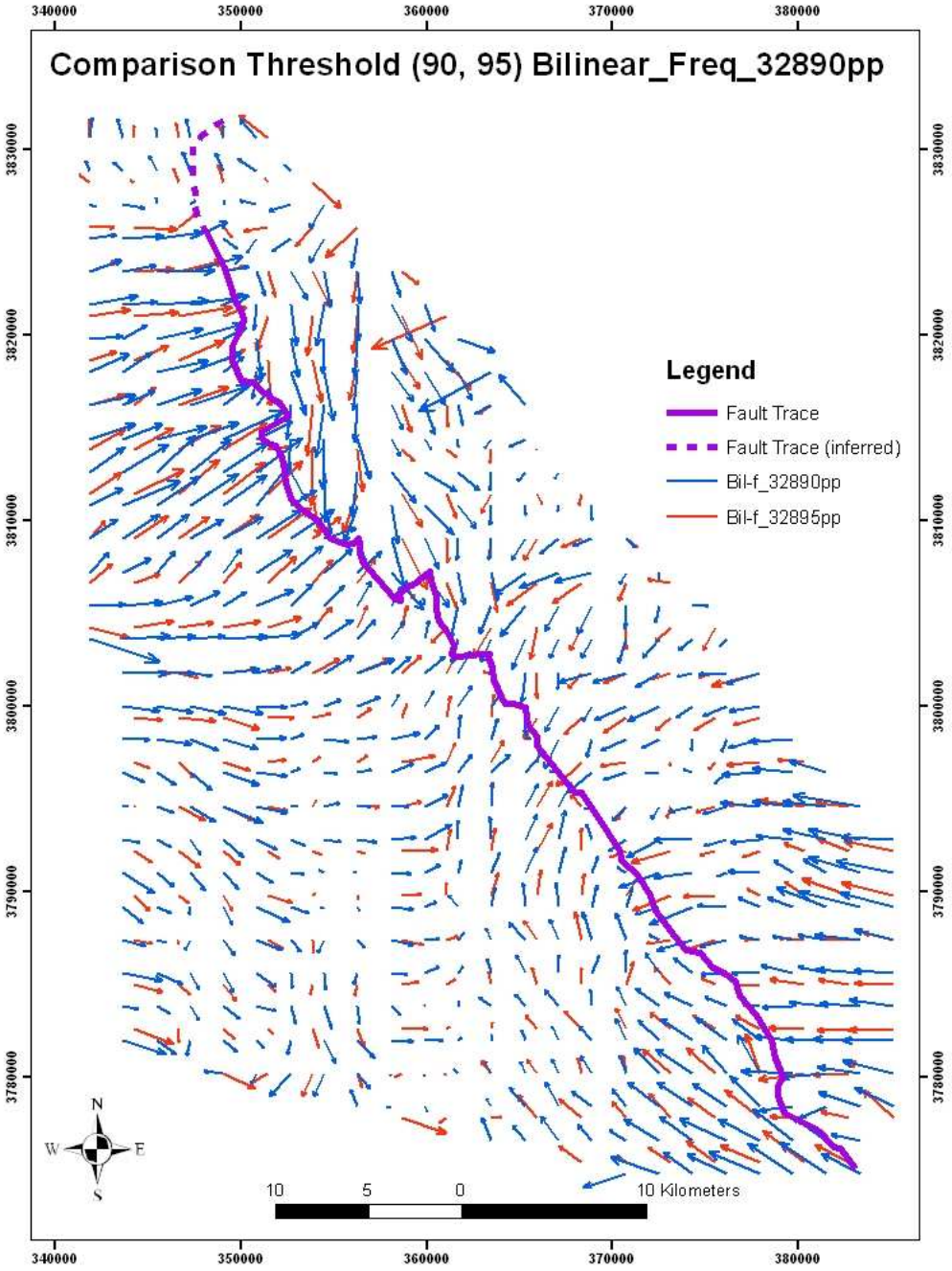

Figure A- 39. Vector Field comparisons of displacement for Threshold of Frequential correlation engine using Bilinear resampling method

.

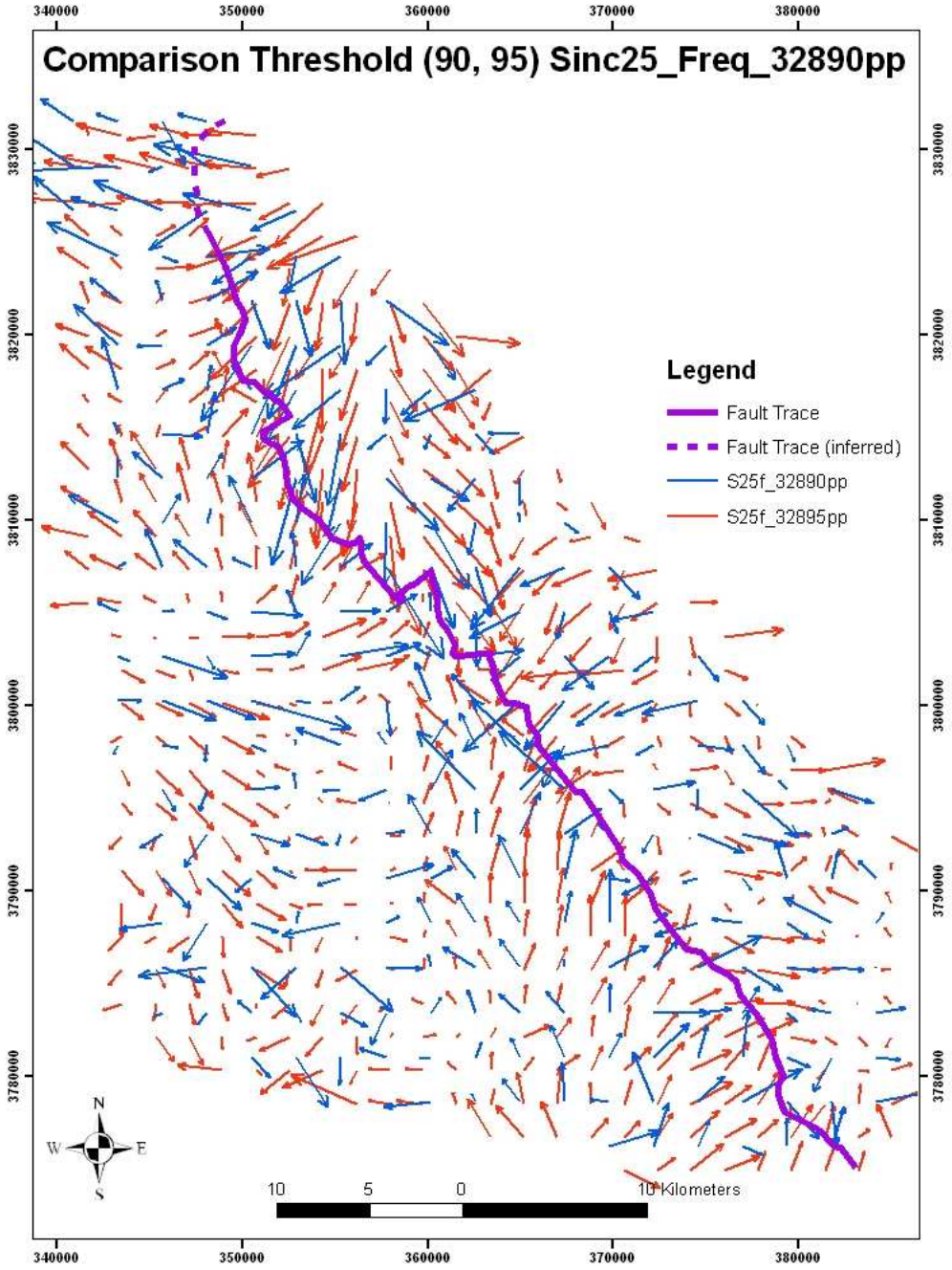

Figure A- 40. Vector Field comparisons of displacement for Threshold of Frequential correlation engine using Sinc25 resampling method

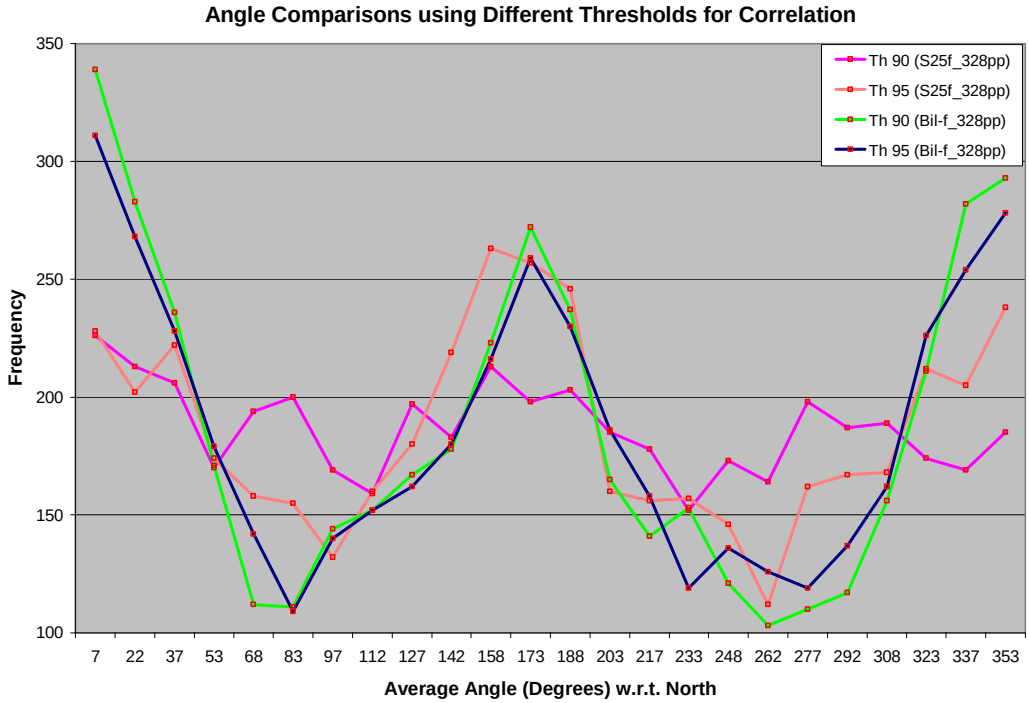

Figure A- 41. Average angle (direction of displacement) of different intervals for Threshold of Frequential correlation method

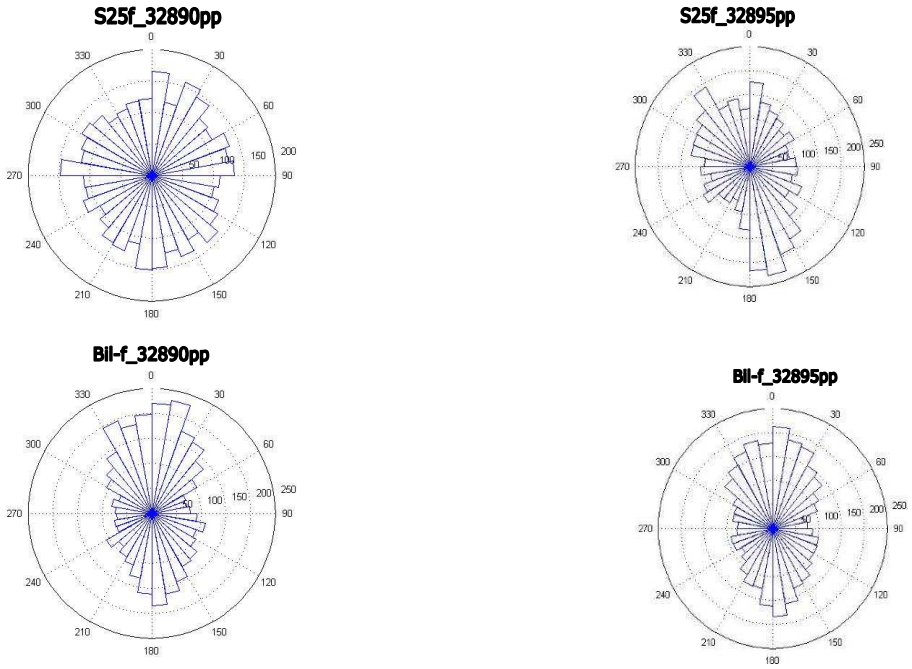

Figure A- 42. Rose diagrams showing displacement directions for different threshold values using Sinc25 and Bilinear resampling methods

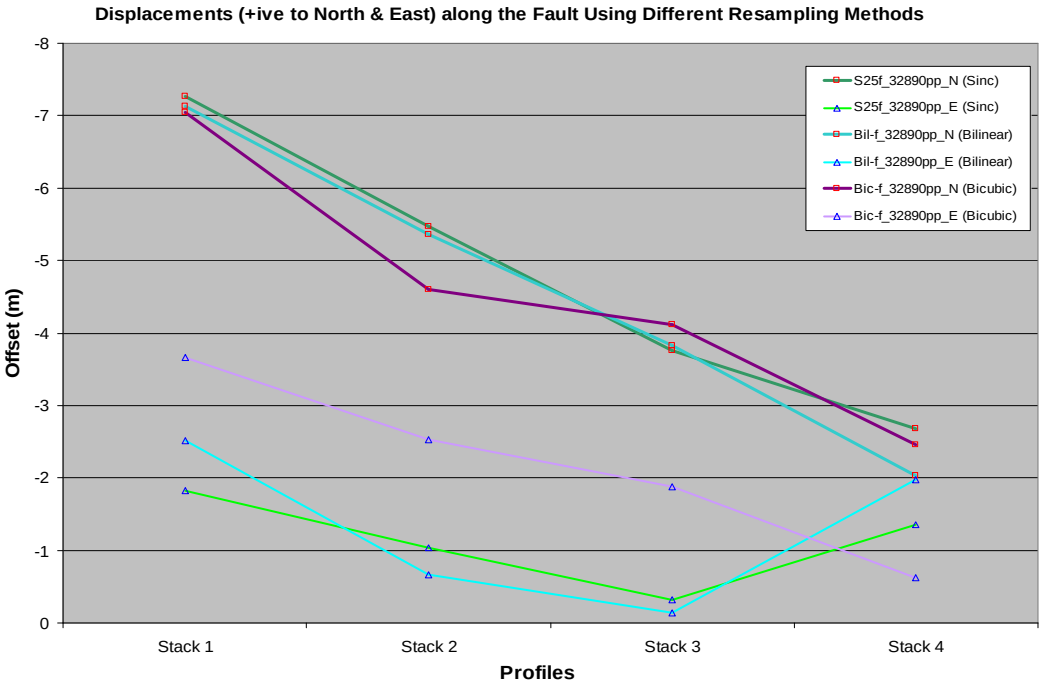

Figure A- 43. Displacement measurement along the fault at selected locations using different resampling methods

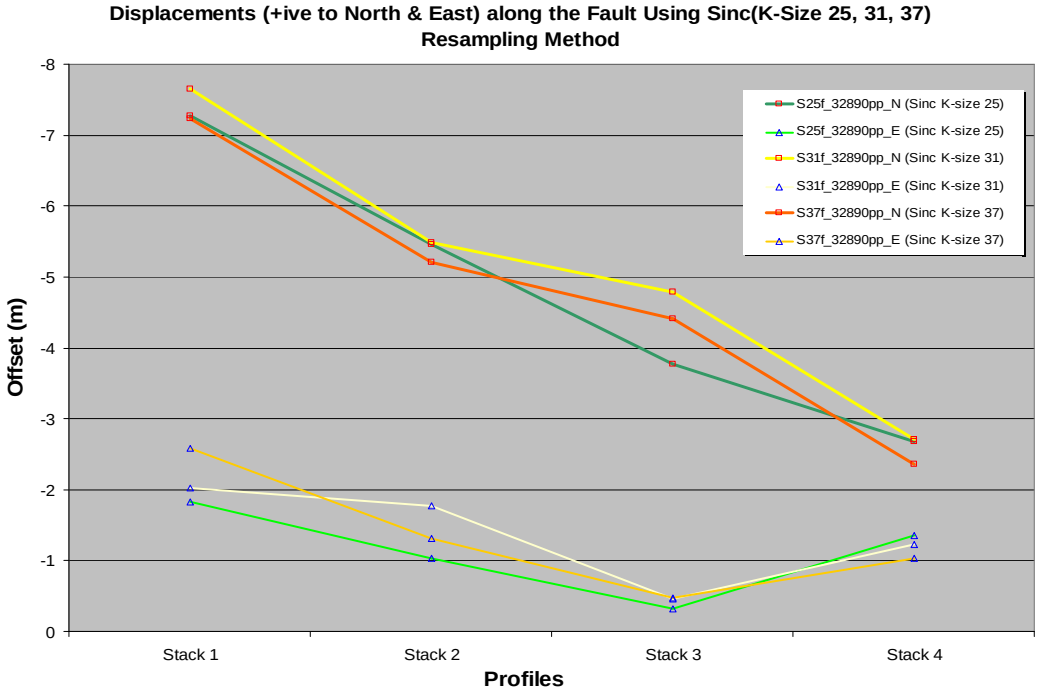

Figure A- 44. Displacement measurement along the fault at selected locations using different kernel sizes of Sinc resampling method

.

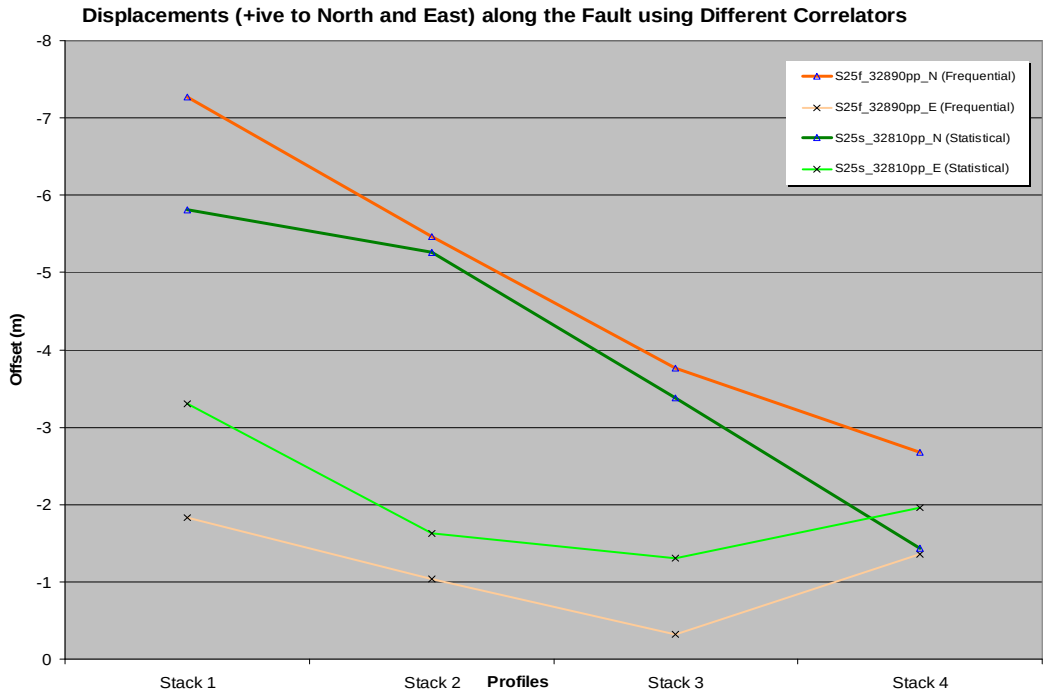

Figure A- 45. Displacement measurement along the fault at selected locations using different Correlators

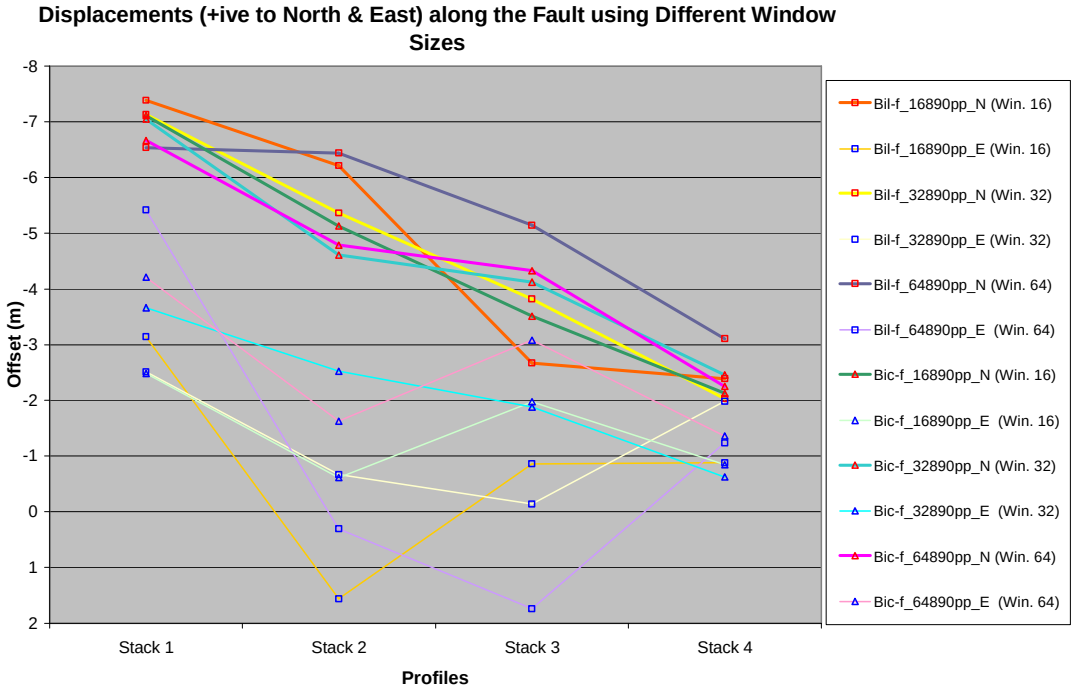

Figure A- 46. Displacement measurement along the fault at selected locations using different window sizes for Bilinear and Bicubic resampling methods

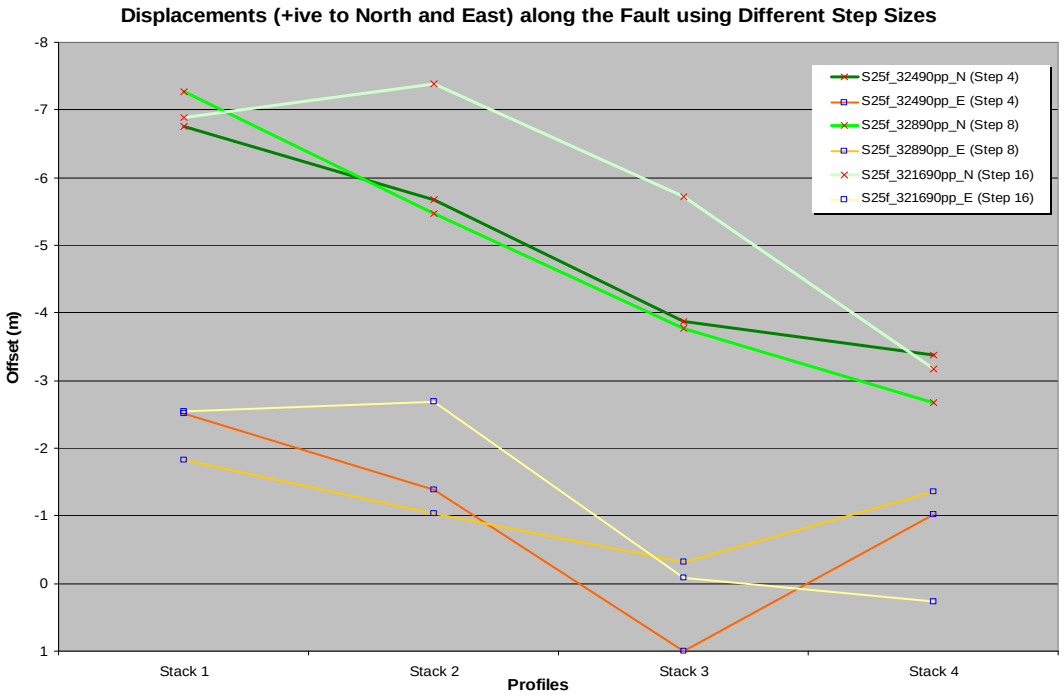

Figure A- 47. Displacement measurement along the fault at selected locations using different step sizes

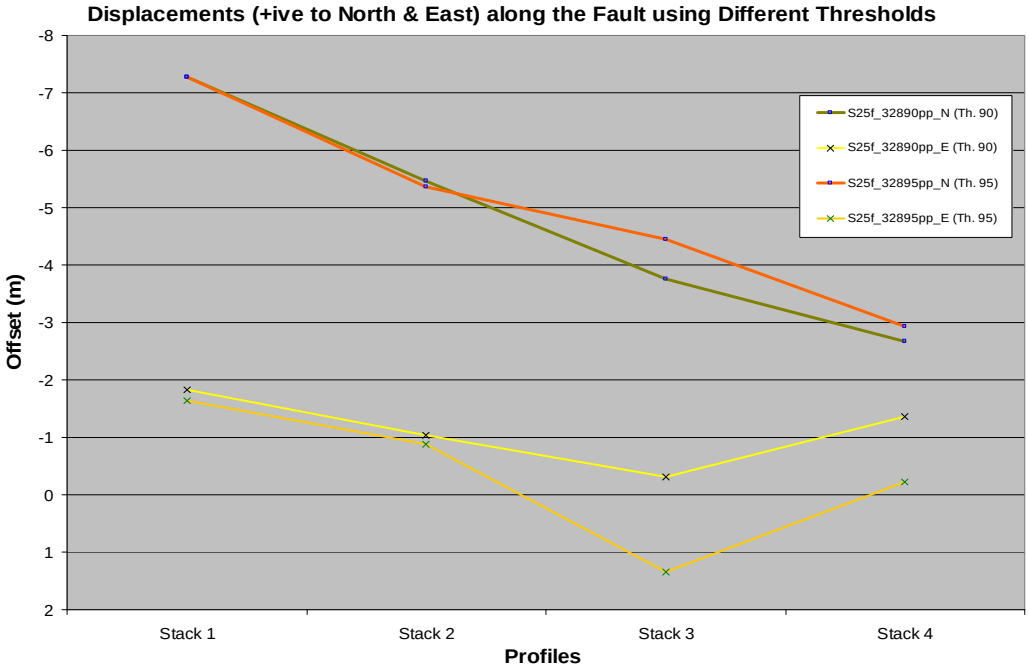

Figure A- 48. Displacement measurement along the fault at selected locations using different threshold values

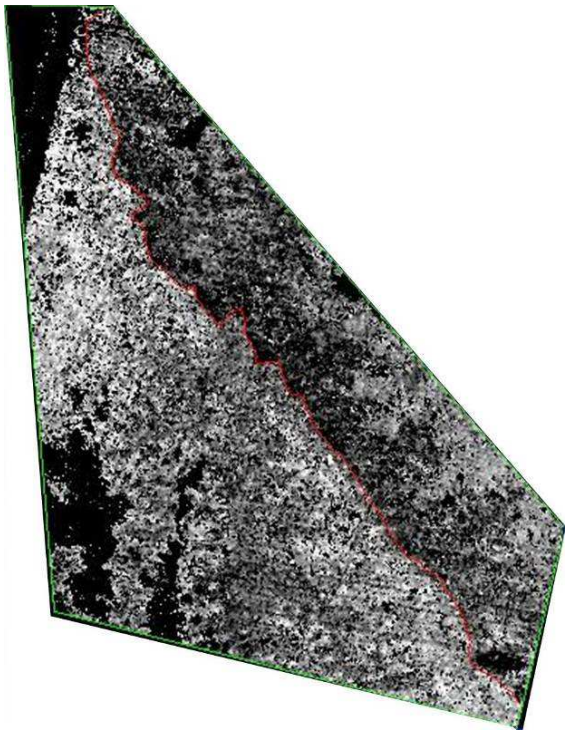

Figure A- 49. Correlation image of 2nd pair of image bracketing the earthquake

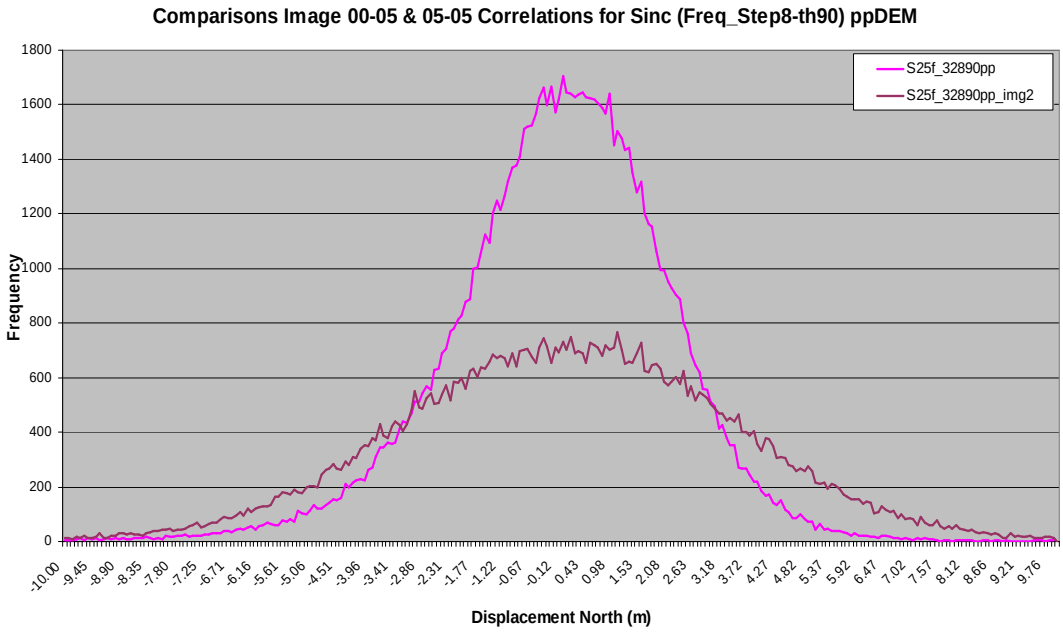

Figure A- 50. Histograms of displacement in North-South direction for two pairs of images bracketing the earthquake

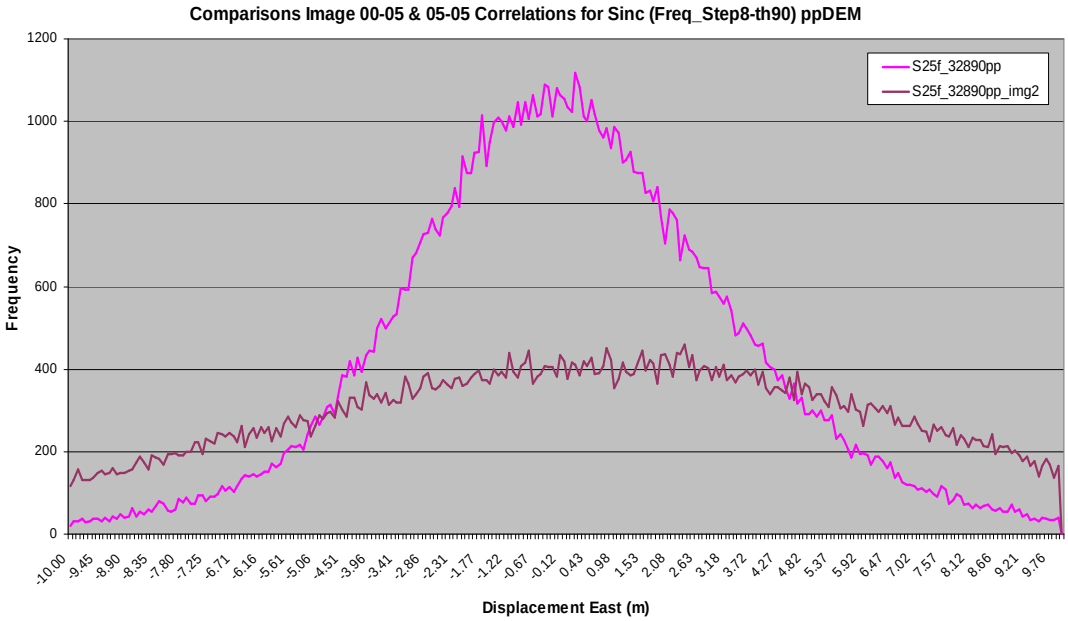

Figure A- 51. Histograms of displacement in East-West direction for two pairs of images bracketing the earthquake

Figure A- 52. Average resultant displacement of different intervals for two pairs of images bracketing the earthquake

.

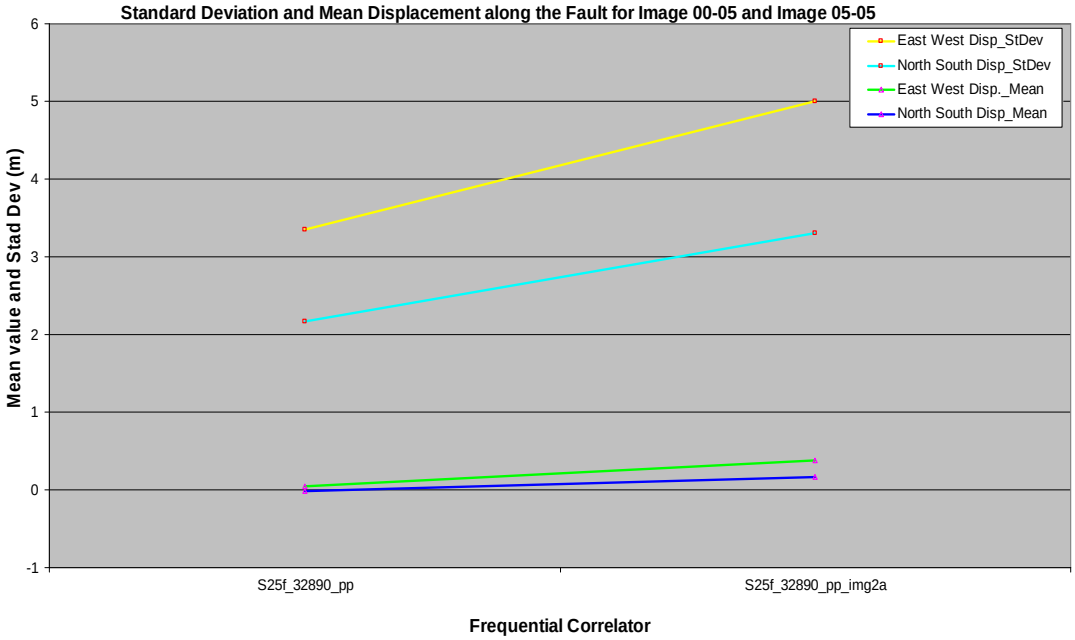

Figure A- 53. Mean and standard deviation both for North-South and East-West components of displacement for two pairs of images bracketing the earthquake

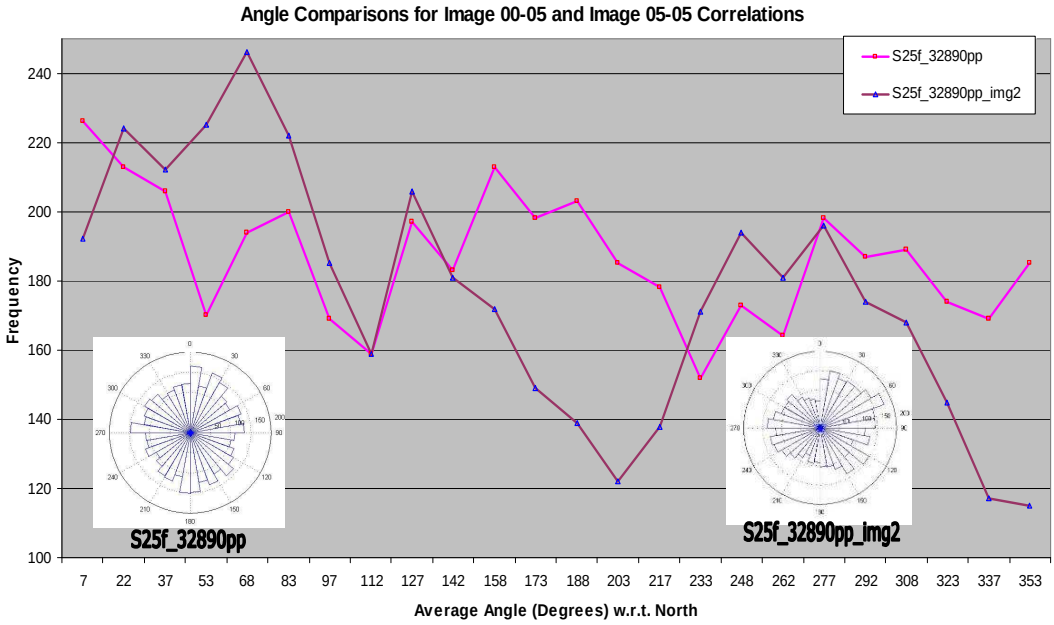

Figure A- 54. Average angle (direction of displacement) of different intervals and their respective rose diagrams for two pairs of images bracketing the earthquake

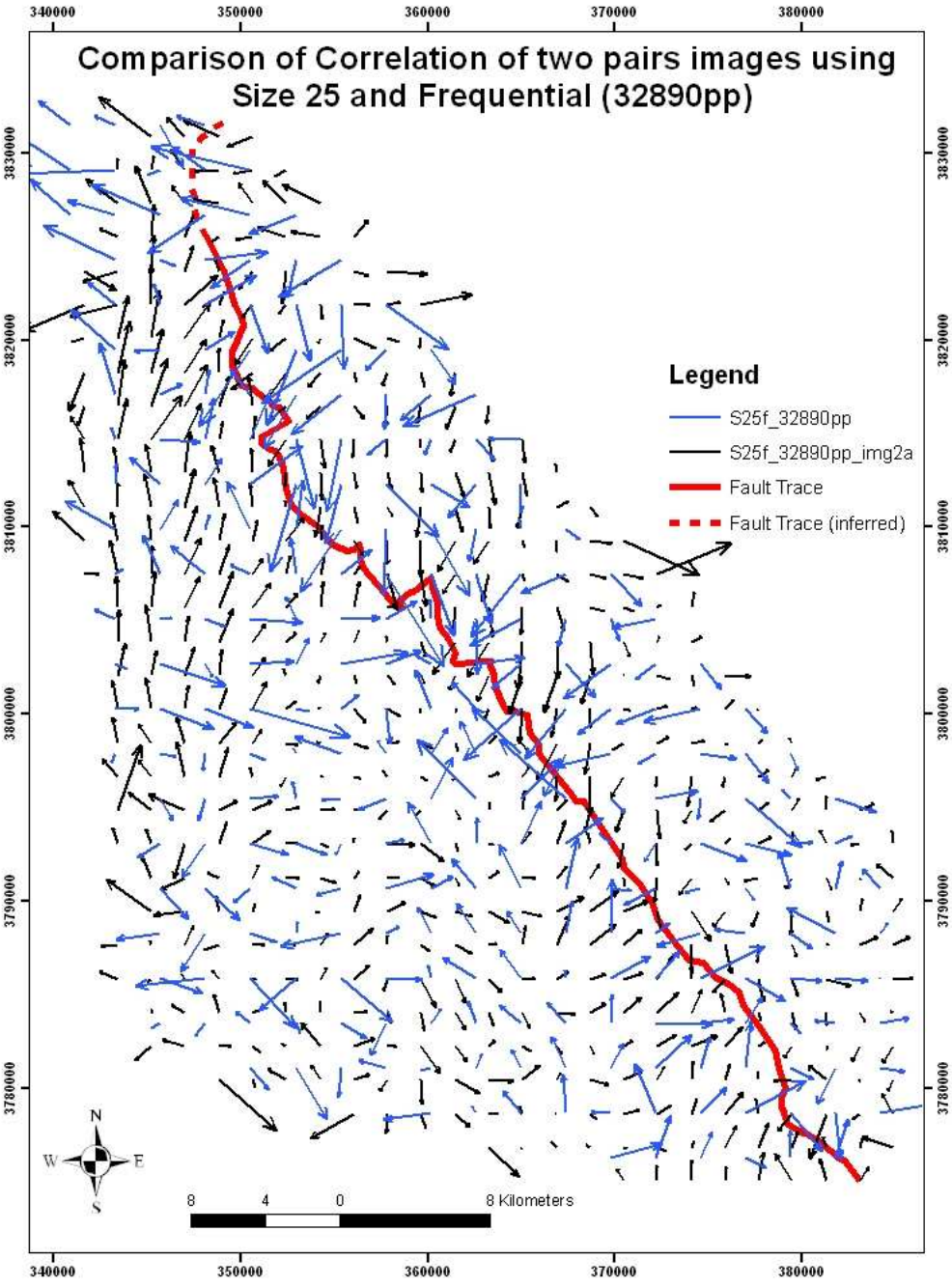

Figure A- 55. Vector Field comparison of displacement for two pairs of images

Appendix B

Nomenclature conventions used to different parameters are given as:

pre-post-DEM	=	pre-earthquake imagery orthorectified with respective pre DEM and post-earthquake imagery orthorectified with respective post DEM.
pre-DEM	=	Both pre- & post-earthquake images are orthorectified using pre-earthquake DEM
post-DEM	=	Both pre- & post-earthquake images are orthorectified using post-earthquake DEM
S25f_32890pp	=	Resampling method Sinc with kernel size 25 and correlation using Frequential method with window size 32, step 8, threshold 90 and pre-post-DEM
S25f_32890pre	=	Resampling method Sinc with kernel size 25 and correlation using Frequential method with window size 32, step 8, threshold 90 and pre-DEM
S25f_32890post	=	Resampling method Sinc with kernel size 25 and correlation using Frequential method with window size 32, step 8, threshold 90 and post-DEM
S25f_321690pp	=	Resampling method Sinc with kernel size 25 and correlation using Frequential method with window size 32, step 16, threshold 90 and pre-post-DEM
S25f_321695pp	=	Resampling method Sinc with kernel size 25 and correlation using Frequential method with window size 32, step 16, threshold 95 and pre-post-DEM
S25f_641695pp	=	Resampling method Sinc with kernel size 25 and correlation using Frequential method with window size 64, step 16, threshold 95 and pre-post-DEM
S25s_32810pp	=	Resampling method Sinc with kernel size 25 and correlation using Frequential method with window size 32, step 8, search range 10 and pre-post-DEM

S31f_32890pp	=	Resampling method Sinc with kernel size 31 and correlation using Frequential method with window size 32, step 8, threshold 90 and pre-post-DEM
S37f_32890pp	=	Resampling method Sinc with kernel size 37 and correlation using Frequential method with window size 32, step 8, threshold 90 and pre-post-DEM
Bil-f_32890pp	=	Resampling method Bilinear and correlation using Frequential method with window size 32, step 8, threshold 90 and pre-post-DEM
Bic-f_32890pp	=	Resampling method Bicubic and correlation using Frequential method with window size 32, step 8, threshold 90 and pre-post-DEM